Investigating the Pathophysiology of Acute Ischaemic Stroke Using Magnetic Resonance Imaging

D.Phil. thesis, University of Oxford

George W. J. Harston

MA, MBBChir, MRCP (UK)

Magdalen College, Oxford

Investigating the Pathophysiology of Acute Ischaemic Stroke Using Magnetic Resonance Imaging

DPhil thesis, George W.J. Harston, Magdalen College

Hilary Term, 2015

Abstract

The original description of the ischaemic penumbra asserted that both cerebral blood flow and metabolism would be required to monitor therapeutic intervention in acute ischaemic stroke. However, imaging in stroke trials has predominantly used biomarkers of infarction or perfusion-weighted signal to identify the pathophysiological processes that occur. This approach has neither identified novel treatment targets, nor been shown to consistently select patients who might benefit from intervention. The aim of this thesis was to use magnetic resonance imaging (MRI) biomarkers to identify and describe the pathophysiology of acute ischaemic stroke in patients.

Patients admitted to the John Radcliffe Hospital in Oxford were recruited into a clinical imaging study. Serial imaging data were acquired, predominantly in the first hours after symptom onset, to capture the early dynamics of brain pathophysiology. Tissue status was meticulously defined over time to ensure robust interpretation of the novel imaging biomarkers: multiple post labeling delay arterial spin labeling to measure cerebral blood flow (CBF), and amide proton transfer to generate an intracellular pH-weighted signal.

At a group level, the regions with the most severe injury had the lowest mean CBF and the greatest acidosis at presentation. There was a gradient of mean CBF and pH-weighted signal from the most ischaemic tissue to healthy tissue, but at the level of the individual there was considerable overlap in both parameters. The dynamics of perfusion were not sufficient to explain tissue outcome. Both acidosis and alkalosis were observed up to 24 hours in tissue that infarcted, and the nature of the pH change correlated with the timing of infarction.

These data show that single imaging biomarkers cannot explain the pathophysiology of stroke and tissue fate. There is heterogeneity of pathophysiology both within and between patients, and the dynamics of these processes vary. Insight from pH-weighted imaging highlights the limitations of using perfusion imaging alone to assess tissue status, and supports the use of complementary metabolic imaging in the investigation of ischaemic stroke.

Table of contents

Abbreviations

ADC	Apparent diffusion coefficient
ADP	Adenosine diphosphate
AIF	Arterial input function
AMICI	Acute Magnetic Resonance Imaging in Cerebral Ischaemia
ANOVA	Analysis of variance
APT	Amide proton transfer
ASL	Arterial spin labeling
ASPECTS	Alberta Stroke Programme early CT score
ATP	Adenosine triphosphate
AUC	Area under the curve
BAT	Bolus arrival time
BBR	Boundary-based registration
BOLD	Blood oxygen level dependent
CASL	Continuous arterial spin labeling
CBF	Cerebral blood flow
CBV	Cerebral blood volume
CEST	Chemical exchange saturation transfer
CNR	Contrast-to-noise ratio
CSF	Cerebrospinal fluid
CT	X-ray computed tomography
CTA	Computed tomography angiogram
CTP	Computed tomography perfusion
DSA	Digital subtraction angiography
DSC	Dynamic susceptibility contrast
DWI	Diffusion weighted imaging
ECASS	European Cooperative Acute Stroke Study
EPI	Echo planar imaging
FLAIR	Fluid attenuated inversion recovery
FLIRT	FSL linear registration tool
FMRIB	Functional Magnetic Resonance Imaging of the Brain
FNIRT	FSL non-linear registration tool
FNR	False negative rate
FPR	False positive rate
FSL	FMRIB Software Library
GH	George Harston, thesis author
LACS	Lacunar stroke
MO	Mean overlap
MPRAGE	Magnetization-prepared rapid gradient echo
MRA	Magnetic resonance angiogram
MRI	Magnetic resonance imaging
MRP	Magnetic resonance perfusion
MTT	Mean transit time

NINDS	National Institute of Neurological Disorders and Stroke
PACS	Partial anterior circulation stroke
PASL	Pulsed arterial spin labeling
PCASL	Pseudocontinuous arterial spin labeling
PD	Proton density
PET	Positron emission tomography
Pi	Phosphate
PLD	Post labeling delay
POCS	Posterior circulation stroke
PVE	Partial volume estimate
PWI	Perfusion weighted imaging
RCT	Randomized controlled trial
RF	Radiofrequency
ROC	Receiver operating characteristic
ROI	Region of interest
SPECT	Single photon emission computed tomography
T1	Longitudinal recovery
T2	Transverse decay
TACS	Total anterior circulation stroke
TCD	Transcranial Doppler
TE	Echo time
T_{max}	Time to maximum
TR	Repetition time
TRAIT	Treatment relevant acute imaging target
TTP	Time to peak
UO	Union overlap
VEPCASL	Vessel-encoded pseudocontinuous arterial spin labeling

List of publications

Publications arising from this thesis:

Harston GWJ, Tee YK, Blockley N, Okell T, Thandeswaran S, Shaya G, Sheerin F, Cellerini M, Payne S, Jezzard P, Chappell M, Kennedy J. (2015) Identifying the Ischaemic Penumbra Using pH-weighted Magnetic Resonance Imaging. ***Brain***. 138: 36-42

Harston GWJ, Rane N, Shaya G, Thandeswaran S, Cellerini M, Sheerin F, Kennedy J. (2015) Imaging Biomarkers in Acute Ischemic Stroke Trials: A Systematic Review. ***AJNR Am J Neuroradiol***. [Epub ahead of print]. DOI: 10.3174/ajnr.A4208

Tee YK, Harston GWJ, Blockley N, Okell TW, Levman J, Sheerin F, Cellerini M, Jezzard P, Kennedy J, Payne SJ, Chappell MA. (2014) Comparing Different Analysis Methods for Quantifying the MRI Amide Proton Transfer (APT) Effect in Hyperacute Stroke Patients. ***NMR Biomed***. 27:1019–1029

Harston GWJ, Batt F, Fan L, Okell TW, Sheerin F, Littlewood T, Kennedy J. (2014) Lacunar Infarction Associated with Anabolic Steroids and Polycythemia: A Case Report. ***Case Rep Neurol***. 6:34–37

Harston GWJ, Sheehan M, Kennedy J. (2014) Emergency medicine research: rites, rituals and consent. ***Emerg Med J***. 31:90-91

Harston GWJ, Tee YK, Jones M, Payne S, Pope G, Sheerin F, Kennedy J. (2013) Ventricular Extension of Intracerebral Hemorrhage during Intravenous Thrombolysis. ***Cerebrovasc. Dis***. 36: 324–325

Presented abstracts arising from this thesis (GH as first author):

Medical Engineering Centres Annual Meeting and Bioengineering 2014 (London):

Harston GWJ, Tee YK, Blockley N, Okell TW, Levman J, Sheerin F, Cellerini M, Jezzard P, Chappell M, Payne S, Kennedy J. Identifying the ischaemic penumbra using pH-weighted magnetic resonance imaging – poster presentation

Harston GWJ, Levman J, Okell TW, Pope G, Reckless I, Sheerin F, Cellerini M, Payne S, Chappell M, Jezzard P, Kennedy J. Serial changes in Apparent Diffusion Coefficient in Acute Ischemic Stroke – poster presentation

International Society of Magnetic Resonance in Medicine Meeting 2014 (Milan):

Harston GWJ, Okell TW, Sheerin F, Cellerini M, Payne S, Jezzard P, Chappell M, Kennedy J. Serial perfusion imaging using arterial spin labeling in acute ischemic stroke (0592) – platform presentation; prize: summa cum laude

Harston GWJ, Tee YK, Blockley N, Okell TW, Levman J, Sheerin F, Cellerini M, Jezzard P, Chappell M, Payne S, Kennedy J. Serial pH-weighted imaging using amide proton transfer in acute ischemic stroke (0763) – platform presentation; prize**:** magna cum laude

Harston GWJ, Levman J, Okell TW, Pope G, Reckless I, Sheerin F, Cellerini M, Payne S, Chappell M, Jezzard P, Kennedy J. Serial changes in Apparent Diffusion Coefficient in Acute Ischemic Stroke (2029) – poster presentation

European Stroke Conference 2013 (London):

Harston GWJ, Tee YK, Chappell M, Blockley N, Okell T, Levman J, Reckless I, Pope G, Sheerin F, Cellerini M, Rane N, Jezzard P, Payne S, Kennedy J. pH-weighted imaging in acute stroke: can metabolic imaging help us better understand the penumbra? – platform presentation Cerebrovasc Dis 35(Suppl 3): 46 (2013)

Harston GWJ, Tee YK, Chappell M, Blockley N, Okell T, Levman J, Reckless I, Pope G, Sheerin F, Cellerini M, Rane N, Jezzard P, Payne S, Kennedy J. Tissue outcome in acute ischemic stroke: how useful is perfusion? – poster presentation Cerebrovasc Dis 35(Suppl 3): 415 (2013)

Harston GWJ, Rane N, Kennedy J. Imaging Surrogates in Acute Stroke Trials: a Systematic Review – poster presentation Cerebrovasc Dis 35(Suppl 3): 418 (2013)

Brain Conference 2013 (Shanghai, ISCBFM):

Harston GWJ, Tee YK, Chappell M, Blockley N, Okell T, Levman J, Sheerin F, Cellerini M, Jezzard P, Payne S, Kennedy J. pH-weighted imaging in acute stroke: how does it compare to conventional techniques? Poster abstract no.: A-551-0024-00404 – poster presentation

Acknowledgements

I am indebted to a large number of individuals for their help and support in the writing of this thesis. In particular I must thank my supervisor, Professor James Kennedy, whose support and guidance over many years have led me to undertake research in stroke medicine. I have benefited enormously from his knowledge and wisdom in both the clinical and research settings. I am also grateful to my co-supervisor, Professor Stephen Payne, who has provided valuable insight over the duration of my research fellowship.

I must also acknowledge the help I have received from clinical fellow colleagues. Dr. Siva Thandeswaran and Dr. Gabriel Shaya both collected data that was used in this thesis. Dr. Neil Rane and Dr. Gabriel Shaya contributed to the systematic review in Chapter 2. I am grateful to Dr. David Minks for his work providing the complementary delineation of the follow up lesions used in Chapter 4.

I am grateful to the Acute Stroke Service at the Oxford University Hospitals NHS Trust for facilitating the recruitment of patients under their care into these research studies. In particular, I am indebted to the stroke consultants at the John Radcliffe Hospital, Rocel Espinosa, and Rachel Teal for their advice and support. To the team in the Oxford Acute Vascular Imaging Centre I am also grateful, especially Juliet Semple, Melanie Jones, and Carol Davey, without whom we would not have been able to deliver acute clinical research imaging in this cohort of patients. From the Department of Neuroradiology, I am thankful to Dr. Martino Cellerini for providing clinical MRI reports, and also to Dr. Fintan Sheerin, not only for providing MRI reports, but also for reviewing the manually delineated follow up lesion definitions in Chapter 4, and for his insightful comments and advice throughout my research fellowship.

I have received invaluable support and advice from the research groups of Professors Jezzard, Payne and Chappell, and the regular input from the group leaders has ensured the technical integrity of this work. Specifically, I am indebted to Dr. Thomas Okell and Professor Michael Chappell, who developed the arterial spin labeling sequence and associated post processing used in Chapter 5. For the work in Chapter 6, I am grateful to Dr. Nicholas Blockley and Professor Peter Jezzard who developed the chemical exchange saturation transfer sequence, and to Dr. Yee Kai Tee and Professor Chappell who provided the post processing software to quantify the pH-weighted signal.

Finally, I would like thank my family and in particular my wife, Sarah, for her tolerance and encouragement. I am also grateful for the support of my parents, and for their lifelong inspiration and backing.

This work was financially supported by the National Institute for Health Research Oxford Biomedical Research Centre Programme, the Dunhill Medical Trust and the Centre of Excellence for Personalized Healthcare funded by the Wellcome Trust and Engineering and Physical Sciences Research Council.

Chapter 1: Introduction

1. Stroke background

The incidence of stroke in the UK since the turn of the millennium has fallen, but improved survival means the prevalence of stroke has remained stable at 25 per 1000.[1] The estimated cost of stroke to the UK economy is around £9 billion per year and accounts for 5% of NHS spending.[2] Despite the societal and economic burden that stroke presents the early treatment options for acute ischaemic stroke remain limited to intravenous thrombolysis and possibly mechanical thrombectomy,[3, 4] with other measures such as stroke unit care and hemicraniectomy aimed at optimizing recovery and minimizing complications of the disease.[5, 6]

Many neuroprotective and reperfusion therapies for acute stroke have shown promise in preclinical experiments, but failed to translate into clinical practice.[7, 8] Possible explanations for this failure include the heterogeneity of stroke and the challenge of distinguishing stroke pathologies acutely,[9, 10] poor study design,[11] and inadequate preclinical models.[7, 8, 12, 13] Better identification of the pathology of human stroke in the acute setting would help meet some of these challenges, by improving diagnosis, identifying specific pathophysiological processes and potential treatment targets, and stratifying patients into homogeneous groups.

1.1. *Pathophysiology of acute ischaemic stroke*

Stroke is a heterogeneous disease consisting of ischaemic and haemorrhagic types, which account for 80% and 20% of the disease burden respectively.[14] Within ischaemic stroke, there are multiple aetiologies which lead to ischaemia (e.g. cardioembolism, *in situ* small vessel disease),[15] and within the cerebral parenchyma there are a range of pathophysiological processes that mediate ischaemic injury.[13]

Ischaemia is the imbalance between the energy requirements of the cell and the blood supply to it. The glucose and oxygen from the blood are required for aerobic synthesis of adenosine triphosphate, ATP, the predominant source of chemical energy within the cell, the level of which is normally maintained by oxidative phosphorylation. During ischaemia, in both neurons and glia, ATP is maintained for a finite period by high energy reserves (via creatine phosphokinase and adenylate kinase reactions) and glycolysis.[16, 17] In addition, following permanent or transient interruption of the cerebral blood flow, processes triggered by ischaemia, such as excitotoxicity and peri-infarct depolarizations, increase the energetic requirements of cells. Collateral blood supply means that cerebral hypoperfusion is rarely total, and its degree and duration will determine the nature of the pathophysiological processes that ensue.[18]

The mechanisms of ischaemic cell injury include: failure of ionic gradients, cell swelling and necrosis; free radical mediated lipolysis or DNA damage; inflammation; and mitochondrial dysfunction and apoptosis.[13] The relative contributions of the injurious pathways depend on the energetic imbalance and the tissue affected.[19] The time course for the different pathological processes range from minutes to weeks,[13, 20] and are dependent on the reperfusion dynamics of the tissue, which can be either beneficial, or deleterious (e.g. in the context of reperfusion injury).[21]

1.2. *Ischaemic penumbra*

The development and implementation of novel stroke therapies has centred on the ischaemic penumbra model. The penumbra was first described by Lindsay Symon's group at the Institute of Neurology in Queen Square (London, UK),[18] and it describes the fate of the brain early after the onset focal cerebral ischaemia. The model

distinguishes infarcted tissue from tissue at risk of infarction, the so-called ischaemic penumbra.

Symon and colleagues used primate models of focal cerebral ischaemia to investigate the electrophysiological and biochemical changes following the onset of ischemia, and the thresholds of blood flow at which these occurred. The group measured electrical evoked responses over the cerebral cortex of the baboon and identified a threshold of cerebral blood flow (CBF, 16-20ml/100g/min) below which electrical activity was suppressed, and then completely abolished (12ml/100g/min).[18, 22] Importantly the abolition of the evoked responses could be reversed by elevating blood pressure and restoring blood flow to suprathreshold levels demonstrating the reversibility of this phenomenon.

A second CBF threshold at which so-called "membrane failure" occurred was also described, below which tissue was thought to become irreversibly injured. Symon's group used ion-sensitive electrodes to measure the cortical extracellular potassium and calcium concentrations. They found that at a CBF level of 8-11ml/100g/min the concentration of extracellular potassium rapidly increased and the concentration of extracellular calcium decreased.[23, 24] The group surmised that this rapid change in ion concentrations was a result of intracellular potassium efflux due the energetic failure, and hence membrane failure, of the cells. This established the presence of a CBF threshold for the ischaemic core and the zone between these two thresholds was named the ischaemic penumbra (both after the area around the dark area at the centre of a candle flame and the bright zone surrounding the shadow during a solar eclipse).[18] Tissue with abnormal perfusion, but not at risk of infarction, is described as benign oligaemia.

Similar CBF thresholds for the cessation of electrical activity were described in patients undergoing carotid endarterectomy,[25] but the first convincing evidence for the presence of an ischaemic penumbra in human stroke came from positron emission tomography (PET) studies in the early 1980s.[26-28] In these studies the ischaemic penumbra was characterized by regions of hypoperfusion, with normal cerebral metabolic rate of oxygen consumption ($CMRO_2$) and elevated oxygen extraction fraction, and the ischaemic core as an area of disrupted $CMRO_2$. Later PET work correlated the regions of the acute PET scan with follow up imaging and final clinical outcome,[29, 30] confirming the presence of a clinically meaningful penumbral region in patients with acute ischaemic stroke, opening the way to patient selection for therapy using penumbral imaging techniques.[31]

Subsequent preclinical and clinical data have suggested that the penumbral concept may be an oversimplification of reality, with artificially binary tissue definitions and a significant heterogeneity of pathologies within tissue types.[32-36] Dynamic changes occur in the CBF and metabolism of the brain and accurate prediction of tissue at risk has been demonstrated to be challenging, even using multitracer PET techniques.[37]

1.2.1. *Lacunar stroke*

The presence of penumbra in lacunar infarction has been questioned as the affected perforator arteries are thought to be without collateral vessels that would create the graduated hypoperfusion required for a penumbra to exist.[38] However, others have hypothesized that penumbral tissue explains the sensitivity to haemodynamic instability in some patients.[39] Despite the challenges to the spatial resolution of neuroimaging in lacunar stroke it has been shown that regions of infarct growth are associated with a peri-infarct region hypoperfusion compared to those that do demonstrate infarct growth,

which would support the presence of a salvageable region of tissue at risk.[40] The size of lacunar infarcts limits the insights that can be provided by neuroimaging, and the generally good prognosis limits the availability of acute post mortem tissue. As a result the pathogenesis of lacunar infarcts remains poorly understood.[41]

1.3. *Recanalization and reperfusion*

Current evidence-based treatments for acute ischaemic stroke (intravenous thrombolysis and mechanical thrombectomy) centre around recanalization of the occluded vessel, which allows perfusion of the distal vascular bed and restoration metabolic substrate to the ischaemic tissue. However, recanalization does not necessarily lead to reperfusion and reperfusion may not result in tissue survival.[42] Reperfusion is superior at predicting both tissue survival (quantified using either infarct volume or penumbral salvage) and clinical outcomes than recanalization.[43, 44]

The dissociation between recanalization and reperfusion occurs because of either perfusion from collateral blood vessels in the absence of recanalization of the feeding artery,[44] or no reperfusion despite recanalization, the so-called "no-reflow" phenomenon.[45] No-reflow is thought to result from emboli from the occluding thrombus, in situ microthromi and inflammatory changes, neurovascular unit dysfunction and pericyte death, and tissue oedema preventing restoration of the microcirculation.[45, 46]

A further dissociation exists between reperfusion and tissue survival. Reperfusion of tissue that has already infarcted will be of no benefit, and delayed neuronal injury may occur in apparently salvageable regions despite reperfusion as the pro-apoptotic pathways are already in motion.[47] Furthermore, reperfusion itself can have deleterious effects, a phenomenon known as reperfusion injury. Reperfusion injury is poorly

understood, but proposed mechanisms include facilitation of oxidative stress and free radical production, and excitotoxicity following glutamate release fuelled by the restoration of blood flow.[45]

This dissociation between recanalization and reperfusion, and between reperfusion and tissue survival, underlies the concept of futile recanalization, where successful recanalization does not lead to clinical improvement.[48, 49] Development of imaging biomarkers has the potential to improve the understanding of the factors that determine outcome in stroke, and the different responses to treatments seen between patients.

2. Imaging biomarkers

Imaging is an appealing medium with which to investigate the pathophysiology of acute stroke in patients. It allows insight into the brain structure, blood supply and metabolism at the time of injury, when invasive investigations are not possible. Histology remains the gold standard of investigation in many human diseases for both research and clinical practice, but the inaccessibility of the brain and the often delayed mortality following stroke mean that acquiring brain tissue acutely is rarely possible. Imaging biomarkers have the potential to provide an alternative to histological investigations. Imaging biomarkers have been used for various purposes in different diseases: prediction, detection, staging, grading and the assessment of response to treatment.[50] In some fields, including oncology, imaging is widely used to guide treatment, but in stroke there is much less evidence to support such an approach.[9]

2.1. *Rationale for using imaging biomarkers*

When considering imaging biomarkers, it is worth making the distinction between biomarkers to provide insight into disease pathophysiology for scientific purposes, and biomarkers for use in routine clinical practice. Biomarkers used in the pathological

investigation of disease are by necessity disease-centred, and ideally directly reflect the underlying biological processes. Such biomarkers provide insight into disease pathways and may aid the identification of novel treatment targets. A degree of data loss and imprecision can be tolerated at a study level, if understood and acknowledged, for these disease-centred biomarkers.

Biomarker development for use in clinical practice has different requirements. Understanding the biological basis for a signal is less important than its clinical validation if it is to be used as a prognostic or risk factor, or a surrogate outcome. The biomarker should be linked to patient-centred variables, outcomes that reflect how the patient "feels, functions and survives".[51] Biomarkers used as surrogate outcomes do not need to be intrinsically biologically meaningful, but must have been validated as a surrogate that reflects patient outcome.[51] Prognostic factors require equally robust validation as surrogate outcomes to demonstrate that they have a clinical utility, especially if they are used to identify subgroups of patients who may benefit from a treatment.

However, having made the distinction between using biomarkers either as an investigative technique or as a clinical tool, a biomarker is more likely to gain clinical validity if it relates to the underlying disease pathophysiology. Whilst correlations with disease outcome are often used to validate imaging biomarkers in the clinical setting, if the relationship to the biology of the disease is properly understood this would provide additional insight into potential treatment targets and improve translation between preclinical models and patients. It would be possible for a biomarker to fulfill both roles, provided the compromises are not too great for either purpose.

2.2. *Limitations of imaging biomarkers*

Despite the appeal of using imaging biomarkers to investigate disease pathology there are several inherent limitations of imaging that must be considered. There are a finite number of physical parameters that can be measured, and the relationship between these physical measures and human biology is not always clear. Furthermore, imaging considers the state of the brain and not the patient as whole, so can miss non-cerebral treatment modifiers or outcomes.[52, 53] Overreliance on imaging biomarkers without rigorous methodology can lead to significant research bias.[54]

There are also practical considerations when developing imaging biomarkers in a clinical setting. Successful translation requires not only the development of the imaging sequence, but the ability to exploit it in a patient population. In stroke, this means getting the patient to the hardware required for image acquisition, with the necessary expertise available to generate and interpret the imaging data. The image acquisition has to be of a duration that is clinically acceptable, relatively resistant to artefact, and without the need for exogenous agents that could be either toxic (risk of anaphylaxis, haemodynamic effects, or direct toxicity) or intolerable in the acute setting (high flow gases, physiological or pharmacological challenges). If imaging is used to guide treatment decisions then analysis and interpretation need to be feasible within a short time frame. Speed of acquisition and processing is of particular importance in stroke as the only treatment modifier for thrombolysis is time from symptom onset.[55] The spatial resolution of neuroimaging is limited to the macroscopic scale, which prohibits the distinction of cell specific responses to ischaemia. There is also no temporal information in a single image, so the dynamics of the disease prior to imaging cannot be known.

3. Imaging guidelines for stroke

3.1. *Clinical guidelines*

Guidelines for the management of acute stroke from the National Institute for Health and Care Excellence (NICE) in the UK and the American Stroke Association recommend urgent brain imaging for patients with suspected stroke, but neither specify the preferred imaging modality (CT or MRI).[56, 57] In practice, the majority of acute stroke imaging involves non-contrast computed tomography (CT) because it is quick and without absolute contraindication, provided the patient can lie flat. CT reliably identifies intracranial haemorrhage and is sufficient to group stroke patients into ischaemic or haemorrhagic subtype, the only distinction that influences management with a strong evidence base.[55] Angiography is used increasingly to identify vascular occlusions where a thrombectomy service is available.

3.2. *Acute stroke imaging roadmap II*

In light of several null trials that used imaging criteria to select patients for intervention, a consensus statement, the Acute Stroke Imaging Roadmap II, was produced to guide imaging based stroke research over a 5 year time frame.[58] This document lists six principle recommendations:

1. The use of standard terminology;
2. A standardized imaging assessment of revascularization;
3. A standardized process to assess whether ischaemic core and penumbral imaging meet required standards;
4. The characteristics of a clinical and imaging data repository;
5. An optimal study design for a clinical trial to evaluate the value added of advanced imaging; and

6. The structure of a stroke neuroimaging network to implement the above;

The Roadmap also defines general requirements of imaging in stroke trials (speed, standardization, quality control, reproducibility and centralization), suggests a variety of potential uses for imaging, and highlights some unresolved issues. The unresolved issues describe the ongoing uncertainty about whether advanced imaging can add any value to the conventional assessment of stroke patients.

The Roadmap advocates the use of the same imaging biomarkers to select patients and demonstrate efficacy in Phase 2 studies, biomarkers it terms Treatment Relevant Acute Imaging Targets (TRAITs). This generic term encompasses modifiable biomarkers that can be targeted by a specific intervention to demonstrate efficacy such as vascular occlusion, perfusion status of tissue, or infarct volume. There is no specific recommendation regarding the optimum methodology to define ischaemic core or penumbra using imaging, a reflection of the lack of strong evidence in this area. There is also no recommendation with regards to whether CT or MRI might be optimal for selecting patients, and within these modalities no suggestion of the parameters that might be best exploited to define tissue at risk.

For validation of penumbral imaging strategies, the Roadmap advocates the use of 24 hour diffusion-weighted imaging (DWI, range 18-36 hours) as the preferred method of measuring final infarct volume, or CT hypodensity at this time if MRI is not available. This recommendation is justified on pragmatic grounds (minimizing drop out compared to later time points), and by a single study correlating 24 hour trace DWI volumes and day 90 infarct volume defined on T2-weighted FLAIR imaging.[59] Importantly, as will be discussed in Chapter 4, this recommendation does not mention image registration and the need for tissue level validation of novel imaging biomarkers. It does not discuss

the use of apparent diffusion coefficient (ADC) versus trace DWI hyperintensity, or the potential errors that imaging at 24 hours might introduce. Accurate registration and determination of tissue fate are of particular importance in interpreting penumbral imaging, because it is a tissue level analysis that is required. Correlation of infarct volumes at different time points within individual patients is inherently biased to produce a strong correlation. Distal vascular occlusions will produce smaller final infarct volumes than proximal occlusions regardless of intervention and, therefore, correlation of volume does not discriminate treatment efficacy. Infarct growth or penumbral salvage at a tissue level is needed to avoid underestimation of treatment effects.

4. CT and CT perfusion

Non-contrast CT and CT perfusion have been used with some success in several imaging studies to select patients for treatment and assess the efficacy of interventions.[60, 61] CT offers a practical and rapid imaging modality that is widely available in centres around the world. However, for the investigation of pathology, CT does have limitations. Non-contrast CT measures X-ray absorption, which is a physical parameter with little evidence regarding the biological substrate.[26] CT hypodensity is thought to qualitatively represent ischaemic core although that has been questioned in some studies.[62-64] When compared to DWI, CT has a lower sensitivity for detecting infarction and relatively poor interrater agreement. The limited ability to manipulate the CT signal and the paucity of knowledge regarding the biological substrate constrain its utility for investigation of tissue pathophysiology.

5. MRI

MRI is an appealing tool for the investigation of stroke pathophysiology as it allows multiple properties of protons in nuclei (typically hydrogen) to be manipulated and measured. In this way, a number of tissue properties with increasingly understood biological substrates can be probed.[65-69]

5.1. *Principles of MRI*

A MRI scanner consists of a high strength magnetic field aligned in the bore of an electromagnet to create the homogeneous resting field, B_0. An imaging subject in the bore causes distortions to this field, which are corrected prior to image acquisition, a process known as shimming. There is a net alignment of protons in the brain with the B_0 field. To generate a signal the protons are excited by a radiofrequency (RF) pulse, B_1, which causes the net alignment of protons to deflect from the longitudinal axis (M_z) and towards the transverse plane ($M_{X/Y}$). The deflected protons rotate around the B_0 axis (precession), the rate of which is determined by the magnetic field strength. The rate of precession is called the Larmor frequency:

$$\omega = \gamma B_0$$

The Larmor frequency, ω, is a product of a constant, the gyromagnetic ratio, γ, and B_0. The Larmor frequency is also the resonance frequency for excitation of a proton and, therefore, by applying a gradient to the magnetic field at the time of the excitation, a single slice can be selectively excited.

Over time the deflected protons realign with the B_0 field, so called longitudinal recovery, the half life of which is denoted by T1. In addition to longitudinal relaxation, the protons precess at subtly different rates according to the differences in their local microenvironment magnetic field. As a result of these different rates of precession, the

protons gradually dephase, diminishing the net signal. This is called transverse decay, and the half life of this is denoted by T2 (Figure 1.1). The magnitude of the signal at the time of acquisition is a composite of both T1 and T2.

To acquire a signal the protons are repeatedly excited by RF pulses separated by the repetition time, TR. During each TR and after each RF pulse the signal is acquired at a time known as the echo time, TE (Figure 1.1). Manipulation of the TR and TE leads to different properties of the protons influencing the signal to different degrees. This is how T1-, T2- and proton density (PD)-weighted images are generated.

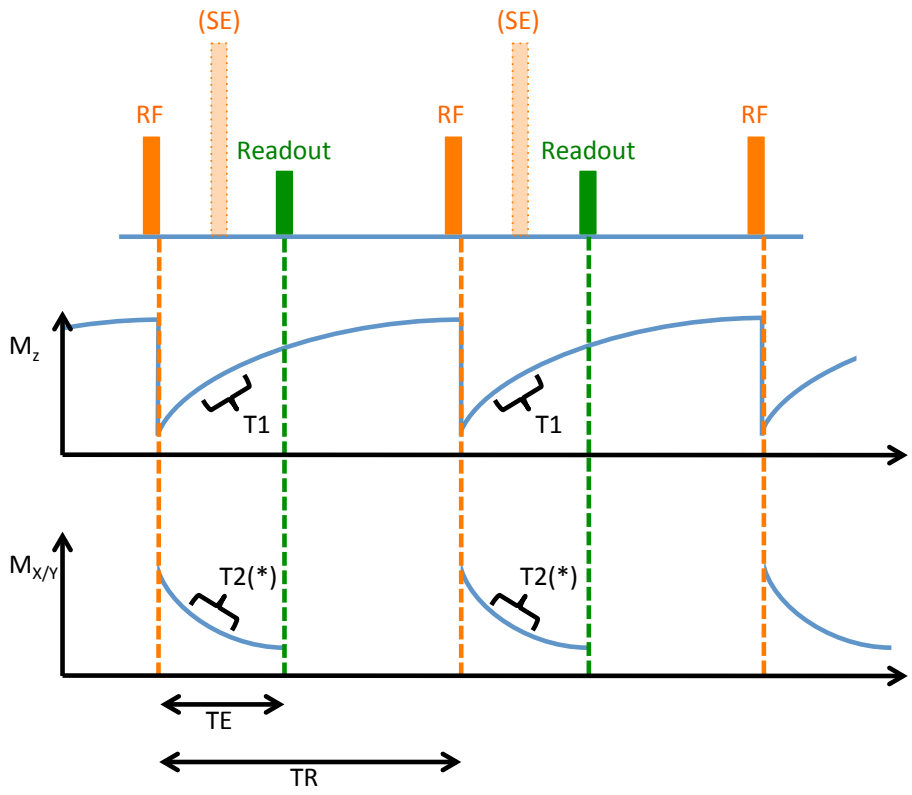

Figure 1. 1 – Schematic of MRI signal. RF: radiofrequency pulse; SE: spin echo inversion pulse used in spin echo sequences; M_z: longitudinal magnetization; $M_{X/Y}$: transverse magnetization; TE: echo time; TR: repetition time; T1: half life of longitudinal relaxation; T2(*) half life of transverse decay, * indicates decay due to B_0 inhomogeneity in addition to T2 decay seen in gradient echo sequences.

In addition to the differences in the microenvironment magnetic field that lead to T2 transverse decay, larger scale inhomogeneities in the B_0 field lead to additional dephasing. The combined effect of T2 decay and B_0 inhomogeneity dephasing is known as the T2* property. This is most apparent in regions of the brain where the B_0 field is distorted, such as near large veins or haemorrhages. This effect can be compensated for by inverting the proton spins 180° half way between the RF pulse and the image readout (i.e. at TE/2 seconds from the RF pulse, Figure 1.1). This is known as a spin echo sequence as to opposed the gradient echo sequence.

To readout the MR signal, the current in the scanner coils, generated by the rotating protons in the B_0 field, is measured. By applying gradients across the B_0 field during the readout, the spin frequencies of the protons are manipulated in such a way that spatial frequencies of the signal intensity are generated. The spatial frequency information creates a "k-space" image that following a Fourier transform generates a conventional MRI picture. Echo planar imaging (EPI) is a rapid method of image readout that allows acquisition of large regions in a short space of time. This is useful for imaging patients or where multiple volumes are required quickly (e.g. functional MRI, diffusion-weighted imaging or cardiac MRI). However, EPI is susceptible to field inhomogeneity artefact because phase change is erroneously ascribed to proton position.

5.2. *Diffusion-weighted imaging*

5.2.1. *Signal generation*

Diffusion-weighted imaging (DWI) exploits the ability of magnetic gradients to change the frequency of precession of a proton, and uses this to determine how much that proton has moved during each image acquisition cycle. DWI is a T2-weighted sequence, but with the addition of two opposite magnetic gradients applied at the

beginning and end of the TE. The first gradient is applied transiently after the RF pulse. This gradient causes the frequency of precession to change for a short time across the gradient. When the gradient is removed the protons return to precessing at the same frequency, but are now systematically out of phase across the direction of the gradient. Before readout an opposite gradient is applied for an equal duration causing the protons to rephase. However, if the protons have moved via diffusion the rephasing is imperfect and hence the signal is reduced. The sequence is then repeated, but with the diffusion gradient in a different plane. This allows directional information regarding proton diffusion to be acquired. Water accounts for the majority of protons in the brain and so by inference the signal provides information about the diffusion of water. Conventional DWI acquires diffusion-weighted data in three orthogonal planes and averages the signal to give a directionless measure of water diffusion. This is known as the trace diffusion-weighted image. If data are acquired in more than three planes then a vector can be generated to provide additional information about any anisotropy of diffusion. This is diffusion tensor imaging.

5.2.2. *Quantification*

How sensitive the DWI signal intensity is to diffusion is dependent on the amplitude and duration of the diffusion gradients, and the time between them. The diffusion weighting of a sequence is quantified using a b-value, with higher numbers representing greater diffusion sensitivity. A b = 0 image is a T2-weighted image with no diffusion weighting. In stroke, DWI typically uses two b-values of around 1000 s/mm^2 and 0. The trace DWI (e.g. b = 1000 s/mm^2) represents both diffusion- and T2-weighted signal ("T2 shine through"). In order to remove the contribution of the T2-weighted signal, an apparent diffusion coefficient (ADC) image is calculated from the trace DWI and b = 0

images. The ADC value is a measure of how easily water can diffuse with lower values representing restricted diffusion (Figure 1.2).

Within the stroke literature the naming conventions around DWI are often applied loosely. For the purpose of this thesis "DWI" will be used to refer to the technique in the broadest terms. "Trace DWI" will be used to describe the b = 1000 s/mm^2 image and "ADC" the apparent diffusion coefficient image.

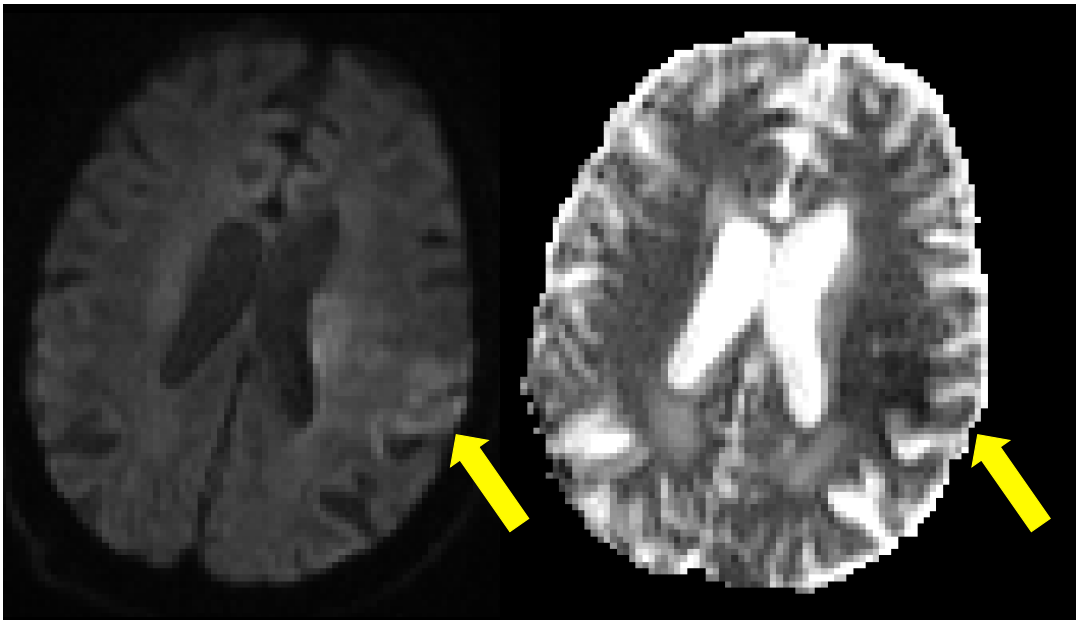

Figure 1. 2 - Diffusion-weighted imaging from a patient with acute ischaemic stroke indicated by the yellow arrow. Left: trace DWI, b = 1000s/mm^2. Right: apparent diffusion coefficient image.

5.2.3. *Biological substrate*

Restricted diffusion of water is thought to occur in cerebral ischaemia due to net movement of water from the extracellular to the intracellular space, and increased tortuosity of the extracellular compartment.[70] This occurs as a result of the energetic failure of the cells, ATP depletion, and loss of ATPase function that would normally maintain ionic gradients across the cell membrane. There is a net influx of sodium ions into the cell and osmotic pressures draw water in from the extracellular space (cytotoxic oedema). The gelatinous intracellular spaces contain large quantities of

macromolecules, and these limit the free diffusion of water, whereas the extracellular space has fewer barriers to diffusion. The net intracellular movement of water restricts the ability of water to diffuse freely, increasing the trace DWI intensity and reducing the ADC values (Figure 1.2).

The natural history of trace DWI signal and ADC differ after the acute phase of ischaemia. After the initial elevation of the trace DWI signal in acute ischaemia and the fall in ADC values, the lesions gain T2-weighted hyperintensity, which maintains the intensity of the trace DWI signal. However, this T2-weighted component is controlled for in the ADC signal, so the ADC image follows the natural history of the diffusion characteristics, i.e. pseudonormalization followed by facilitated diffusion in the days to weeks that follow ischaemia.[71] This mismatch between ADC and trace DWI is thought to be due to concurrent vasogenic oedema, which increases extracellular diffusivity and also increases T2-weighted signal, and cytotoxic oedema, which restricts diffusion, but has no effect of T2-weighted signal. Thus the net effect on ADC can be little of no change from normal whereas the trace DWI remains hyperintense from the vasogenic oedema. Further ADC and trace DWI mismatch can occur adjacent to cerebrospinal fluid (CSF). ADC signal can be contaminated by the partial volume effects of CSF in voxels containing a proportion of freely diffusing fluid, which increases the mean diffusivity of that voxel.

5.3. ***Perfusion MRI***

CBF is the delivery of blood to the brain. Measurement of CBF requires a contrast agent in the blood that can be used to quantify its arrival in the brain tissue.[72] In practice, imperfect contrast agents are used, including exogenous intravenous contrast (e.g. gadolinium, Gd) that remain in the vasculature, and arterial spin labeling, the signal of

which decays over time. In order to quantify CBF the effect of the contrast on the MRI signal, the concentration profile of the agent, and its compartmental distribution need to be known.[72]

5.3.1. *Exogenous contrast perfusion*

MRI measures of cerebral perfusion in stroke are most commonly achieved by dynamic susceptibility contrast perfusion-weighted imaging (DSC-PWI).[73] Intravenous paramagnetic contrast, typically Gd-based, is injected peripherally and the passage is measured through the cerebral vasculature. The concentration profile of tracer is estimated by repeatedly measuring the effect of Gd on the T2* relaxivity as the bolus passes through the vasculature. Concentration-time curves are generated from these images, but in order to calibrate these curves it is necessary to know the concentration profile of the contrast as it enters the brain: the arterial input function (AIF). If the AIF is known, then the deconvolved concentration-time curve produces the cerebral blood volume (CBV, area under the curve), CBF (peak of curve), and mean transit time (MTT, CBV/CBF).

DSC-PWI is not reliable for absolute quantification of CBF because the deconvolution process is subject to multiple sources of error.[74-78] These errors include the challenges of accurately measuring the AIF, dispersion of the contrast as it flows through the vasculature, variations in cardiac output, the effect of the contrast on the tissue relaxivity, assumptions about the integrity of the blood brain barrier, and venous outflow. For this reason DSC-PWI is more commonly quantified using relative CBV or surrogates of CBF such as time to peak (TTP), MTT or T_{max}. TTP is the time from the first detection of the arrival of contrast to the peak signal, and T_{max} is the deconvolved equivalent.[79]

Several studies have demonstrated the correlation of thresholds of perfusion biomarkers in predicting tissue at risk of infarction,[80] but they have yet to be translated into routine clinical practice.[78] The parameters allow perfusion maps to be generated with a reasonable contrast to noise ratio in a clinically acceptable time frame. However, for the investigation of pathophysiology, the biological substrates for some of these parameters are not clear and the difficulty in quantifying physiological measurements absolutely limits the application of the DSC-PWI.[81]

5.3.2. *Arterial spin labeling*

Arterial spin labeling (ASL) is a non-contrast MRI technique, which quantifies CBF by measuring the passage of magnetically labeled water in blood as it arrives in the cerebral parenchyma.[66] Whereas DSC-PWI requires knowledge of the AIF to deconvolve the tracer signal, ASL uses labeled water, which freely diffuses into the tissue compartments, making quantification more straightforward.[72] Routine access to high field strength magnets (3.0T is preferred) and improvements in suppression of noise and signal generation have meant that ASL is increasingly used to quantify CBF in both healthy individuals and patients. It is available as a standard option on most MRI platforms.[82] Furthermore, no requirement for exogenous contrast or exposure to radiation means that serial acquisitions are possible within individuals providing a platform for the "repeatable non-invasive 3-dimensional imaging of regional cerebral blood flow" called for by Astrup *et al*.[18, 73]

The paradigm of ASL is in 3 parts: labeling of inflowing blood in the feeding arteries supplying the brain; a post labeling delay (PLD) whilst the blood travels to the brain; and image acquisition (Figure 1.3).

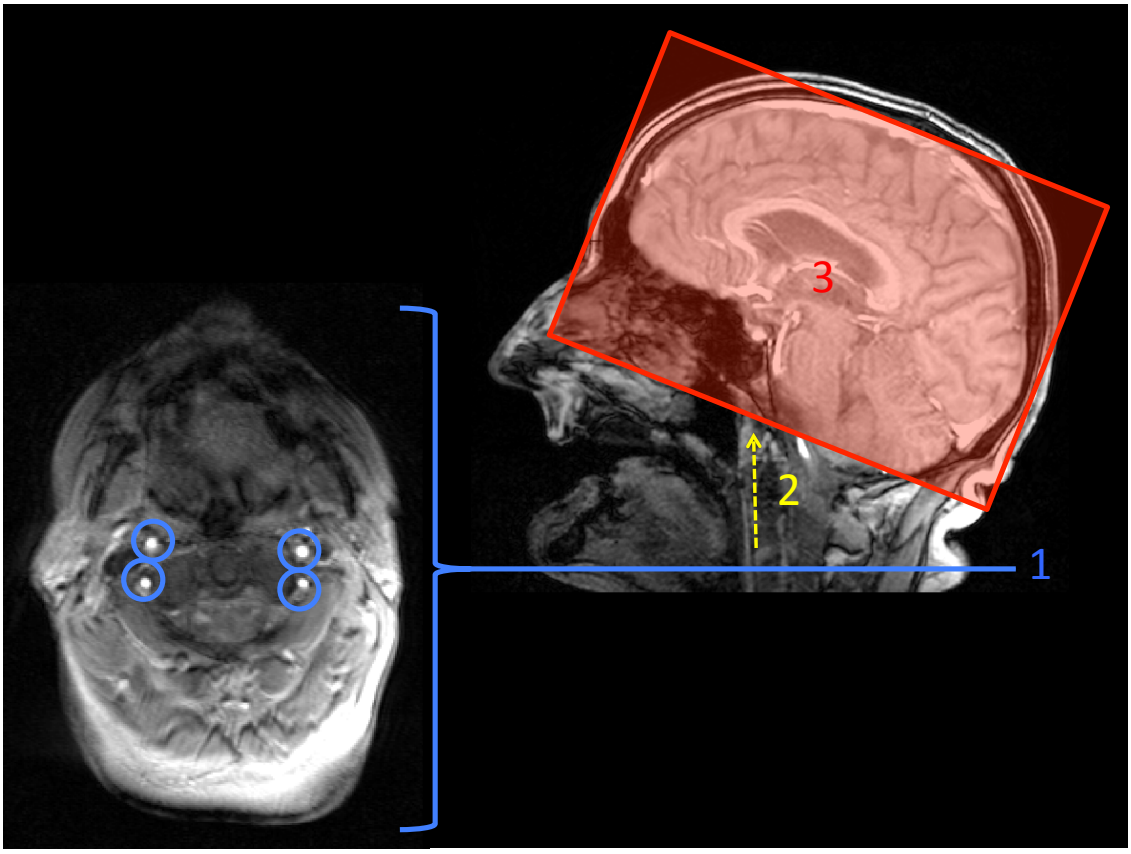

Figure 1. 3 - Arterial spin labeling. 1: magnetic labeling of blood in the large arteries of the neck; 2: post labeling delay; 3: image acquisition.

There are three options for labeling the inflowing blood: pulsed, continuous, and pseudocontinuous ASL (PASL, CASL and PCASL). PASL involves the labeling of a thick slab over the neck in a short period of time. In contrast, CASL and PCASL label a single slice in the neck over a longer period of time, with PCASL providing a superior labeling efficiency. PASL has a lower signal-to-noise ratio than the other techniques. Therefore, PCASL is the preferred imaging technique for clinical use.[82]

A particular challenge when using ASL is selecting the optimum PLD. The PLD needs to be sufficiently long to ensure that the bolus of labeled blood has completely arrived in the brain by the time of image acquisition. However, if the PLD is too long then signal will be lost due to magnetization decay. In health, blood arrival times are rarely delayed, meaning there is little conflict between these two considerations. This is in

contrast to patients with cerebrovascular disease, where arrival times can be delayed, resulting in CBF underestimation. To overcome this problem, a multiple PLD approach can be used, in which signal is measured after a series of different PLDs. A model is fitted which incorporates both delays in the bolus arrival and signal decay into the quantification of CBF, extending the range of arrival delays that can be accurately measured.[66, 83] However, even using multiple PLDs, there is a theoretical bolus arrival time limit of approximately 3.5s, beyond which ASL cannot measure perfusion.[84] It is not clear from the literature what the bolus arrival times are in stroke patients. There are known to be delays in MTT, TTP and T_{max} measured using DSC-PWI commonly in the order of 4-6s, although it must be noted that these parameters do not reflect bolus arrival time.[79]

CBF is measured by subtracting an image where there is no arterial labeling from one where blood has been tagged and the difference is the signal from the inflowing blood. Approximately 2% of the grey matter water is replaced by inflowing blood-borne water every second. Including the signal losses from magnetic decay this results in a signal of less than 1% of the background.[82] Background suppression is used to maximize the signal contrast.[82, 85]

In white matter, low signal to noise ratio, delays to arrival and partial volume contamination limit the ability of ASL to measure CBF.[86] In healthy volunteers advances in imaging hardware, improved imaging sequences and analysis techniques have made white matter CBF quantification possible,[87] but this has yet to be demonstrated in patients, in whom the signal to noise ratios are poorer.

5.4. *Metabolic MRI*

MRI advances in metabolic imaging have been more limited than in perfusion imaging. PET has traditionally been the metabolic imaging technique of choice for stroke studies, but there are few MRI based alternatives. Blood oxygen level dependent (BOLD) techniques, with or without use of stimulus gases, generate signal utilizing the T2* effect of deoxygenated haemoglobin, and from this the oxygen extraction fraction can be inferred.[88-90] BOLD techniques rely heavily on the perfusion of blood and can be impractical, often requiring gaseous stimuli such as carbogen for meaningful calibration.[91] Magnetic resonance spectroscopy provides detailed information about molecular profiles in individual voxels, but it does not give sufficient spatial resolution to be used in a clinically meaningful way.[92-94]

5.4.1. *Chemical exchange saturation transfer*

Chemical exchange saturation transfer (CEST) includes of a range of MRI techniques that measure the exchange of protons between endogenous or exogenous contrast molecules, and water.[95] The low concentration of the protons in the contrast precludes their direct measurement. However, the resonance frequency of these protons is offset from that of water, meaning they can be selectively saturated. As saturation occurs over a period of time, the saturated protons exchange into the water pool and the accumulated attenuation of the water pool signal can be measured (Figure 1.4).

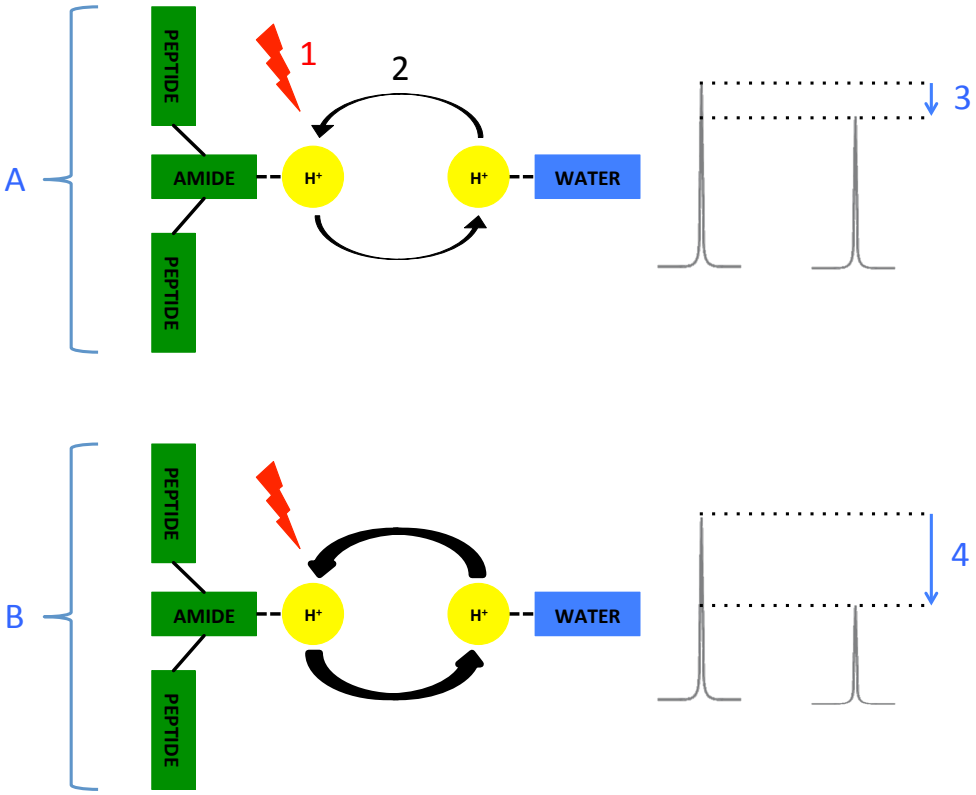

Figure 1. 4 – Chemical exchange saturation transfer under slow (A) and fast (B) exchange rate conditions. The protons in the contrast are selectively saturated (1) over a prolonged period allowing exchange into the water pool (2). This attenuates the measured water signal (3), which occurs to a greater extent in the fast exchange conditions (4) allowing the exchange rate to be estimated.

To measure the CEST effect at a given frequency, signal is repeatedly measured using a range of saturating frequencies offset from water, relative to an unsaturated signal (S_{sat}/S_0). This produces the Z-spectrum, from which the CEST effect can be quantified at the frequency offset of interest (Figure 1.5). The magnitude of the CEST effect can be estimated using asymmetry measures or model based approaches.[96-99] The latter have the advantage of not assuming symmetry of the non-CEST signal about the water frequency, an assumption that is rarely correct.[95-97]

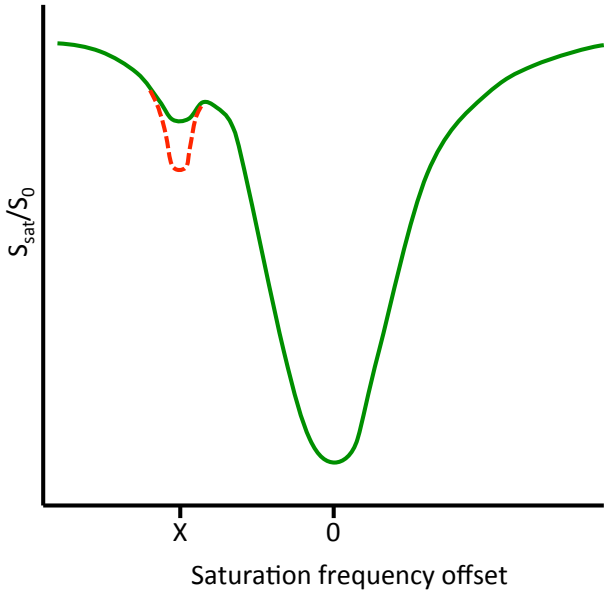

Figure 1. 5 - The Z-spectrum is acquired by measuring the water signal following a range of saturation pulses at various frequencies offset from water, S_{sat}, relative to the unsaturated signal, S_0. The magnitude of the diminution of the water signal at the frequency of interest, X, is used to quantify the proton transfer rate. If the proton transfer rate increases the magnitude of the CEST effect increases (intermittent red line).

5.4.2. *Amide proton transfer*

The CEST effect at 3.5 parts per million (ppm) offset from water represents the exchange of protons between the amide groups of proteins and peptides, and water, known as the amide proton transfer, APT.[67] The magnitude of the APT effect is dependent on the concentration of available amide groups and the exchange rate of protons. The exchange rate is base catalyzed and hence pH-dependent. Therefore, for a given concentration of amide, the APT represents a pH-weighted signal. In preclinical models the amide concentration has been shown to constant for the first few hours following the onset of ischaemia although it is not known what changes to the available amide concentration occur after this time.[67]

6. Thesis aim

The aim of this thesis is to investigate the pathophysiology of acute ischaemic stroke using serial MRI measurements. Specifically, these include diffusion-weighted imaging, quantified using ADC, absolute CBF, quantified using vessel-encoded pseudocontinuous ASL (VEPCASL), and pH-weighted imaging, quantified using APT CEST.

Chapter 2: Systematic Review of Imaging Biomarkers in Acute Stroke Trials

1. Introduction

Treatment options for patients with acute ischaemic stroke are limited. Despite attempts to develop novel neuroprotectants and strategies for reperfusion, few have made it into routine practice. This failure of progress is multifactorial in origin, but includes failure to properly account for patient heterogeneity and a lack of proven surrogate outcomes.[53] Imaging has been widely embraced, both in clinical practice and research studies. It is an appealing tool for the investigation of patients with acute stroke because it can provide insight into the pathophysiology underlying the disease. Identification of pathology within patients provides a means to reduce heterogeneity of participants in a trial, to stratify patients into those that may or may not benefit from treatments, and to assess intervention efficacy and/ or safety.[58, 100]

As outlined in Chapter 1, the Acute Stroke Imaging Research Roadmap II was developed on the background of recent null acute stroke trials incorporating selection using penumbral imaging.[58] It reinforced the need for rigorous definition of regions of interest, and defined a framework for using imaging biomarkers in studies (with the specific example of revascularization). However, this consensus statement made few recommendations regarding the details of the specific imaging biomarkers used, which reflects a lack of consensus amongst the stroke imaging community.

1.1. *Aims*

In this Chapter, randomized controlled trials (RCTs) were systematically reviewed in patients with acute ischaemic stroke, using the groupings developed in the Acute Stroke Imaging Research Roadmap II, and with the following aims:

- To describe the purposes for which imaging is used in RCTs;

- To determine the imaging modalities that are used for each purpose, in particular for defining infarction and tissue at risk of infarction; and

- To determine which strategies, if any, have been used with success.

2. Methods

2.1. *Eligibility Criteria*

Studies analyzing data from randomized controlled trials (RCTs) of acute ischaemic stroke therapies (e.g. intravenous thrombolysis, glycemic control, hypothermia) were included. Enrollment was required within 48 hours of symptom onset and imaging biomarkers had to be used to select patients, measure outcome, or define subgroups (preplanned or *post hoc*). Any form of imaging including CT, MRI, single photon emission CT (SPECT), or transcranial Doppler (TCD) was allowed. Studies that used imaging solely to exclude patients with intracranial haemorrhage at trial enrollment were not included in the analysis. Other exclusion criteria were: studies of haemorrhagic stroke or transient ischaemic attack; cluster trials; studies in children; those not comparing treatment and control groups; and those using historic controls. Where two or more papers described the same populations both studies were included provided different imaging biomarkers were used in each.

2.2. *Search strategy*

MEDLINE and EMBASE (1995 to March 2014) were searched using a combination of terms, their derivatives and related terms: RCTs, acute stroke, and imaging (for example search terms see Appendix A). Searches were limited to English language papers in adult human subjects. Additional searches were made of strokecenter.org and the Virtual International Stroke Trials Archive. Two of the three reviewers screened each title and abstracts independently (GH plus one of two fellows). The same reviewers independently reviewed the full texts of all potentially relevant studies and those included were agreed by consensus (Figure 2.1).

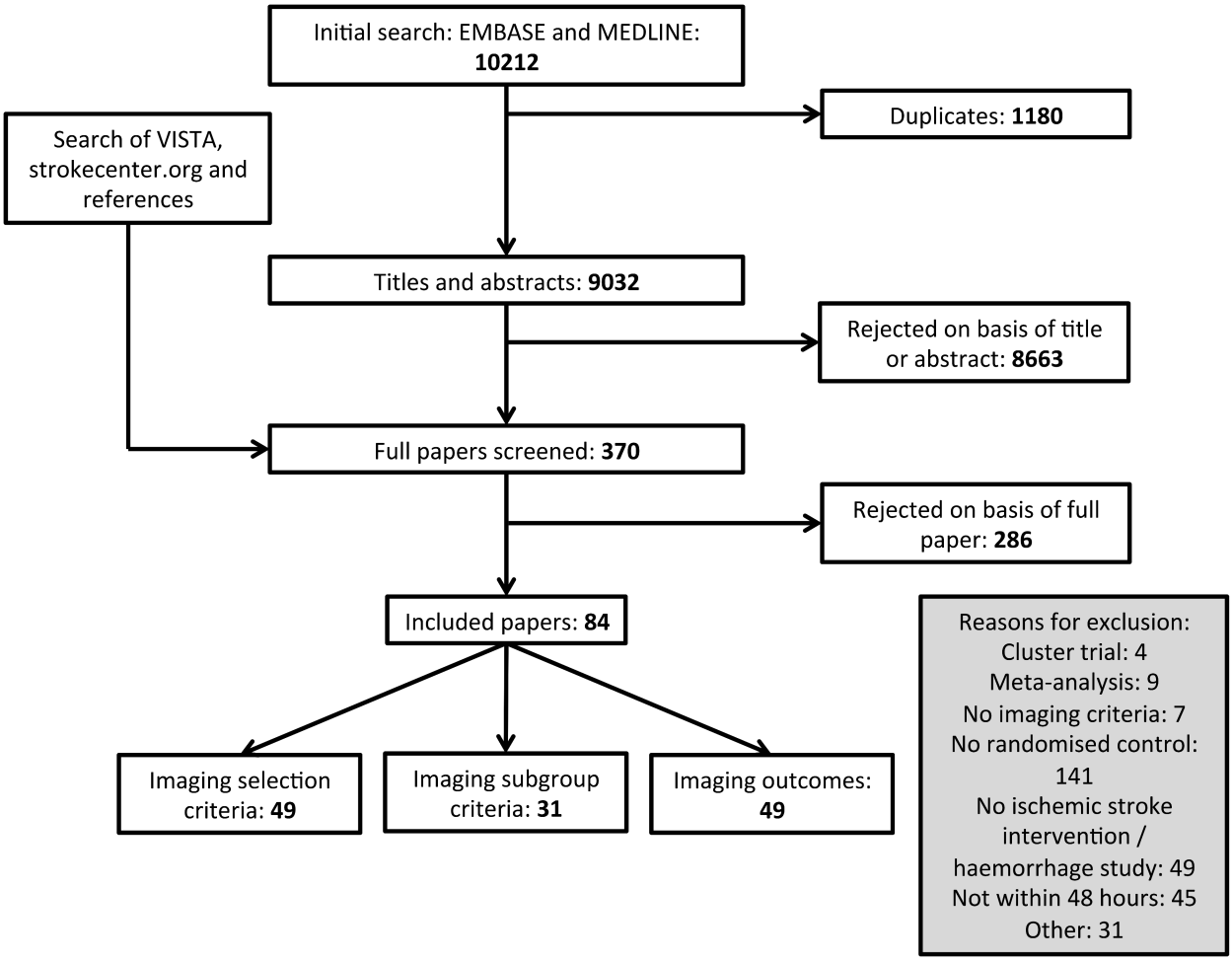

Figure 2. 1 – Schema of systematic review

2.3. ***Data extraction***

Data extracted included year, number of patients enrolled, details of the imaging biomarker, and the result of the trial. The imaging biomarkers were classified into the groups identified in the Acute Stroke Imaging Research Roadmap II with particular attention to TRAITs.[58] The purpose for which each biomarker was used (trial eligibility, outcome measure, or subgroup analyses (preplanned or *post hoc*)) was recorded.

3. Results

3.1. *Search Results*

The electronic search yielded 10,212 titles of which 1180 were duplicates. Screening of the remaining studies and additional manual searching produced 370 to be appraised. 286 were excluded following review of the paper, leaving 84 to be included in the final analysis (Figure 2.1, Appendix B). Eight groups of imaging biomarkers were identified: infarct volume; oedema; diagnosis/ territory of infarction; vessel status; ischaemic penumbra; perfusion status; collaterals; and, composite/ other (Table 2.1).[58] 49 studies used imaging for trial eligibility, 49 studies used one or more imaging outcome (e.g. infarct volume or recanalization rate etc.), and 31 studies used imaging criteria to define one or more subgroup (e.g. stratification by infarct volume). 85 different imaging-defined subgroups were identified in these 31 studies, 17 of which were preplanned and the remaining 68 subgroups defined *post hoc*.

	Trial eligibility	Outcome measure	Subgroup analysis
Infarct volume	29	62	34
Oedema	5	NA	0
Diagnosis / territory of infarction	9	NA	5
Vessel status	16	17	23
Ischaemic penumbra	10	7	22
Perfusion status only	2	27	1
Collaterals	0	0	2
Composite / other	0	4	2

Table 2. 1 – Use of imaging in stroke trials

3.2. *Imaging Biomarkers*

Infarct volume was extensively used as an exclusion criterion from trial recruitment and subgroup eligibility assessment (Table 2.1). The most consistent definition used was an

infarct volume on non-contrast CT scan of greater than one third of the MCA territory (16/29 studies) (Appendix C). Other definitions used ranged from any evidence of ischaemia on non-contrast CT to greater than two thirds of the MCA territory demonstrating restricted diffusion on DWI. One trial of hemicraniectomy for malignant MCA syndrome excluded patients with an infarct volume less than a predefined level (145ml on DWI).[101]

Imaging of infarction was used in a variety of other ways to establish trial eligibility: DWI to confirm diagnosis prior to enrolment; the presence of oedema on CT to exclude patients; and, location of infarction within a specific vascular territory for either inclusion or exclusion (Appendix C).

Vessel occlusion identified using angiography (computed tomography angiography, CTA, magnetic resonance angiography, MRA, or digital subtraction angiography, DSA), and TCD was commonly identified prior to enrollment in a trial. Of the 16 trials that selected according to vessel occlusion status, 12 used imaging to identify a target for the intervention and the remaining 4 excluded patients with carotid occlusions on the basis of futility of intervention (Appendix C).

Perfusion deficit alone was used in only 2 studies to select patients for inclusion (Table 2.1), whereas 13 studies used reperfusion as an outcome criterion in 27 different efficacy analyses. There was considerable heterogeneity in the timing of timing of assessment of reperfusion (4 hours to 3 months), which was made using a variety of modalities (magnetic resonance perfusion, MRP, computed tomography perfusion, CTP, SPECT) (Appendix D).

Author	Intervention	No. of participants	Criterion	Inclusion or subgroup	Pre-planned
Hacke (2005)	Desmoteplase	104	20% PWI/DWI mismatch and PWI lesion >2ml involving grey matter (MTT/TTP)	Inclusion	Y
Singhal (2005)	Normobaric oxygen	16	20% PWI/DWI mismatch (MTT)	Inclusion	Y
Els (2006)	Hypothermia (HC patients)	25	DWI and PWI >2/3 hemisphere, no mismatch, (PWI modality not specified)	Inclusion	Y
Furlan (2006)	Desmoteplase	37	20% PWI/DWI mismatch and PWI lesion >2cm diameter and involving cortex (MTT)	Inclusion	Y
Davis (2008)	Alteplase	80	20% PWI/DWI mismatch and PWI lesion-DWI lesion >10ml (Tmax+2s)	Subgroup	Y
Hacke (2009)	Desmoteplase	193	20% PWI/"core" mismatch (CT or MRI)	Inclusion	Y
Kidwell (2009)	Magnesium	44	20% PWI/DWI mismatch (Tmax+2s)	Subgroup	N
		40	20% PWI/DWI mismatch (Tmax+2s) and DWI >3ml	Subgroup	N
Parsons (2010)	Alteplase	85	20% PWI/DWI mismatch (Tmax+2s)	Subgroup	N
		37	PWI lesion <190ml, DWI lesion <25ml (Tmax+2s)	Subgroup	N
		30	PWI lesion 20-190ml, DWI lesion <25ml (Tmax+2s)	Subgroup	N
		31	PWI lesion <190ml, DWI lesion <18ml (Tmax+2s)	Subgroup	N
		24	PWI lesion 20-190ml, DWI lesion <18ml (Tmax+2s)	Subgroup	N
		65	20% PWI/DWI mismatch (Tmax+2s), ICA occlusion excluded	Subgroup	N
		40	PWI lesion >20ml, DWI lesion <25ml (Tmax+2s), ICA occlusion excluded	Subgroup	N
		32	PWI lesion >20ml, DWI lesion <18ml (Tmax+2s)	Subgroup	N
		62	20% PWI/DWI mismatch (Tmax+8s)	Subgroup	N
		52	PWI lesion <150ml, DWI lesion <25ml (Tmax+8s)	Subgroup	N
		40	PWI lesion 10-150ml, DWI lesion <25ml (Tmax+8s)	Subgroup	N
		43	PWI lesion <150ml, DWI lesion <18ml (Tmax+8s)	Subgroup	N
		33	PWI lesion 10-150ml, DWI lesion <18ml (Tmax+8s)	Subgroup	N
Schabitz (2010)	Granulocyte-colony stimulating factor	44	PWI/DWI mismatch, any size (PWI unspecified)	Inclusion	Y
Bi (2011)	Hypothermia	93	20% PWI/DWI mismatch (TTP/MTT)	Inclusion	Y
Michel (2012)	Alteplase	6	Favorable CTP profile	Inclusion	Y
Nagakane (2011)	Alteplase	80	20% PWI/DWI mismatch and PWI lesion-DWI lesion >10ml (Tmax+2s, co-registered)	Subgroup	N
Nagakane (2012)	Alteplase	62	20% predicted infarct volume/DWI mismatch	Subgroup	N
Parsons (2012)	Tenecteplase	75	20% PWI/CT mismatch and >20ml mismatch volume (CT MTT)	Inclusion	Y
Warach (2012)	Desmoteplase	66	PWI/"core" mismatch >60ml (CT or MRI)	Subgroup	N
Kidwell (2013)	Embolectomy	68	"Core"/PWI <70% and "core" less than 90ml (CT or MRI)	Subgroup	Y

Table 2. 2 - Studies using imaging to define ischaemic penumbra as an inclusion criterion for a trial or subgroup. PWI: perfusion weighted imaging; DWI diffusion weighted imaging; MTT: mean transit time; TTP: time-to-peak; T_{max}: time to maximum

Identification of the ischaemic penumbra, as either a means of patient selection or outcome assessment was common (Table 2.1). Table 2.2 demonstrates the variety of ways in which penumbra has been defined. All but one study defined penumbra using MRP measures, such as mean transit time or Tmax, to identify hypoperfused tissue that extended beyond the DWI lesion, and most used a threshold of 20% penumbra-core volume mismatch to select patients. No RCT using MRP has resulted in a positive outcome. However, the 20% penumbra-core threshold was used with success in an evaluation of tenecteplase using CTP (Table 2.2).[60] In addition to trials of reperfusion therapies, several neuroprotective trials also used penumbral imaging for inclusion.

3.3. ***Subgroup analyses***

The comparison of the results of studies with preplanned imaging-defined subgroups or imaging-based outcomes compared with *post hoc* analyses can be seen in Table 2.3. There are significantly more positive results in studies using *post hoc* analyses. For instance, no preplanned subgroup analysis of mismatch eligibility criteria has demonstrated a positive effect of what otherwise had been a null trial by primary analysis, whereas, two *post hoc* defined subgroup analyses have demonstrated a positive effect (Table 2.2): those patients with very large perfusion deficits and small DWI lesions;[102] and, patients with a 20% mismatch profile only once images were properly co-registered.[103] More generally, the definitions used for subgroup selection were less consistent than those used for trial eligibility criteria (Appendix E). Using the example of quantification of cerebral infarction, subgroup definitions ranged from strata of absolute volumes to scoring systems such as the Alberta Stroke Programme Early CT score.[104]

		Preplanned	*Post hoc*	P-value
Inclusion/exclusion	**Subgroup studies**	3/17	28/68	
	RCTs	10/49		
	Total	13/66	28/68	0.009*
Outcome		13/84	19/42	0.0005*

Table 2. 3 - Proportion of analyses showing a positive outcome using imaging biomarkers for inclusion/exclusion or outcome assessment. *Fisher exact test

4. Discussion

This review reinforces the frameworks outlined in the Acute Stroke Imaging Research Roadmap II.[58] It identifies groupings of imaging biomarkers that have been used across RCTs reflecting the individual needs of those trials. However, there is marked heterogeneity in the definition of these imaging biomarkers between trials with a large number of *post hoc* subgroup analyses exploring further imaging biomarker definitions. No strategy to select patient using imaging biomarkers has been used consistently with success in stroke RCTs.

4.1. *Purpose of imaging biomarkers in RCTs*

In general terms, the use of imaging biomarkers is intended to produce a more homogenous population within a trial with the hope of limiting patient selection to those for whom the intervention is most likely to be of benefit. This should allow smaller trials to be conducted over shorter periods of time. Eight groupings of imaging biomarkers used in acute stroke trials were identified: infarct volume; oedema; diagnosis/ territory of infarction; vessel status; ischaemic penumbra; perfusion status; collaterals; and, composite/ other. All were used to assess trial eligibility, outcome assessment or for subgroup analysis.

4.2. *Defining infarction*

Tissue infarction was commonly defined at presentation using either hypodensity on CT or by restricted diffusion on DWI, inferred from hyperintensity on a trace DWI. Despite the potential for objective automated definition of infarcted tissue,[105] ADC values have not been used routinely for this purpose. When imaging biomarkers were used prospectively to enroll patients, visual inspection at a workstation was the norm, despite the low interrater reliability described when using this approach.[106]

One-third MCA territory as a threshold on non-contrast CT was the most consistent imaging biomarker used for trial eligibility. This criterion was adopted by the ECASS group of studies following the findings of a single-centre observational cohort study that suggested extensive ischaemic change on CT predicts an increased chance of a fatal clinical outcome.[107] However, retrospective analysis of the randomized data from the NINDS trial showed that while 14% of patients randomized had greater than 1/3 MCA territory affected by early ischaemic change, the presence of this change on the pre-treatment scan was not a treatment modifier, nor did it predict increased risk of harm from intervention when patients are treated within 3 hours of onset.[108]

There was less consistency of imaging biomarkers when infarct volume has been used to assess outcome. Timing of measurements, modality used and measurement technique were all highly variable between trials. Infarction has been defined by CT, DWI, or T2-weighted MRI, over a range of times from 4 hours to 90 days. Measurement of efficacy has generally been by measurement of total infarct volume or change in volume over time. Coregistration to define tissue level change has been infrequent and details of registration techniques have not been not provided.[109] Interestingly, when coregistration

has been used *post hoc* it has transformed null trials into positive analyses of efficacy.[103, 110]

4.3. ***Defining tissue at risk***

Tissue at risk was defined by the difference between a presenting perfusion deficit and either a DWI lesion or CT hypodensity. 20% has commonly been used as the visually determined mismatch threshold for enrolment, (this threshold is not justified by the studies in this review and appears arbitrarily determined), and within this a variety of parameters have been used to define the perfusion deficit. For example, within studies that used DSC-MRI perfusion, T_{max}, MTT and TTP have all been used. Even within single studies, different definitions of the perfusion deficit have been used.

Importantly, no study used electrophysiological or metabolic biomarkers to define penumbral tissue. As discussed in Chapter 1, it was a combination of electrophysiology, metabolism, and cerebral blood flow that were originally used to define the ischaemic penumbra.[18, 22, 26-28] This omission reflects the difficulty in measuring electrophysiology and metabolism in acute stroke patients and so perfusion measures alone have been used as surrogates. However, this may explain the failure of imaging biomarkers to consistently select patients for intervention and highlights the need for improved biomarkers that measure metabolic or electrophysiological properties.

4.4. ***Inconsistency of measurement***

The impact of the inconsistent measurement of imaging biomarkers is important and this exemplified by when using infarct volume as an outcome assessment. Oedema and atrophy impact on infarct volume at different times, so assessment of infarction will be dependent on the timing of imaging following onset.[111] Within the same patients, the blinded adjudication of FLAIR and T2 images by neuroradiologists results in different

infarct volume estimates and discrepant interrater agreements.[112] The reliability and repeatability of a biomarker in defining a pathological process will be affected by the contrast-to-noise ratio afforded by the imaging modality.[113] For example, DWI has a greater contrast-to-noise ratio than T2-weighted MRI, CT, and CTP, allowing clearer definition of the extent of a lesion,[113, 114] thus reducing measurement error and improving interrater agreement.[59] Even where there is excellent interrater agreement between neuroradiologists, substantial measurement errors can still exist that affect sample size calculations for a RCT, particularly where the infarct volumes are small or moderate.[115] Automated approaches to volume measurement offer the prospect of limiting human measurement error, but introduce challenges of their own in the accommodation of thresholds that vary between individuals and which are also influenced by timing from stroke onset.[115]

4.5. ***Relationships with patient outcomes***

The relationship between patients, imaging biomarkers, treatments, and eventual clinical outcomes is complex. Failure to accurately understand these relationships and, thus, selecting an inappropriate biomarker has contributed to the criticisms of recent RCTs. Defining a treatment responsive group using an imaging biomarker is a different task to selecting those who are destined to do well independent of treatment, as was seen in MR-RESCUE.[116, 117] The only positive RCT of intravenous thrombolysis used within three hours of stroke onset is not included in this review because patients were not excluded by infarct volume criterion,[118] and as described above *post hoc* analysis demonstrated that infarct volume was not a treatment modifier within three hours.[108] The existence of an optimum threshold of infarct volume used to exclude patients from trial enrolment remains unclear.[102, 119]

Several prospective observational studies have explored various thresholds of the ischaemic core volume to select patients for endovascular therapy (e.g. DEFUSE-2 used a threshold of greater than 70ml on DWI to exclude patients).[119-122] These data suggest that patients selected using lower infarct volume thresholds than used previously have a greater capacity to benefit from endovascular treatment. However, this approach from observational studies now needs to be translated into RCTs.

Expected treatment effects on a biomarker used as an imaging outcome and its relationship with clinical outcomes also need to be understood when designing a RCT. For example, the recanalization rate with intravenous tPA in the IMS-3 trial was twice what was predicted and the highly significant increase in revascularization was not associated with improvement in clinical outcomes.[123]

4.6. ***Stratification and subgroups***

The Acute Stroke Imaging Research Roadmap II outlines a framework for use within a RCT advocating the use of a consistent TRAIT within all arms. This would allow secondary analyses to address the additional value of imaging while the primary focus remains on the therapeutic intervention. This is an area that deserves further methodological consideration. This Chapter highlights the large number subgroup analyses, typically *post hoc*, performed utilizing data from the RCTs. An excess of positive *post hoc* subgroup analyses was found, suggesting that any apparently useful subgroups should be viewed with caution given the risk of publication bias.[53, 54] This may give a false sense of promise from apparently successful *post hoc* attempts to stratify patients, meaning that these positive results should only be used for hypothesis generation. Validation in separate patient research cohorts is required before widespread clinical adoption.[124]

4.7. *Meta-analysis and sample size*

Successful meta-analyses of pooled data from RCTs of intravenous thrombolysis and hemicraniectomy have contributed to their wide adoption into national stroke clinical guidelines and practice.[116, 117] The inconsistent use of imaging biomarkers highlighted in this review, markedly hampers such meta-analyses. For instance, it would be inappropriate to combine cohorts in whom mismatch was defined using different modalities and thresholds. It is equally challenging to interpret results from individual studies where different imaging modalities are used to define enrollment criteria, for instance MR-RESCUE used either MRI or CT to assess the favorability of penumbral pattern.[116] The advantage of this approach is to maximize the number of sites that may take part in a RCT hopefully reducing study duration and broadening the generalizability of the results. However, unless the equivalence of the biomarkers is robustly established then the reliability of data interpretation is potentially compromised. The Acute Stroke Imaging Research Roadmap II begins to address these difficulties with the example of the clarification of revascularization status and associated concepts.[58, 125]

4.8. *Biomarker development*

There remains an unmet need for a robust pathway for stroke imaging biomarker development from pre-clinical studies through translational and observational studies ready for utilization in RCTs and clinical settings. This pathway needs to accommodate the fact that the imaging that drives scientific discovery may or may not be available for clinical use in acute stroke. For example, diffusion MRI is a widely used and validated method for identifying core infarct in animal model studies, and has been used in several RCTs. On the other hand perfusion CT has almost no preclinical validation, but is commonly employed in RCTs. The relationship between how and if different imaging

modalities measure the same pathophysiology must be established. Existing initiatives developed from expert consensus may expedite this process and ensure a more homogenous use of biomarkers in RCTs.[50, 126]

5. Conclusions

In this Chapter the practice of using of imaging biomarkers in RCTs has been explored. There is a heterogeneity, and by implication a lack of consensus, in the definition of presenting and final infarction, and tissue at risk. In addition, no study uses biomarkers other than perfusion to define penumbral tissue, in contrast to the electrophysiological and metabolic biomarkers that were originally used to define penumbra. Using imaging to select patients for treatment has not translated into clinical practice and the only treatment modifier for reperfusion therapies identified to date is time from onset to intervention.[4, 55, 118] Assessing efficacy using imaging is done in a variety of ways with little attention to methodological consideration such as coregistration and automation of definition. Imaging biomarkers offer the opportunity to refine the trial cohort by minimizing participant variation, to decrease sample size and to personalize treatment approaches for those who stand to benefit most. However, within imaging modalities there has been little consistency between stroke trials. Greater efforts to use consistent imaging biomarkers, which are biologically understood and prospectively validated, should help improve the development of novel treatment strategies in acute stroke and improve comparison between studies.

Chapter 3: General Methods

1. Overview

The Acute Magnetic Resonance Imaging in Cerebral Ischaemia (AMICI) feasibility study was a year long observational cohort study designed to test the feasibility of recruiting patients with acute ischaemic stroke into a MRI-based imaging study at the John Radcliffe Hospital site. The results of the feasibility study informed the design of the AMICI cohort study. Both studies acquired imaging serially over the first month from stroke onset. The data in this thesis is from both the feasibility study and the first year of the cohort study. The imaging time points were the same for both studies, but in the cohort study patients could be recruited beyond 6 hours up to 24 hours. Imaging was "front-loaded" to capture the early dynamics of cerebral injury.

1.1. *Ethical approval*

Ethical approval for the AMICI feasibility and cohort studies was given by the National Research Ethics Service Committee South Central (Oxford C) under references 12/SC/0292 and 13/SC/0362.

2. Study participants

Participants were recruited from patients admitted to the John Radcliffe Hospital with ischaemic stroke between August 2012 and May 2014. Recruitment was considered for all patients who met the study criteria and who could be scanned in the operating hours of the Oxford Acute Vascular Imaging Centre (Monday to Friday, 8am until 5pm).

Inclusion criteria were as follows:

- Clinical diagnosis of stroke within 6 hours (feasibility study) or 24 hours (cohort study) of symptom onset;

- Patient or representative able to give a clear medical history and participate in the consent process;
- Age over 18.

Patients with contraindication to MRI, or severely impaired conscious level (score greater than 1 on question 1a of the National Institute for Health Stroke Scale (NIHSS)) were excluded. Patients with intracranial haemorrhage on CT or MRI at presentation were recruited into the AMICI cohort study, but the data are not included in this thesis.

3. Study procedures

A flow diagram of the study procedures is detailed in Figure 3.1. Patients were identified and screened either in the Emergency Department or on the Stroke Unit once the clinical team had assessed whether the patient or their family was agreeable to being approached by a member of the research team. Clinically indicated imaging and treatments were initiated prior to research scanning. Non-contrast CT was the standard imaging modality used by the clinical stroke service. Neither CT angiography nor MRI scanning was routinely available to the clinical team. Within 6 hours of symptom onset the patients were admitted to the Recovery Area in AVIC directly from the Emergency Department. Having completed pre-MRI safety checks the patient underwent the first research MRI as soon as possible. The second MRI scan was performed after 2 hours if time was available. Once, the second MRI was complete the patient was transferred to the Acute Stroke Unit to continue routine clinical care.

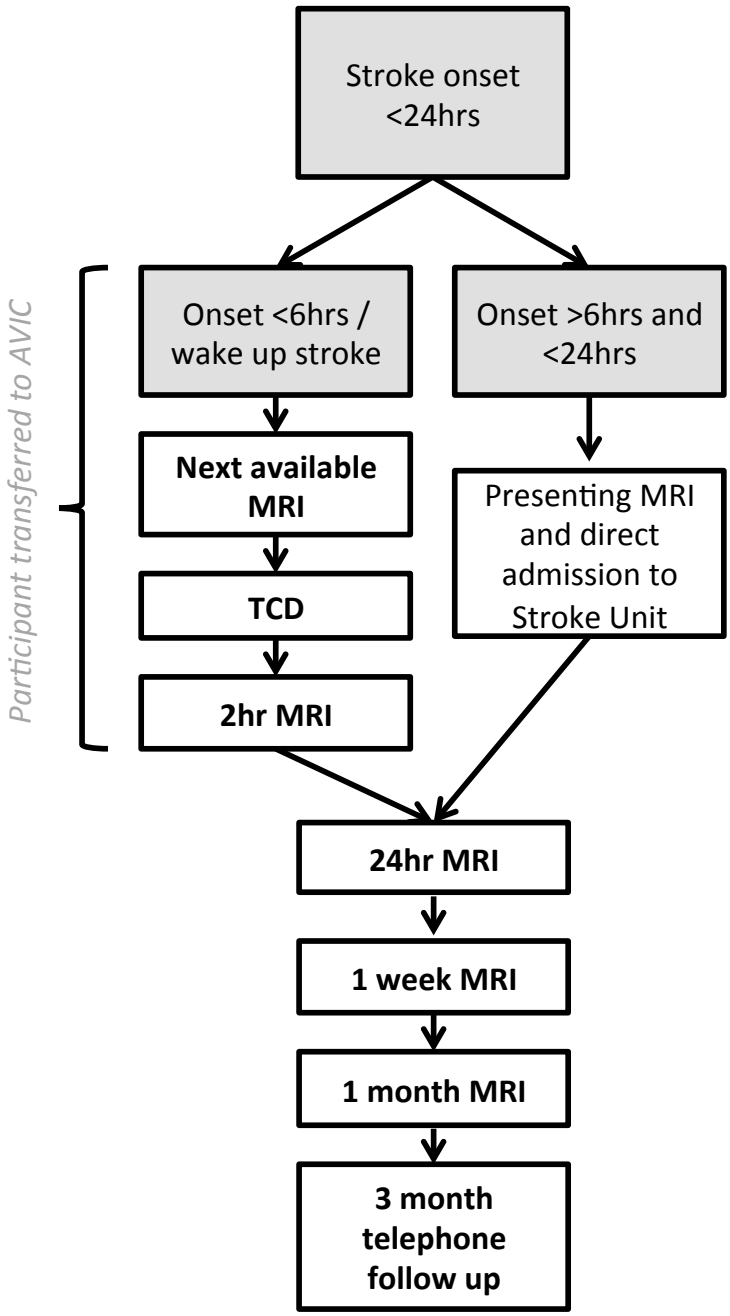

Figure 3. 1 – Patient flow as part of the AMICI study. Note that for the AMICI feasibility study patients were only recruited within 6 hours of symptom onset.

Patients presenting within 24 hours underwent a similar pathway to those presenting within 6 hours, but assessments did not include a 2 hour scan. If the presenting MRI

was later than 18 hours from symptom onset this was categorized as the 24 hour scan. The recruitment window was extended from 6 to 24 hours following the feasibility study because it became clear that even at 24 hours useful observations of blood flow and pH-weighted imaging were being made. This also increased the number of patients eligible for recruitment.

Further MRI scanning was performed at 24 hours (18-36 hours), at 1 week (3-7 days) and at 1 month (21-42 days). Transport arrangements were made from home or community hospitals to acquire follow up imaging whenever the patient or consultee agreed to this.

Demographic data were collected at presentation. Clinical assessments were made at each scan time point. These included blood pressure, oxygen saturations and NIHSS. Patients were followed up by telephone assessment at 3 months. This consisted of a short conversation to establish the modified Rankin scale (mRS).[127] For the purpose of this thesis analyses have been limited to tissue based data from imaging. This is justified by the number of patients and the effect that single outliers can have on small subgroups defined by clinical criteria. For correlations of imaging biomarkers with clinical outcomes larger cohorts are required.

3.1. *Consent*

The use of a consent waiver in this study was not possible due to the need for a reliable medical history to screen for MRI safety. For this reason a verbal consent process was developed, which minimized the time to research MRI. A contemporaneous, witnessed, written record was kept and written consent was gained when time allowed. For those without capacity, a Personal Consultee was contacted to advise about recruiting the patient and to ensure that no contraindication to MRI existed. This bespoke approach to

informed consent was piloted in the AMICI FS to optimize time to imaging and was used without significant modification in the AMICI cohort study.[128]

4. Imaging

4.1. *Patient imaging time points*

Imaging time points were defined as follows:

- Presenting imaging: the first MRI performed within 18 hours of symptom onset.
- Acute imaging: a subgroup of the presenting MRIs performed within 6 hours of symptom onset. If thrombolysis was indicated the initial MRI occurred during the infusion of tPA.
- 2 hour imaging: a second MRI performed 1-3 hours following acute imaging.
- 24 hour imaging: MRI performed between 18 and 36 hours from stroke onset.*
- 1 week imaging: MRI performed between 3 and 7 days after stroke onset.*
- 1 month imaging: MRI performed between 21 and 42 days after stroke onset.*

*where imaging could not be acquired between these time points later or earlier times were used to maximize data capture.

4.2. *Imaging protocols*

All scans were acquired using the 3.0T Siemens Verio scanner in the Acute Vascular Imaging Centre, University of Oxford, using a 32-channel head coil. Total duration of scanning at each time point was 25 (feasibility study) or 30 minutes (cohort study). Depending on the volume and location of the presenting lesion visualized on DWI, one of two imaging protocols for ischaemic stroke was selected: lacunar (<15mm in axial diameter and subcortical) or large volume.

For both protocols standard imaging was acquired at every time point:

- DWI (3 directions, 1.8×1.8×2.0mm, FoV=240mm, 4 averages, b=0 and 1000s/mm^2 TR=9000ms, TE=98ms);
- T1-weighted structural imaging (MPRAGE, 1.8×1.8×1.0mm, FoV=228mm, TR=2040ms, TE=4.55ms);
- Gradient and magnitude fieldmaps (3.0×3.0×5.0mm, FoV = 240mm, TR = 488ms, TE = 5.19ms and 7.65ms);
- T2-weighted turbo spin echo fluid attenuated inversion recovery sequence (FLAIR) (1.9×1.9×2.0mm, FoV=240mm, TR=9000ms, TE=96ms) at 1 week and 1 month time points; and
- Short, low resolution planning sequences including localizing scans to plan the main imaging sequences and time of flight imaging of the feeding arteries in the neck used to plan the perfusion sequence.

In addition, patients imaged using the large volume protocol had VEPCASL perfusion images acquired, and a single slice CEST sequence localized to the DWI lesion. Specific details of the VEPCASL and CEST preparation and acquisition protocols are detailed in Chapters 5 and 6 respectively. Vascular imaging was not routinely collected as part of the research protocol because of the time required to perform the other imaging sequences. In addition, the need to give contrast would have excluded some patients and limited the sample size.

The lacunar imaging protocol, in addition to the core sequences above, acquired a 12-direction diffusion tensor image and either a high resolution ASL perfusion sequence or blood oxygen level dependent (BOLD) imaging for functional MRI assessment. These lacunar-specific sequences will not be discussed further.

4.3. *Image processing*

All image analysis was performed using FSL (Oxford Centre for Functional MRI of the Brain Software Library), in-house UNIX shell scripts, and MATLAB 7.14 software (The Mathworks Inc.).[129-131] Details of the specific image processing and analysis are outlined in the relevant Chapters.

All analysis, other than postprocessing of the conventional imaging modalities, was performed off line and did not influence patient management. Standard imaging sequences (T1- and T2-weighted imaging, and DWI) were made available to the clinical team and were reported by a consultant neuroradiologist.

4.4. *Regions of interest*

4.4.1. *Patients*

Binary infarct definitions and perfusion deficits were created in the native image space. Masks were registered to the required image space for analysis before thresholding at 0.5 to minimize registration-induced error (see Chapter 4 for details of registration techniques used). The following regions of interest (ROIs) for patients were used in every Chapter.

- *ADC lesion*: within the automatically generated region of restricted diffusion defined on the presenting scan, using an ADC threshold of 620 $x10^{-6}mm^2/s$;[105]
- *Ischaemic core*: within the presenting ADC lesion and also within the final infarct;
- *Infarct growth*: within the final infarct and not within the presenting ADC lesion; *early infarct growth*: infarct growth up to 24 hours; *late infarct growth*: infarct growth beyond 24 hours;

Additional ROIs specific to each Chapter are outlined in the respective Methods sections. Contralateral ROIs were created by non-linear registration of the masks to standard MNI152 space,[132] reflection in the sagittal plane, and returning to structural image space.

4.4.2. *Healthy volunteers*

ROIs for use in the healthy volunteers were generated from the Harvard-Oxford Atlas.[132] Six regions were selected on the basis of their distribution throughout the brain (precentral gyrus, postcentral gyrus, insular cortex, middle temporal gyrus, lateral occipital cortex, paracingulate gyrus). The ROIs were non-linearly coregistered to the structural image at each scan time using a rigid body and then non-linear registration technique.[131, 133, 134] before the required coregistration described in each Chapter. The masks were thresholded at 0.5 and binarized for data extraction.

5. Recruitment results

5.1. *Summary details*

54 patients were recruited between August 2012 and May 2014, of which 50 had an ischaemic stroke. One patient was excluded from all analyses because the presenting scan was aborted within minutes of starting. Of the remaining 49, 32 underwent the large volume protocol and 17 received the lacunar imaging protocol. Summary demographic are presented in Table 3.1 and are comparable to other imaging-based acute stroke studies.[110, 116, 119] Data for individual patients is presented in Table 3.2.

5.2. *Recruitment rate*

Approximately 700 patients with stroke are admitted to the John Radcliffe hospital each year. Recruitment occurred only when acute MRI scanning was available during

working hours (8am-3.30pm). Recruitment was not possible at the weekend or on public holidays, during scanner service and repair, and when a radiographer or clinical research fellow was not available. Over the first 6 months of the feasibility study the scanner was operational on 44% of days.

Following the completion of the feasibility study recruitment rates were analysed. 73 patients whose symptom onset was within 6 hours were screened. 44 of 73 screened patients met the study inclusion criteria and 24 were recruited. Consultees were required for 9 participants. Reasons for non-recruitment can be seen in Figure 3.2: one patient did not have a contactable consultee, one patient and one consultee declined participation, and the majority of reasons were due to patient related factors.

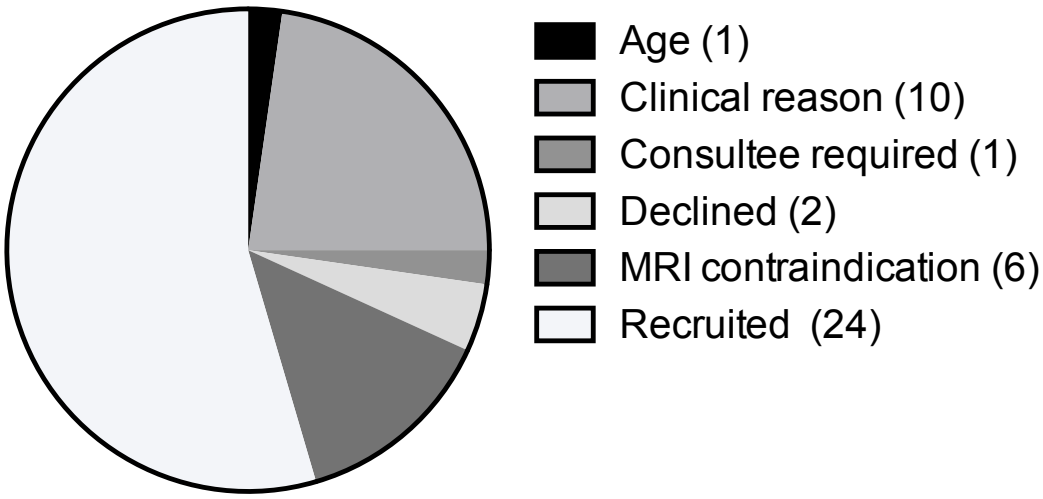

Figure 3.2 - Reasons fro non-recruitment in the AMICI feasibility study

	All patients	Large volume protocol	Large volume protocol (acute)
Number	49	32	25
Mean age (SD), yrs	72.6 (15.2)	74.3 (15.2)	76.1 (15.6)
Female sex, %	49	59	64
Thrombolysed, %	35	44	48
Prior stroke / TIA, %	26	32	37
Hypertension, %	50	54	53
Diabetes mellitus, %	17	16	17
Atrial fibrillation, %	30	38	47
Cigarette smoker (current), %	20	12	11
Median NIHSS (IQR)	7 (12)	10.5 (16.5)	13 (15)
Median ED to MRI (IQR), h:mm	1:35 (2:47)	1:35 (3:30)	1:24 (0:35)
Median onset to MRI (IQR), h:mm	3:22 (3:18)	3:04 (2:03)	2:48 (1:05)
Median presenting ADC lesion volume (IQR), ml	1.7 (10.4)	5.7 (23.1)	4.8 (26.2)

Table 3. 1 – Summary demographic data. SD = standard deviation, TIA = transient ischaemic attack, IQR = interquartile range.

Patient	Stroke syndrome	Scan protocol	Hemisphere	Sex	Age	Presenting NIHSS	Thrombolysis	Time to presenting scan
1	LACS	Lac	L	M	78	1	N	02:41
2	LACS	Lac	R	M	74	2	N	05:00
3	LACS	LV	L	F	84	3	N	03:25
4	TACS	LV	L	M	92	25	Y	02:50
5	PACS	LV	R	M	64	3	N	01:41
6	LACS	Lac	R	F	51	4	N	03:58
7	TACS	LV	L	F	86	27	N	03:09
8	LACS	Lac	L	M	40	0	N	04:05
9	TACS	LV	L	F	88	25	N	02:15
10	TACS	LV	R	F	94	15	N	03:20
11	POCS	Lac	R	F	79	2	N	07:05
12	TACS	LV	R	F	70	19	Y	02:20
13	TACS	LV	L	F	81	21	N	03:25
14	POCS	Lac	L	M	35	7	Y	03:15
15	PACS	LV	R	M	50	6	Y	03:49
16	PACS	LV	L	M	95	19	Y	04:14
17	PACS	LV	L	F	91	10	N	04:53
18	TACS	LV	L	F	53	13	Y	02:48
19	LACS	LV	R	M	57	7	N	01:43
20	PACS	LV	R	M	86	2	N	01:46
21	PACS	LV	L	M	49	1	N	04:25
23	TACS	LV	R	F	92	25	N	02:32
24	LACS	Lac	R	M	79	2	N	03:33
25	TACS	LV	L	F	68	23	Y	01:00
27	TACS	LV	R	F	80	14	Y	09:50
29	PACS	Lac	R	M	73	3	N	ND
30	POCS	LV	L	M	80	3	N	11:06
31	PACS	LV	L	M	54	0	N	02:40
32	LACS	Lac	R	M	66	4	Y	03:06
33	PACS	LV	L	F	76	10	Y	02:40
34	PACS	LV	L	F	78	9	Y	02:50
35	POCS	LV	R	F	66	2	N	16:03
36	POCS	Lac	R	F	69	3	N	06:40
37	PACS	LV	L	F	56	7	Y	01:35

39	LACS	Lac	L	M	70	2	N	15:00
40	LACS	Lac	L	M	80	2	N	05:30
41	LACS	LV	L	M	71	8	Y	14:36
42	LACS	Lac	L	M	93	4	N	17:00
43	PACS	LV	L	M	48	3	N	16:10
44	TACS	LV	L	F	103	18	Y	03:10
45	PACS	LV	L	M	82	13	Y	03:00
47	LACS	Lac	R	M	78	4	N	05:45
48	LACS	Lac	R	M	81	2	N	02:08
49	LACS	Lac	L	F	62	7	Y	02:25
50	TACS	LV	L	F	76	25	Y	02:40
51	LACS	LV	L	F	76	11	N	11:25
52	PACS	LV	R	F	77	2	N	02:15
53	TACS	LV	L	M	56	24	N	06:45
54	LACS	Lac	R	F	72	9	N	06:45

Table 3. 2 - Individual patient details. LACS = lacunar stroke, TACS = total anterior circulation stroke, PACS = partial anterior circulation stroke, POCS = posterior circulation stroke, Lac = lacunar imaging protocol, LV = large volume imaging protocol.

5.3. *Healthy volunteer data*

Data from healthy volunteers used in Chapters 5 and 6 was acquired from 6 individuals working in the AMICI study. All experiments were performed under an agreed technical development protocol approved by the Oxford University Clinical Trials and Research Governance office. Median age was 34 years, range 30 to 43. Volunteers were scanned initially, and then 24 hours and 1 week later. T1-weighted structural images, fieldmap images protocols, planning sequences, plus 4 repeats of the VEPCASL and CEST sequences at each time point.

Chapter 4: Optimization Of Infarct Definition

1. Introduction

Robust definition of tissue outcome and the accurate registration of imaging are essential for the investigation of tissue fate following a stroke. Determining tissue fate is a requirement both for the validation of novel imaging modalities, and for early stage clinical trials using imaging biomarkers as a surrogate of clinical efficacy. In Chapter 2, the imaging outcomes relied predominantly on changes in total volumes, rather than coregistered data. Errors in infarct definition can have significant effects on study sample sizes and power calculations.[115] Additionally, the accurate assessment of tissue fate at serial time points would allow insight into the dynamics of pathophysiology of cerebral ischaemia in patients, thus improving the development of preclinical models. Such information may identify the reasons underlying the difficulties of successfully translating novel treatment approaches from preclinical to clinical trials.[135]

1.1. *Registration*

Without accurate coregistration, imaging analysis is limited to the use of total lesion volumes. Use of lesion volumes at a patient rather than tissue level to assess outcome means that the heterogeneity within the lesion can be overlooked and any changes underestimated.[111, 136] For example, concurrent lesion growth in one region and resolution in another would not be identified using total lesion volumes as there would be little net volume change. Coregistration allows for the heterogeneity of the infarct, a well described phenomenon preclinically, to be investigated at a tissue level.[32, 137] Coregistration is also required to objectively compare signals between imaging modalities, essential for development of novel imaging biomarkers.

The majority of stroke studies do not use coregistration of imaging to define tissue fate, or, if they do, do not routinely give any specific details regarding the registration methodology.[109] Those that do give details use a simple linear registration approach based on manual identification of landmarks and do not account for any structural changes over time due to oedema or atrophy.[103, 136] There is little methodological work aimed at determining the optimum strategy for defining infarction and coregistration, and this is limited to *post hoc* analysis of RCT data.[103]

Alternatives to linear registration strategies include: non-linear registration, which allows local deformations to align the anatomy of brains with different structures and is commonly used when registering to a standard space image;[131] boundary-based registration, which is widely used in functional MRI experiments to register EPI data to structural images;[138] and techniques that incorporate information about field inhomogeneity to correct for imaging distortions, also used in functional experiments.[131]

1.2. ***Infarct definition***

The Acute Stroke Imaging Roadmap II advocates the use of DWI or non-contrast CT acutely to define ischaemic core, although these two modalities do not appear to measure the same pathophysiology.[63, 64, 139] Restricted diffusion on DWI is thought to represent cytotoxic oedema and therefore irreversible cellular injury.[140, 141] There is debate about whether restricted diffusion is reversible or represents permanent injury. In a systematic review Kranz and Eastwood found the reported prevalence of diffusion lesion reversal varied from 0% to 83%.[142] Many of the studies included in this review suffer from flawed methodology: using absolute volumes to define lesion progression / reversal, not using coregistration, and using subacute outcome assessments without correcting for oedema. More recent studies using more objective methodologies have

questioned the significance of diffusion lesion reversal and whether such reversal is sustained.[111, 143]

An optimum ADC threshold for defining infarction of 620 $x10^{-6}mm^2/s$ has been defined in a small but homogeneous group of patients with proven revascularization in the DEFUSE study cohort.[105] The threshold had a high sensitivity and specificity for irreversible infarction, but has yet to be validated prospectively. The appeal of using ADC to define infarction is the potential to automatically define infarction consistently across imaging platforms, removing the problems of inter-rater disagreements.[144]

Despite the need for accurate and consistent definition of final tissue fate, there is no consensus on which imaging biomarkers should be used in stroke trials to assess final infarction or at what time points (Chapter 2). The Acute Stroke Imaging Roadmap II advocates that "24 hour DWI" (range of 18-36 hours) is used to define tissue outcome, although it does not expand on the choice of ADC or trace DWI images, the need for coregistration, methods of infarct delineation, or the correction of anatomical (e.g. oedema) or imaging (e.g. echo planar imaging) distortions.[58] The justification for using "24 hour DWI" is a study by Campbell *et al.* that compared manually defined infarct volumes at 24 hours on trace DWI with 90 day T2-weighted FLAIR.[59] Unsurprisingly the infarct volumes of lesions at 24 hours and 90 days correlated well, but they were not equal, and the 24 hour scan consistently underestimated the final infarct volume at day 90.

1.3. *Aims*

The aims of this Chapter are:

- To assess the optimum method of registering imaging between imaging time points, comparing non-linear and rigid body registration on the premise that a non-linear registration may correct for structural distortion due to subacute oedema;
- To assess the optimum method of registering EPI data within imaging time points, comparing boundary-based registration and correction for field map inhomogeneity with rigid body registration;
- To determine the strengths and limitations of different imaging outcome time points (24 hour trace DWI and ADC, and 1 week and 1 month T2-weighted FLAIR);
- To describe the relative frequencies of ischaemic core, infarct growth, and diffusion lesion reversal within the patient cohort;
- To determine the validity of $620\times10^{-6}mm^2/s$ as an ADC threshold of infarction and whether it can be used to objectively define infarction at presentation;
- To use the optimum infarct definition strategies to objectively investigate the dynamic properties of diffusion characteristics over time;
- To define the framework with which to investigate both perfusion and pH-weighted imaging in Chapters 5 and 6.

2. Methods

2.1. *Patients*

All patients with ischaemic stroke recruited into the AMICI study were considered for inclusion in this analysis. Patients were excluded if there was no index ischaemic lesion visible on any of the presenting or follow up scans.

2.2. *Infarct definition*

2.2.1. *Final infarction*

A neuroradiology fellow and a clinical research fellow (GH) independently outlined the index stroke lesions using the 24 hour, 1 week and 1 month datasets using the masking tool in FSLView.[131] At 24 hours the lesion was defined on the trace DWI ($b=1000s/mm^2$), and at 1 week and 1 month the lesion was outlined on the T2-weighted FLAIR image. Where the mean overlap agreement (see Section 2.5) between the assessors was less than 80%, a third rater, a consultant neuroradiologist, resolved discrepancies.

2.2.2. *Infarction defined by ADC within 24 hours*

ADC lesions at presenting and 24 hour time points were objectively defined using a threshold of 620 $x10^{-6}mm^2/s$ to create binary lesion masks at these time points.[105] A cluster-based analysis was performed on the thresholded mask of the ADC data. The maximum volume cluster was automatically identified and smoothed with a kernel of standard deviation 1mm, followed by repeat cluster analysis and automated selection of the maximum cluster volume.[145] This mask was then restricted to the original thresholded mask to minimize suprathreshold voxels included by smoothing. The

automated masks were inspected to ensure the cluster or clusters representing the acute infarct were correctly selected.

Once in the image space for analysis all masks were further masked using a coregistered tissue mask generated using the FSL automated segmentation tool on the structural T1-weighted image.[146] Mirrored contralateral lesion masks were created by reflection in standard (MNI152) image space.[147]

2.3. *Registration steps*

Comparisons of registration or masks at different time points were made in the presenting structural T1-weighted image space. Comparison of diffusion-weighted images and masks at the same time point were made in the native diffusion image space.

2.3.1. *Within time point registration*

Registration within each time point was achieved using either FMRIB's linear registration tool (FLIRT)[133, 134] or the *epi_reg* tool in FSL.[131] *epi_reg* and FLIRT were compared for registering of the trace DWI and ADC images to the structural T1-weighted images within scan time points. Only linear registration using FLIRT was used to register T2-weighted FLAIR images to the T1-weighted image as these sequences do not use EPI readout and hence do not suffer EPI distortions.

Linear registration was achieved using the rigid body (6 degrees of freedom) schedule available in FLIRT. The rigid body schedule maintains the structure of the brain applying 3 rotations and 3 translations to the source image to match the orientation and positioning of the target image. As the images are acquired at the same time there are no structural changes between image acquisitions (e.g. oedema). DWI was acquired using

an EPI readout that is susceptible to field map inhomogeneities and distorts the image, most noticeably in those regions close to the skull base. *epi_reg* uses BBR to identify changes in intensity over white matter boundaries to align EPI to structural images in addition to incorporating fieldmap information.[138]

2.3.2. ***Between time point registration***

Registration between time points was rigid body, using FLIRT (as described above), or non-linear, using FMRIB's non-linear registration tool (FNIRT). FNIRT generates a deformation warp that maps the voxel of one structural image onto another, according to the relative signal intensity and by inference the tissue type. The transformation matrix output from FLIRT and the warp-field coefficients from FNIRT were generated by registering the structural T1-weighted image at each scan time to the presenting T1-weighted image. For both tools an input weighting image of the lesion mask was used to prevent errors of registration due to T1-weighted signal change at the follow up time point. Subsequent registrations of images or masks between time points were performed by applying the transformation matrix or warp-field to the image or mask after it had been registered to the structural image at its own time point (Figure 4.1).

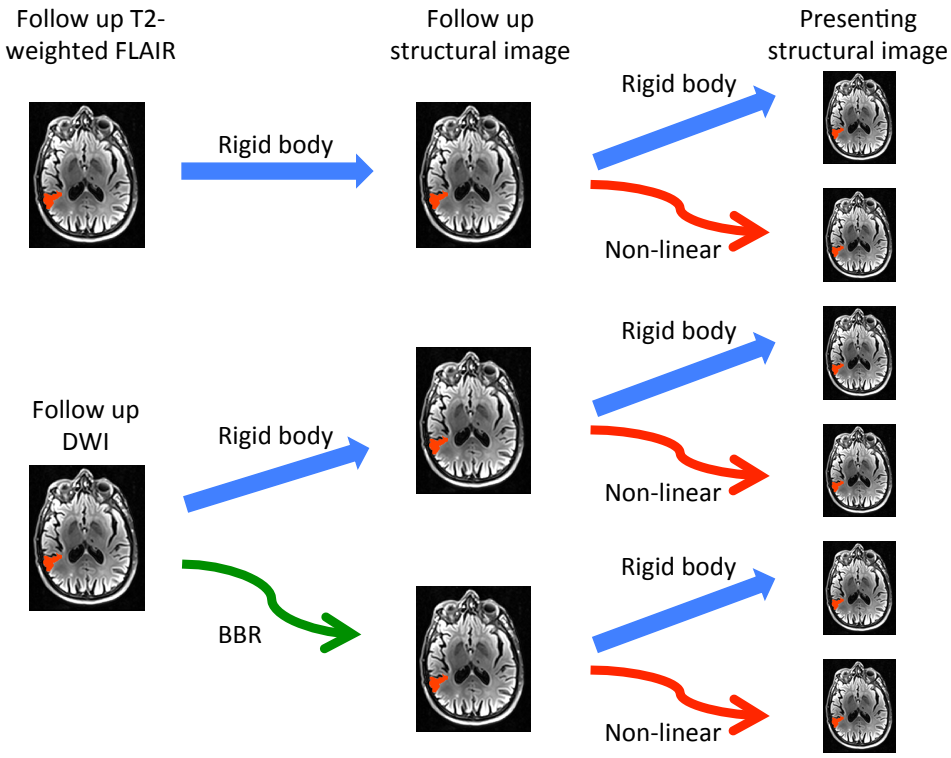

Figure 4. 1 Schematic representing the possible registration steps from the source image to the presenting structural image. DWI = diffusion-weighted imaging; BBR = boundary based registration

2.4. *Assessments of agreement*

Agreement of defined ROIs between and within time points was evaluated using volume overlap statistics. These were mean overlap (MO, also known as Dice coefficient) and union overlap (UO, also known as Jaccard coefficient) measures. False positive rate (FPR), false negative rate (FNR), and sensitivity (also known as target overlap) were calculated.[148, 149]

$$MO = \frac{2\times(S \cap T)}{T + S}$$

$$UO = \frac{S \cap T}{S \cup T}$$

$$FPR = \frac{S \setminus T}{S}$$

$$FNR = \frac{T \setminus S}{T}$$

$$Sensitivity = \frac{S \cap T}{T}$$

Where S is the source region being mapped onto the target region, T (Figure 4.2).

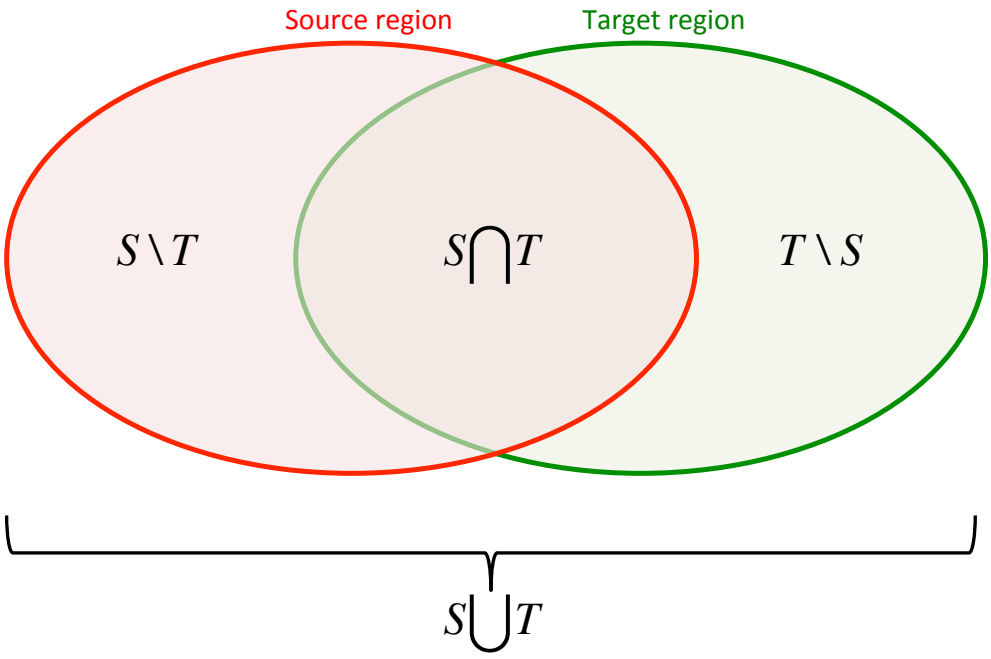

Figure 4. 2 - Schematic demonstrating the overlap regions used to calculate the volume overlap coefficients

2.5. *Contrast-to noise ratio*

Contrast-to-noise ratios (CNR) were calculated using the following formula:

$$CNR = \frac{(\mu_l - \mu_c)}{\sigma_c}$$

Where μ_l is the mean intensity within the lesion mask, μ_c is the intensity in the contralateral region, and σ_c is the standard deviation of the signal in the contralateral lesion.

2.6. *Receiver operating characteristic curve analysis*

Receiver operating characteristic (ROC) curve analysis was performed on the presenting ADC data to determine the areas under the curve (AUCs) for predicting infarction. Youden index was used to estimate optimum thresholds for defining infarction.[150] Analysis was performed in DWI space using the registration techniques outlined above. The analysis was confined to voxels within the tissue mask and within the range 200 to $1200x10^{-6}mm^2/s$ to reduce noise.

2.7. *Regions of interest*

Regions of interest were defined as described in Chapter 3.

2.8. *ADC dynamics*

To investigate diffusion characteristics over time ROIs were translated into DWI space at each time. Both patient level mean data and voxel-wise data were extracted from ROIs. For the temporal analysis of ADC data acute and 2 hour imaging rather than all presenting imaging was used to explore the dynamics.

3. Results

3.1. *Patient details*

Details of the patient lesions and scans used in this analysis are presented in Table 4.1. 42 patients met the criteria for inclusion.

Patient	Presenting scan		2 hour scan		24 hour scan			1 week scan		1 month scan	
	Time from onset (hrs:mins)	ADC lesion volume (ml)	Time from onset (hrs:mins)	ADC lesion volume (ml)	Time from onset (days)	ADC lesion volume (ml)	Trace DWI lesion volume (ml)	Time from onset (days)	FLAIR lesion volume (ml)	Time from onset (days)	FLAIR lesion volume (ml)
01	02:41	0.2	N		N			N		N	
02	05:00	0.5	N		0.9	0.6	1.0	3	1.4	30	1.2
03	03:25	0.3	04:35	0.4	1.0	0.8	1.3	9	1.7	37	2.1
04	02:50	26.5	04:15	36.3	0.9	52.5	88.1	7	115.0	N	
05	01:41	0.9	03:30	2.1	1.1	3.3	8.5	4	10.6	37	4.5
06	03:58	0.5	N		1.0	0.7	1.1	5	1.8	35	0.9
07	03:09	38.3	05:00	37.6	1.1	52.3	67.2	4	93.0	25	69.3
08	04:05	0.1	05:05	0.1	N			4	2.0	32	4.6
09	02:15	41.7	04:05	45.0	N			N		N	
10	03:20	29.3	05:10	31.4	1.3	29.0	83.0	N		19	72.8
12	02:20	129.5	N		N			N		N	
13	03:25	56.0	05:46	67.6	1.0	234.3	278.2	4	443.7	N	
14	03:15	1.7	04:35	2.0	1.1	1.9	1.6	6	1.6	29	1.2
15	03:49	4.8	06:10	3.4	1.1	2.7	4.8	4	4.0	28	6.0
16	04:14	22.8	06:10	22.1	N			3	59.5	47	44.8
18	02:48	21.9	04:51	19.9	1.0	30.6	36.3	4	49.1	34	28.6
19	01:43	12.2	03:50	16.3	1.0	34.9	33.5	4	59.6	67	18.1
23	02:32	39.4	04:30	30.4	0.9	34.6	63.3	4	138.7	N	
24	03:33	0.5	05:09	0.5	N			7	0.9	35	2.2
25	01:00	5.1	N		0.9	14.3	15.6	6	27.5	28	29.4
27	09:50	11.4	N		1.5	1.9	19.8	N		27	22.9
30	11:06	7.6	N		1.4	2.4	12.3	8	20.6	37	4.0
32	03:06	1.8	N		1.1	2.1	2.8	4	3.7	33	2.3
33	02:40	0.1	04:45	0.0	N			4	0.0	38	0.0
34	02:50	2.4	04:20	3.0	1.2	5.1	10.3	N		N	
35	16:03	1.2	N		N			N		29	1.4
36	06:40	0.0	N		N			3	0.2	25	0.1
37	01:35	6.3	03:45	7.5	N			3	17.8	31	11.7
39	15:00	0.6	N		N			8	0.9	43	0.5
40	05:30	0.1	07:00	0.2	N			N		N	
41	14:36	4.0	N		1.5	5.9	9.0	N		29	7.4
42	17:00	3.0	N		1.6	5.8	7.5	5	14.7	42	10.7
43	16:10	10.5	N		N			6	35.9	27	12.8
44	03:10	0.6	N		0.9	4.6	6.3	N		N	

45	03:00	0.5	04:50	1.2	1.0	1.7	4.6	7	7.0	N	
47	05:45	0.3	N		0.9	0.0	0.8	7	1.1	27	0.6
49	02:25	0.6	04:25	0.1	1.0	0.6	1.5	8	1.6	35	0.6
50	02:40	1.8	N		N			N		N	
51	11:25	10.6	N		1.5	13.3	10.5	8	14.9	22	10.8
52	02:15	0	04:20	0.0	1.0	0.0	0.9	6	0.2	27	0.0
53	06:45	82.5	N		1.2	116.7	114.0	7	189.4	29	161.9
54	06:45	2.9	N		N			5	5.8	33	2.9

Table 4. 1 - Scan times and lesion characteristics for patients included in the infarct analysis. N = data not available.

3.2. *Inter-rater agreements of infarct definition*

The mean overlap agreement for manual infarct definition between the two raters was 92%, 86% and 80% at 24 hours, 1 week and 1 month respectively. The agreements in individual patients and their relationship with infarct volume are presented in Figure 4.3. On an individual level agreement was generally good with mean overlaps of around 80%. Those with lower overlap agreements were smaller lesions in the presence of extensive white matter hyperintensities. However, there was no significant correlation between lesion size and inter-rater overlap agreement at any time point.

3.1. *Automated presenting ADC lesion identification*

Presenting ADC lesions were detected in 40 of the 42 patients included in the analysis using the objective cluster-based approach for ADC lesion definition. The lesions that were not identified at presentation (patients 36 and 52) were a small cerebellar lesion, which was not visible in the noise of the posterior fossa, and a very small lacunar infarct amongst extensive white matter hyperintensities. Of the 40 ADC lesions that were identified, 17 were detected automatically, a further 17 required manual selection to determine which cluster represented the infarct and the remaining 6 needed some manual correction to remove incorrectly included noise.

3.2. *Contrast-to-noise ratios*

Mean lesion contrast-to-noise ratios were greatest for the 24 hour trace image (7.0), followed by the 1 week T2-weighted FLAIR image (2.2) and lowest for the 1 month T2-weighted FLAIR image (1.9).

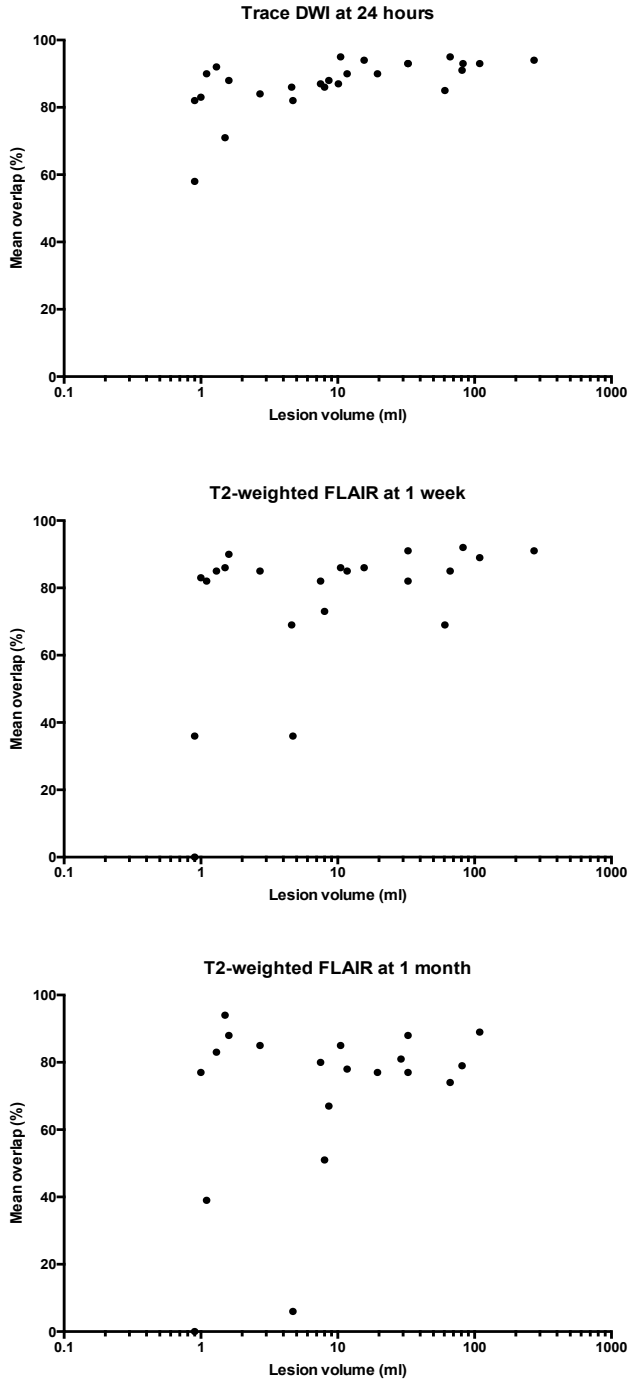

Figure 4. 3 - Inter-rater volume overlap agreements against lesion volume at different outcome times. Note logarithmic scale of x-axis.

3.3. *Between scan registration*

3.3.1. *Infarct volume*

Comparisons of rigid body versus non-linear registration of the lesion mask at each time point to the presenting structural image are presented in Table 4.2. Non-linear registration to the presenting structural scan reduced the final infarct volume at 1 day and 1 week. The greatest volume change occurred when registering the 1 week scan, which resulted in 18.2% volume reduction (absolute change: -7.1ml, paired t-test, p=0.04). This volume change corresponded to the lowest of the volume overlap agreements between rigid body and non-linear registration (MO=87.6%, UO=77.9%). There was no significant change in volume following the non-linear registration of the 1 month scan and these registrations had the greatest volume overlap agreements (MO=91.1%, UO=83.7%).

Time point	Number of patients	Volume following rigid body registration (ml)	Volume following non-linear registration (ml)	Paired t-test of volumes	Percentage change (%)	Mean overlap (%)	Union overlap (%)
24 hours	27	30.1	26.1	0.004	-13.1	90.6	82.9
1 week	30	39.0	31.9	0.04	-18.2	87.6	77.9
1 month	29	17.5	17.2	0.13	-2.2	91.1	83.7

Table 4. 2 – Volume changes and overlap agreements of lesion masks following non-linear registration to the presenting structural image compared to rigid body registration of the same masks.

Comparison of mean post-registration infarct volumes when all 3 outcomes were available is presented in Figure 4.4. The post-registration volumes following rigid body registration to the presenting scan varied significantly between time points. Although a

similar trend was seen in volumes following non-linear registration there was a lower statistical significance (ANOVA, p=0.045 (rigid body) and 0.058 (non-linear)). Using either rigid body or non-linear registration, 1 week lesions were of greatest mean volume followed by 1 month and then 24 hour scans. On inspection of the images the reduction in volume following non-linear registration appeared to be due to correction of distortion secondary to oedema (Figure 4.5).

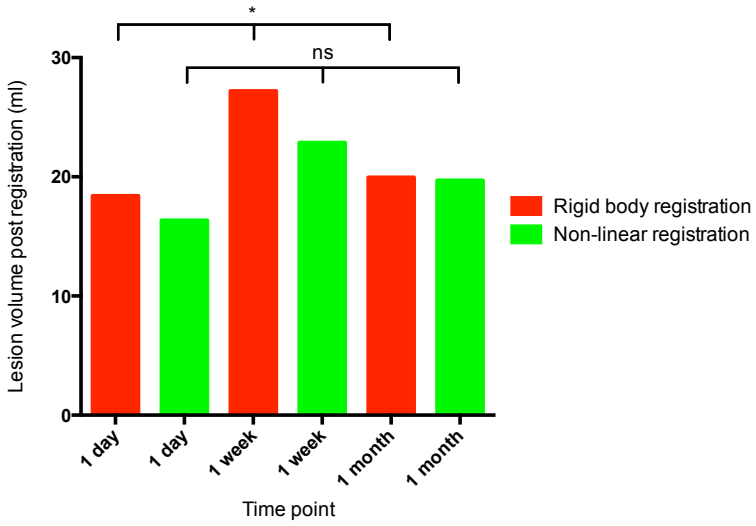

Figure 4. 4 - Mean lesion volumes following registration to the presenting structural image where all three endpoints were available. 17 patients. ANOVA: * = p<0.05, ns = not significant.

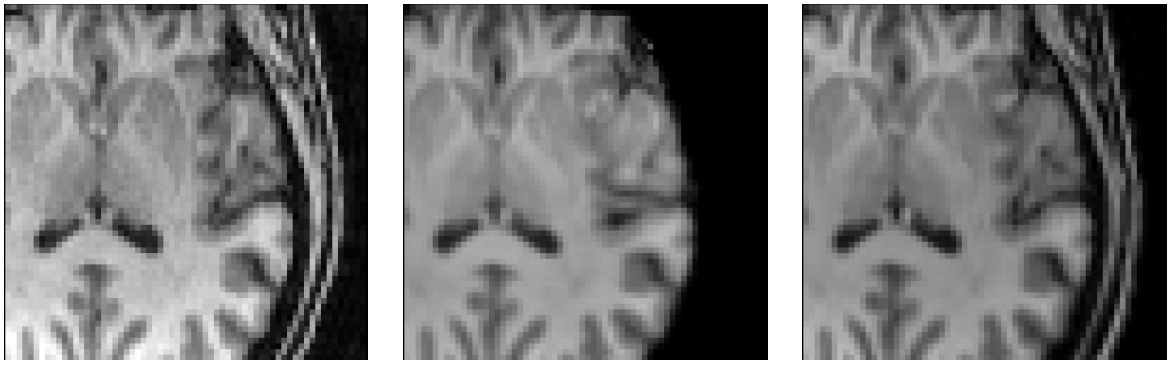

Figure 4. 5 Images demonstrating the ability of non-linear registration to correct for anatomical distortions at the subacute time point when registered to the presenting scan. A: presenting structural image. B: 1 week structural image registered to the presenting image using a rigid body transformation. C: 1 week structural image registered to the presenting image using a non-linear registration.

3.3.2. *Tissue overlap*

Agreements between lesion masks derived from T2-weighted FLAIR images at 1 month and 1 week are presented in Table 4.3. Using 1 month non-linearly registered lesion masks as the target regions, the non-linear registration of the 1 week scan was found to give improved volume overlap coefficients (MO and UO) and a lower false positive rate than rigid body registration of the 1 week regions. Furthermore, volumes are more comparable between time points using non-linear registration as would be expected given the correction of structural distortion demonstrated above (Table 4.2, Figures 4.4 and 4.5). The larger volume of the 1 week lesion following rigid body registration resulted in improved sensitivity (larger source volume) and therefore false negative rate compared to non-linear registration. However, in light of the marked distortion due to oedema demonstrated here, this does not represent improved tissue level registration as was indicated by the greater FPR (Table 4.3).

Non-linear registration provided improved registration between time points particularly at 1 week and 24 hours because it corrected for structural distortion due to oedema. Given this finding the default registration between time points was subsequently set to be non-linear registration unless otherwise stated.

3.4. *Optimum infarct definition: 1 week versus 1 month*

The final comparison in Table 4.3 uses the 1 week non-linearly registered lesion mask as the target region and the 1 month lesion mask as the source region. The data demonstrate an apparent insensitivity (68.6%) of the 1 month scan and a correspondingly high false negative rate (31.4%). To ascertain whether the 1 week masks were overestimating infarction or whether the 1 month masks were underestimating infarction the lesion the masks were visually inspected. A reduction in

T2-weighted signal intensity at 1 month, compounded by partial volume effects, and a resulting difficulty in defining the lesion was found to be responsible for the underestimation of the lesion at 1 month rather than uncorrected oedema at 1 week or atrophy at 1 month. An example of such an effect is presented in Figure 4.6.

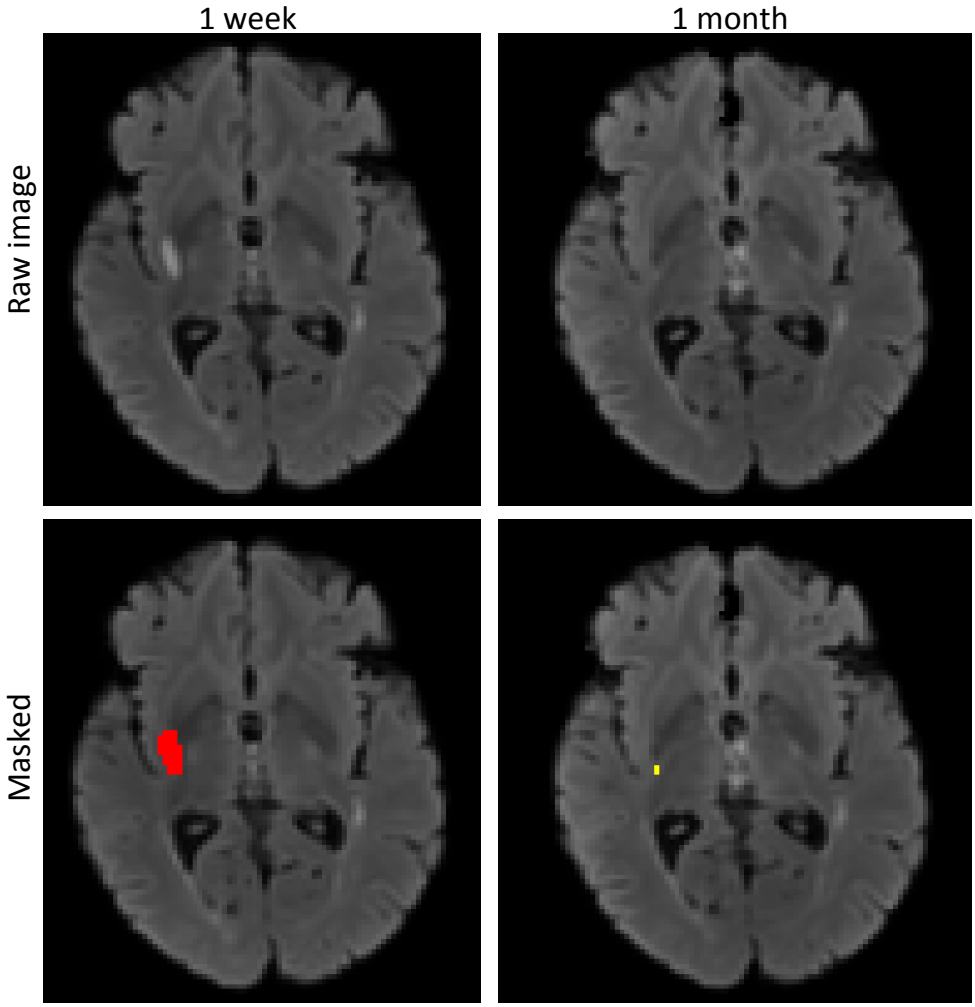

Figure 4. 6 - An example of reduced T-2 weighted signal intensity on FLAIR images at 1 month leading to an underestimation of the lesion at this time point.

Source	Target	Mean difference in volume to target (ml,%)	Mean overlap (%)	Union overlap (%)	False negative rate (%)	False positive rate (%)	Sensitivity (%)
1 week rigid body	1 month non-linear	7.0ml, 40.7%	72.8	57.2	12.4	37.8	87.6
1 week non-linear	1 month non-linear	3.4ml, 19.9%	74.9	59.8	17.7	31.4	82.3
1 month non-linear	1 week non-linear	-3.4ml, -19.9%	74.9	59.8	31.4	17.7	68.6

Table 4. 3 - Comparison of lesion masks registered to the presenting structural image. Number of patients = 24.

3.5. *Within time point registration at 24 hours: rigid body versus BBR*

Registration agreements using either rigid body or BBR for within scan time registration of the 24 hour trace DWI lesion masks are presented in Table 4.4. BBR correcting for fieldmap inhomogeneity did not register the images as well as rigid body linear registration: BBR reduced the lesion volume relative to the target with corresponding reductions in overlap coefficients and sensitivity, and it also increased the false positive rate despite the reduced lesion volume.

Within scan registration technique	Mean difference in volume to target (ml,%)	Mean overlap (%)	Union overlap (%)	False negative rate (%)	False positive rate (%)	Sensitivity (%)
Rigid body	-10.5, -27.0%	77.4	63.1	33.1	8.0	66.9
BBR	-13.2, -34%	62.6	45.6	48.1	21.2	51.9

Table 4. 4 – Comparison of rigid body and BBR registration of DWI to the structural image at 24 hours using the 1 week lesion mask as a target. BBR: boundary-based registration. DWI: diffusion-weighted imaging. All between scan time point registration was non-linear. Number of patients = 22.

3.6. *ADC versus trace DWI at 24 hours*

Comparison of automated ADC mask definition and manual delineation of the trace DWI is presented in Table 4.5. The ADC lesion mask had lower overlap coefficients than the manually delineated trace DWI lesion masks (using the 1 week lesion masks as a reference). Direct comparison of trace DWI and ADC lesion masks in diffusion space confirmed that this observation is due to an insensitivity of the ADC lesion to the trace DWI (sensitivity: 53%, false negative rate: 31%). An example of this insensitivity is presented in Figure 4.7. The voxels not included in the ADC lesions that were included in the trace lesions had a positive predictive value of 85% for infarction at 1 week and were therefore predominantly diffusion lesion pseudonormalization (i.e. recovery of ADC values in tissue destined to infarct) rather than representative of true tissue recovery.

Source	Mean difference in volume to target (ml,%)	Mean overlap (%)	Union overlap (%)	False negative rate (%)	False positive rate (%)	Sensitivity (%)
24 hour trace DWI lesion	-10.5, -27.0%	77.4	63.1	33.1	8.0	66.9
Automated ADC lesion	-18.4, -43%	67.9	51.4	46.8	6.3	53.2

Table 4. 5 – Comparison of 24 hour trace and ADC lesion masks with 1 week lesion masks. All within scan time point registration was linear and between scan time point registration was non-linear. Number of patients = 22.

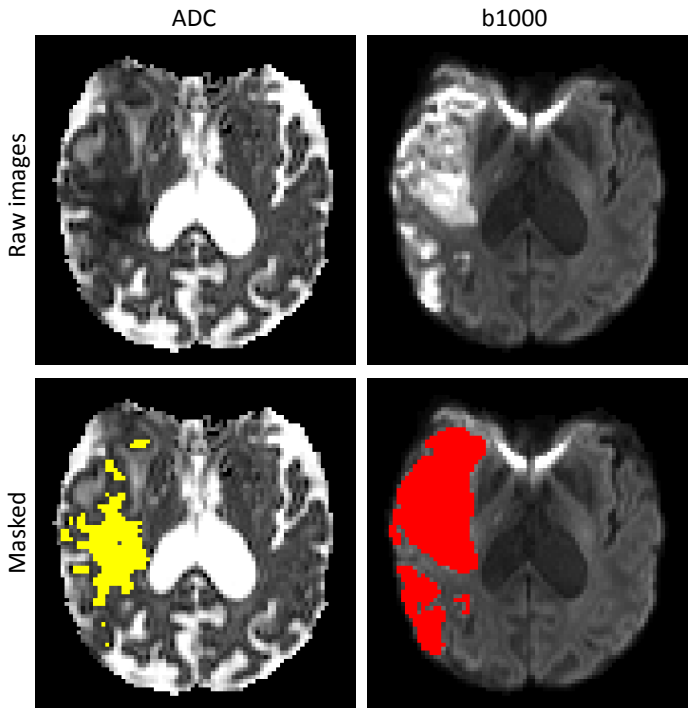

Figure 4. 7 – An example of underestimation of the trace lesion at 24 hours using a thresholded ADC lesion mask.

3.7. *Comparison of 24 hour and 1 month lesions to 1 week lesions*

Both 24 hour and 1 month lesion masks showed insensitivity to infarction as defined on the 1 week scan in terms of absolute volume (Figure 4.4) and coregistered volume overlap results confirmed this (Table 4.6). The 1 month lesions had volumes more similar to those at 1 week than the 24 hour lesions (Figure 4.4), but this was explained by a higher false positive rate and not by an improved sensitivity (Table 4.6). Visual inspection of the data demonstrated that the high false positive rate using 1 month scans was in part attributable to a lower CNR at this time and inclusion of white matter hyperintensity probably not linked to the index event (Figure 4.8).

Given the apparently similar insensitivities of the 24 hour and 1 month lesions to the 1 week outcome an exploratory analysis of the false negative voxels was made. Only 40% of the false negative voxels using the 24 hour lesion were also falsely negative by the 1

month lesion, and 49% of the false negative voxels using 1 month lesions were falsely negative on the 24 hour scan. This indicated that the insensitivity was for different reasons at the different time points and not because of a high FPR at 1 week.

Source	Target	Number of patients	Mean difference in volume to target (ml,%)	Mean overlap (%)	Union overlap (%)	False negative rate (%)	False positive rate (%)	Sensitivity (%)
24 hour b1000	1 week FLAIR	22	-10.5, -27.0%	77.4	63.1	33.1	8.0	66.9
1 month FLAIR	1 week FLAIR	24	-3.4ml, -19.9%	74.9	59.8	31.4	17.7	68.6

Table 4. 6 - Comparison of optimized 24 hour and 1 month lesion masks with 1 week lesion masks. Between scan registration was non-linear and within scan registration was rigid body.

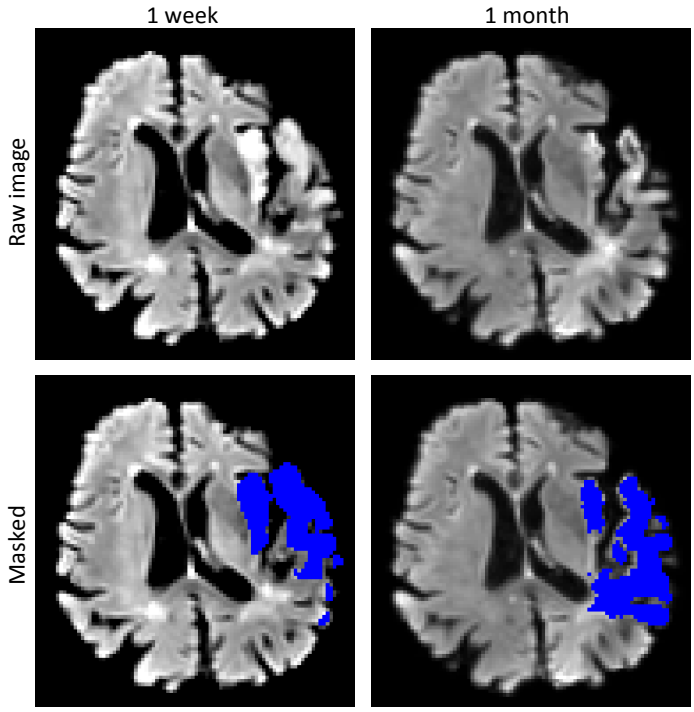

Figure 4. 8 – An example of lower contrast-to-noise of the lesion at 1 month leading to inappropriate inclusion of pre-existing white matter hyperintensity. Greater contrast-to-noise ratios at 1 week allow discrimination of infarct from pre-existing white matter hyperintensity.

3.8. *Regions of interest prevalence*

Using the optimized infarct definitions determined in this Chapter the relative frequencies of tissue fates for the dataset were determined. The ischaemic core represented 31% of the final infarct voxels (patient median: 26%, range: 0-70%). There was no correlation between time from symptom onset and the proportion of final infarct that was represented by infarct growth (R^2=5%, p=0.2). Where both 24 hour DWI and follow up 1 week FLAIR images were available, 52% of the infarct growth was apparent on the 24 hour trace image (early infarct growth) and the remaining 48% was identified on the FLAIR image beyond this time point (late infarct growth).

Of the presenting ADC lesions 12% of voxels were not included in the final infarct (radiographic recovery) and the remaining 88% represented the ischaemic core. Of the ADC lesions at 24 hours 8% of voxels were not included in the final infarct. In contrast, 22% of the ADC lesion voxels had above threshold ADC values at 24 hours, but were included in the final infarct (diffusion lesion pseudonormalization).

3.9. *ADC analysis*

3.9.1. *Receiver operating characteristic curve analysis*

ROC curve analysis of presenting ADC data generated AUCs of 0.68 for all presenting scans and 0.66 for acute scans only (Figure 4.9). Youden analysis estimated the optimum ADC threshold to be $630\times10^{-6}mm^2/s$ both for all presenting scans and when analysis was restricted to the acute datasets. The corresponding sensitivities and specificities were 48% and 82% (all presenting) and 45% and 82% (acute only). Analysis of patients with acute scans that had reperfused by 24 hours produced an AUC of 0.72 and an optimum threshold of $615\times10^{-6}mm^2/s$ for final infarction, with a sensitivity and specificity of 53% and 83% respectively.

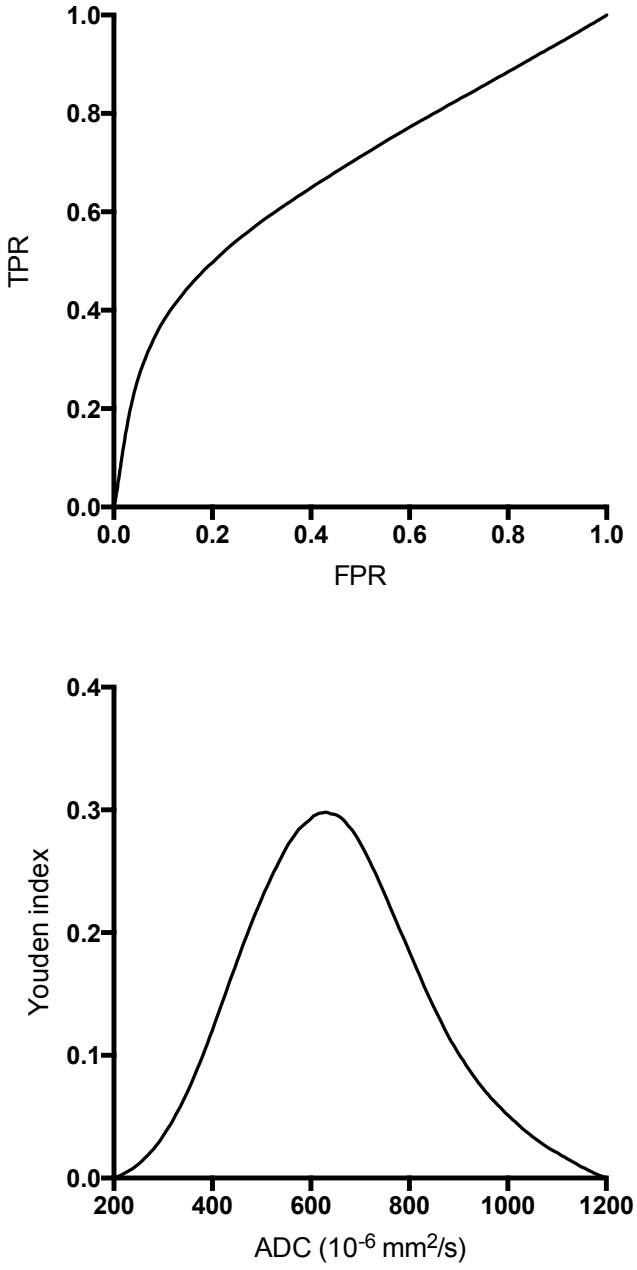

Figure 4. 9 – Top panel: receiver operating characteristic curve for ADC in predicting final infarction for all presenting scans, area under the curve = 0.68. Bottom panel: Youden analysis to determine optimum ADC threshold for defining infarction, optimum threshold = 630×10^{-6}mm/s.

3.9.2. *ADC dynamics*

Mean patient ADC values within the final infarct ROIs were found to decrease over the first 24 hours remaining lower at 1 week, before demonstrating facilitated diffusion at 1 month (Figure 4.10). Voxelwise analysis of the distributions of the ADC values within

the ischaemic core showed heterogeneity of diffusion dynamics (Figure 4.11 and 4.12). A proportion of voxels were found to undergo diffusion lesion pseudonormalization (22%) by the 24 hour time point. However, the mean ADC value within the ischemic core did not rise above the threshold of 620 $x10^{-6}mm^2/s$ until after 1 week. The ADC values in the regions of diffusion lesion pseudonormalization remained lower than those in the contralateral ROI at 24 hours, but rose above the threshold of 620 $x10^{-6}mm^2/s$ and are therefore not included in the objectively defined ADC lesion at this time.

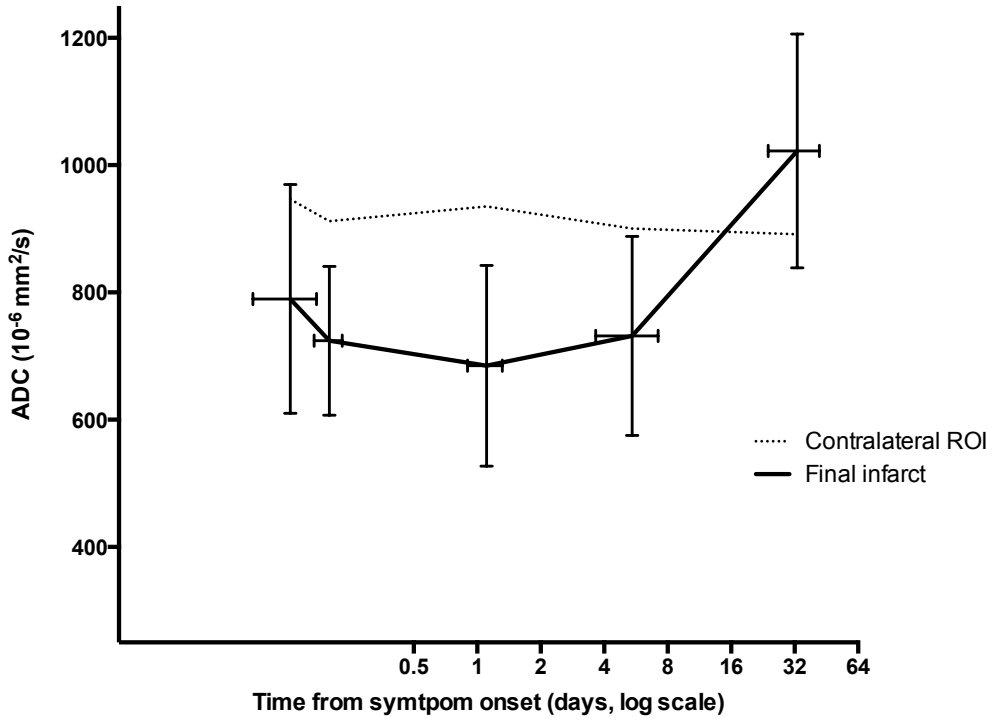

Figure 4. 10 – Mean patient ADC values within the coregistered final infarct masks over time. Error bars = standard deviation.

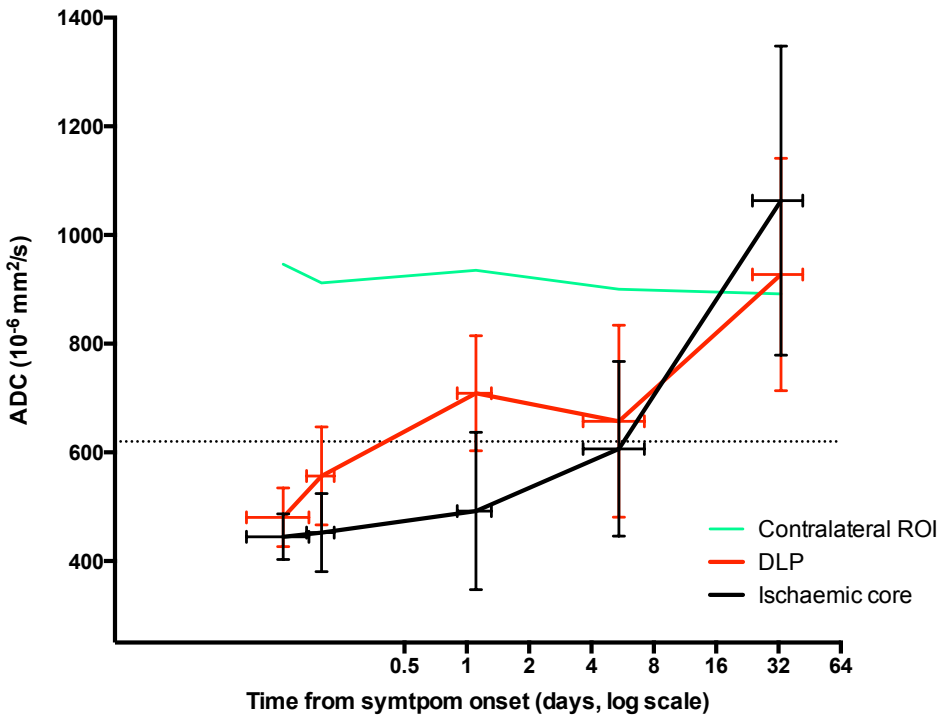

Figure 4. 11 – Mean voxel ADC values within the ischaemic core and the diffusion lesion pseudonormalization (DLP) regions. Error bars = standard deviation.

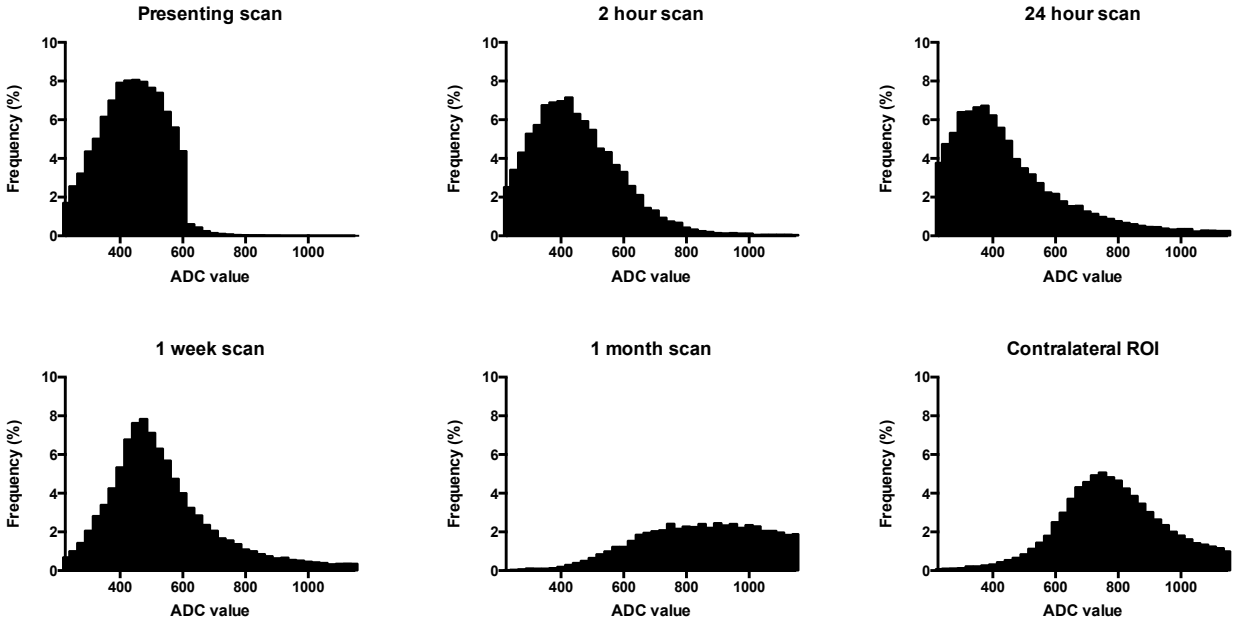

Figure 4. 12 - Distribution of ADC values within the ischaemic core ROI over time and the contralateral ROI for reference (bottom right).

4. Discussion

In this Chapter the different imaging time points that might be used to assess outcome in the study were used to assess the optimum method of registration and final infarct definition. The preferred techniques were then used to define and describe the ROIs at a tissue level. These ROIs were used to investigate the dynamics of the diffusion characteristics over time.

4.1. *Registration*

Non-linear registration to the presenting structural scan produced more consistent total infarct volumes across time points. More importantly, at a tissue level, non-linear registration improved overlap agreement between time points in defining infarction. This improved agreement was achieved by the non-linear warp applied to the follow up images, which uses image details outside the infarct to correct for the distorting effect of oedema within the infarct.

Concerns regarding the use of 24 hour to 1 week outcomes in stroke studies have primarily centred on the over estimation of infarction due to oedema.[58] Non-linear registration to the presenting structural image compensates for this potential confounding error. Using non-linear registration between scan times will improve confidence when assessing the fate of the brain tissue within a voxel. This is of particular value when interpreting a novel imaging technique or the efficacy intervention at a tissue level. Non-linear registration between scan times should be the preferred registration strategy in stroke studies.

4.2. *24 hour imaging outcome*

Using ADC to define infarction at 24 hours is appealing because it would allow cross platform objective infarct definition. However, ADC is less sensitive than trace image at

this time point because of diffusion lesion pseudonormalization at 24 hours, a phenomenon that had been thought to occur later than this when patient level have been interrogated.[71, 151, 152] These data show that within individual patients some regions undergo diffusion lesion pseudonormalization sooner than the patient mean data. Trace DWI is less susceptible to this insensitivity because it combines both T2-weighted signal and restricted diffusion. Therefore, regions that have undergone pseudonormalization are still included in infarct definitions because of the T2-weighted signal contribution.

Attempts to use BBR and corrections for fieldmap inhomogeneity to improve registration of EPI data did not improve the registration of lesion masks, and rigid body registration within scan time was superior. This relative failure of BBR may be due to the different grey and white matter contrast in the trace DWI compared that of blood oxygen level dependent imaging used in functional MRI for which the BBR technique was developed. For practical purposes, EPI distortions do not appear to have a significant effect on the lesion definition as the lesions are typically in areas not significantly affected by fieldmap inhomogeneity. However, such distortions would be more important in studies of posterior fossa pathology.

4.3. *Defining final infarction*

4.3.1. *1 week versus 1 month outcome*

The 1 week lesions on T2-weighted FLAIR imaging provided optimum infarct definition following non-linear registration to the presenting imaging space for several reasons. Compared to 1 month, the 1 week imaging had higher T2-weighted signal intensity and a correspondingly higher CNR, and this improved sensitivity to infarction. At 1 month, the lower CNR led to a higher false positive rate, because it is harder to

distinguish infarct from pre-existing white matter hyperintensities. Finally, the higher CNR improved inter-rater agreements at 1 week compared to 1 month.

4.3.2. *24 hour trace DWI*

The trace DWI at 24 hours, a combination of diffusion- and T2-weighted signal, underestimated the final infarct, in particular when oedema is corrected for using non-linear registration. This insensitivity of 24 hour trace DWI is consistent with other work that measured unregistered lesion volumes,[59] and may be either due to radiographic insensitivity to completed infarction or a reflection of ongoing pathophysiological processes beyond 24 hours. Such processes include reperfusion injury,[21] failure of collateral or critically restricted perfusion in the presence of haemodynamic compromise, or extension of the occluding thrombus. These factors may be responsible for those patients who clinically deteriorate following presentation, a phenomenon that is often poorly explained. In addition, the histological changes that occur as a result delayed neuronal injury are seen hours to days after ischaemia and may not be radiographically visualized until beyond 24 hours.[47] DWI lesions have been observed to grow even after proven recanalization.[153]

Trace DWI had a similar degree of insensitivity as the 1 month T2-weighted FLAIR, albeit in different voxels, but had a lower FPR. 24 hour trace DWI should be preferred to 1 month imaging as a tissue outcome when 1 week is not available. If 24 hour imaging is used, the insensitivity to final infarction must be considered in the study design and in the interpretation of the data.[115]

4.4. *Presenting ADC data*

4.4.1. *Automated infarct definition*

ROC curve analysis of these data produced an ADC threshold that was essentially the same as that derived from a homogeneous subset of the DEFUSE cohort (630×10^{-6}/mm versus 620×10^{-6}/mm).[105] This threshold was not greatly affected by subsequent reperfusion status or restricting data to those within 6 hours only.

Automated presenting lesion definition, using an objective ADC threshold, was feasible in the majority of a heterogeneous cohort of patients presenting with acute stroke. This approach would allow consistent infarct definition across imaging platforms and sites. This is particularly important when using imaging to select patients for studies, as quantification of volumes by eye is not reliable.[106, 144]

4.4.2. *Dynamic diffusion changes*

In acute stroke, diffusion restriction is thought to be due to cytotoxic oedema and intracellular movement of water.[140] Facilitated diffusion observed at later time points is a result of changes in tissue integrity and an increase in the number of free water molecules, and has been described at a patient level as occurring between 48 hours and 1 week.[71, 141, 151, 152] The patient level data presented in this Chapter are consistent with this temporal pattern. However, voxel-wise analysis revealed heterogeneity of ADC dynamics at a tissue level with pseudonormalization in some voxels earlier than previously described. The early pseudonormalization may be a consequence of increased capillary permeability and vasogenic oedema, in addition to necrosis and cell lysis,[154, 155] representing an acceleration of the natural history of the ADC dynamics within the ischaemic core. This reversal of ADC characteristics does not represent tissue recovery.

Sustained radiographic recovery did occur in around 12% of the presenting ADC lesion and 8% of the 24 hour ADC lesion. However, this may be an overestimate because the proportion could have been increased by minor errors of registration.[111] This low frequency of radiographic recovery is consistent with findings of recent studies that reported diffusion lesion reversal was infrequent and predominantly transient.[111, 156]

The observed heterogeneity of ADC dynamics is consistent with the heterogeneity of metabolism within the ischaemic region demonstrated using PET imaging[33, 157] and seen in experimental models.[13, 32, 158] There are a variety of injurious pathologies, including energy failure and excitotoxicity, free radical production, peri-infarct depolarization, inflammation and apoptosis that occur following cerebral ischemia and each will have different effects on the diffusion properties of water at different times.[13]

4.5. *Limitations*

4.5.1. *Registration*

Non-linear registration was shown to be the optimum technique for between time point registrations. Although it is difficult to be certain whether all structural distortions have been completely corrected, the volume changes and visual inspection do support this being the case. Defining accuracy of image registration globally, without well-defined ROIs (such as infarct volume), is problematic as the same algorithms that are used to assess the accuracy are used to optimize the registration.

4.5.2. *Infarct definition*

As with all tissue-based analyses, the infarct definitions are susceptible to errors of registration. Potential error can be introduced when registering masks through one or more registration steps. Each step introduces uncertainty, or blurring, at the edge of the

mask. Once registered to the destination image space the masks were thresholded at 0.5 to prevent overestimation of the intended region. This introduces errors of partial volume in lesion definition. As a result, some overestimation of infarct growth or lesion reversal may occur once registered masks are combined, in addition to any under correction of distortions due to oedema.

Ischaemic injury might have occurred outside of the defined final infarct and be below the limit of detection on conventional imaging. Such sub-radiographic injury has been described in PET and preclinical studies although the clinical implications of this are not known.[36, 159, 160]

4.5.3. *ADC dynamics*

The heterogeneity of the patient population demonstrates how optimum image registration, final infarct definition and automated presenting ADC lesion definition might be used and interpreted in an unselected cohort of stroke patients encountered in clinical practice. However, together with the sample size, the heterogeneity of patients does limit the interpretation of dynamic ADC properties with respect to stroke subtypes. Perfusion analysis is not fully presented here, given that the purpose of this Chapter has been to explore the optimum methodology to define tissue fate. Interpretation of perfusion dynamics in the framework of tissue outcome described in this Chapter will form the basis of Chapter 5.

5. Conclusions

In this Chapter the optimum registration techniques and infarct definitions have been defined for the subsequent analyses. Non-linear registration is the preferred registration technique between scan time points and rigid body registration should be used between protocols within scan times. 1 week T2-weighted FLAIR is the optimum method for

defining infarction following non-linear registration to the presenting scan to correct for oedema. 24 hour trace DWI is a less sensitive alternative. Finally, using optimized lesion definition it was shown that ADC dynamics are heterogeneous and diffusion changes may represent different biological processes at different time points. The rigorous definition of tissue outcome is essential for the robust interpretation of not only ADC, but also the perfusion and metabolic imaging techniques that form the basis of the following Chapters.[18]

Chapter 5: Quantification of Cerebral Blood Flow In Acute Stroke

1. Introduction

Perfusion-weighted imaging (PWI) has been used to investigate and define tissue at risk of infarction since the ischaemic penumbra was first described.[18] However, as seen in Chapter 2, no strategy using PWI to select patients for intervention has been successfully translated into clinical practice. The Acute Stroke Imaging Research Roadmap II was developed on the background of recent null acute stroke trials incorporating selection using PWI.[58] Although this consensus statement emphasizes the importance of imaging biomarker definitions and the consistency of imaging parameters, it falls short of questioning the validity of the perfusion-diffusion mismatch and associated concepts.

1.1. *Experimental models*

Thresholds of cerebral blood flow (CBF) have been proposed in animal models at which a variety of pathophysiological processes occur,[19] although the effects of duration of hypoperfusion on tissue outcome has been more challenging to describe.[34, 161, 162] The defined thresholds range from those of electrical activity failure and selective neuronal loss,[18, 163] through to changes in metabolic pathways and overt energy failure with loss of cellular ionic gradients.[164, 165]

Absolute CBF thresholds of macroscopic infarction range from 10ml/100g/min to 24ml/100g/min depending on the experimental model (e.g. species) and the duration of ischaemia.[166, 167] The longer the duration of ischaemia the higher the threshold, reaching a plateau 3-4 hours after stroke onset.[166, 168] Data from experimental models suggest that histological changes also occur in hypoperfused tissue outside the macroscopic infarct,

a finding that has been corroborated in human stroke using PET imaging, although the relationship with the time course of perfusion to these changes is not clear.[36, 159, 163]

1.2. *Clinical data*

Evidence from large randomized trials shows that reperfusion therapies improve clinical outcome if administered early following stroke onset.[55] By inference there is a lower threshold for non-viable tissue at earlier time points and therefore is a greater amount salvageable penumbra available to benefit from reperfusion. As the duration of ischaemia increases the CBF thresholds increase and a smaller volume of the perfusion deficit is viable.

The natural history of absolute CBF values and ischaemic thresholds are less well described in stroke patients than in experimental models. Attempts have been made to quantify CBF using contrast MRI and CT, but generating absolute measures is challenging and giving repeated boluses of contrast and radiation has limited serial acquisitions.[74, 75, 77] For reasons of pragmatism contrast MRI or CT studies often use surrogates of perfusion that correlate with tissue outcome, such as T_{max}, but the physiological significance of such surrogates is not known.[81] Reliably quantifying absolute CBF has required the use of radioisotopes (e.g. oxygen-15 PET). These studies are usually small and not validated in multiple centres, but do allow perfusion thresholds to be linked to metabolic activity.

Estimates from contrast perfusion and PET studies suggest that the grey matter CBF threshold for tissue at risk of infarction is approximately 20ml/100g/min, but range from 12 to 40ml/100g/min.[80, 169-171] Thresholds for non-viable tissue (i.e. the ischaemic core) are less well described and generally lower than those for tissue at risk.[80] White matter thresholds for tissue at risk are lower than those for grey matter and estimated to

be around 12ml/100g/min, although this is harder to estimate owing to the poor perfusion signal to noise ratio encountered in white matter.[82, 171, 172]

1.3. *Perfusion dynamics*

The available evidence suggests heterogeneity in the degrees of reperfusion following human stroke.[173] In experimental models, heterogeneity of reperfusion characteristics is also seen, including both hypoperfusion and hyperperfusion following recanalization.[21, 174] A variety of factors may affect the degree of reperfusion in addition to the tissue state including microvascular thrombi and endothelial dysfunction.[175, 176] Furthermore, reperfusion may be deleterious in some instances, a phenomenon known as reperfusion injury.[21] Data examining the natural history of perfusion over time are limited in human stroke and often restricted to binary assessments of reperfusion or vessel status.

1.4. *Arterial spin labeling*

As discussed in Chapter 1, arterial spin labeling (ASL) is increasingly being used to measure perfusion in the context of acute ischaemic stroke because it is non-invasive, can be performed serially without repeated contrast administration, and allows estimation of absolute CBF.[72, 84] As such ASL has the potential to meet the criteria of "repeatable non-invasive 3-dimensional imaging of regional cerebral blood flow" outlined by Astrup *et al.* for monitoring therapeutic intervention.[18]

In this Chapter, multiple post labeling delay (PLD) vessel-encoded pseudocontinuous ASL (VEPCASL) will be used to investigate the natural history of perfusion in stroke. Vessel encoding improves the estimation of CBF where voxels have a mixed arterial supply without compromising the signal to noise ratio.[177] Using multiple PLD VEPCASL permits the estimation of the bolus arrival time (the time from labeling to arrival in the cerebral parenchyma, BAT) and hence improved CBF quantification if

there is delayed arrival of blood to the tissue. BAT using ASL has not been measured before in acute stroke, but is an important parameter to validate the single post labeling delay of 2.0s recommended by the International Society for Magnetic Resonance in Medicine perfusion study group.[82]

1.5. *Aims*

The aims of this Chapter are:

- To assess the ability of VEPCASL to investigate CBF in acute ischaemic stroke;
- To quantify CBF in the regions on interest defined in Chapters 3 and 4;
- To explore the utility of using absolute CBF in distinguishing viable from non-viable tissue and at risk from not at risk tissue;
- To determine the influence of perfusion dynamics on tissue fate; and
- To explore the strengths and limitations of using absolute CBF measurements acutely to explain the pathophysiology of acute ischaemic stroke;

2. Methods

2.1. *Patients and data quality*

Six healthy volunteers were scanned with four repeated VEPCASL sequences at 3 time points as described in Chapter 3. All patients recruited into the large volume imaging protocol were included in a qualitative assessment of data integrity. Patients were included in quantitative analyses if there was non-corrupted VEPCASL perfusion data available and there were the required lesions with which to define the regions of interest (ROIs).

All images were inspected by a clinician (GH) and assessed for quality. Images were judged to be of good quality if there was the expected distribution of perfusion within the grey matter and appropriate labeling of the perfusion from the feeding vessels.

2.2. *Perfusion imaging*

CBF was measured using a multiple PLD VEPCASL sequence.[177] Imaging was acquired by placing a labeling plane approximately 8cm below the level of the circle of Willis, through the proximal V3 segment of the vertebral arteries. Labeling of the arterial blood was achieved using a 600μs Gaussian radiofrequency pulse once per millisecond over 1.4s. A single shot echo planar imaging readout was used, acquiring 24 slices sequentially from inferior to superior to give whole brain coverage (TR = 4080ms, TE = 14ms, voxel size = 3.4×3.4×4.5mm). Volumes were acquired following a range of 6 PLDs (0.25s, 0.5s, 0.75s, 1s, 1.25s, 1.5s). Vessel encoding of the four arteries in the labeling plane was achieved by means of 8 paired encoding cycles in a range of orientations.[177, 178] Calibration scans were acquired using identical parameters to the VEPCASL sequence, but without ASL or background suppression applied, to allow absolute CBF quantification and to correct for uneven spatial sensitivity. Total acquisition time was 5min 55s.

2.3. *Image processing*

Retrospective motion correction was applied using the MCFLIRT tool found in FSL.[131, 133] Calculation of the perfusion signals arriving from each artery at each PLD was achieved using a maximum *a posteriori* approach to the general Bayesian framework for vessel encoded data.[178, 179] A kinetic curve was fitted to the data for each feeding artery separately to estimate CBF and BAT with a corresponding variance using a variational Bayes approach.[66, 130] Signal calibration was performed using the

cerebrospinal fluid signal within the calibration images as a reference, defined using a ventricle mask transformed from standard space (MNI152)[147] to the ASL image space and superimposed with the subject's own CSF mask registered from T1 image space.[146]

The resulting vessel-specific CBF maps were summed to generate a map of the total CBF from all arteries. Vessel-specific BAT and variance maps were combined using a voxelwise weighting for vessel-specific CBF as a proportion of total combined CBF.

2.4. *Perfusion masks*

Masks of the presenting perfusion deficit were generated using a thresholded approach to identify and cluster all grey matter voxels with a CBF of less than 20ml/100g/min. This threshold was chosen as it is thought to represent the approximate threshold for identifying tissue at risk in patients with acute stroke.[80, 169-171] These thresholded clusters were used as a guide for manual delineation of the perfusion deficit. The resulting masks were then "closed" by sequential dilatation and erosion before registration into perfusion image space at each time point.

2.5. *Regions of interest and registration*

The patient regions of interest (ROIs) used in this analysis are described in Chapters 3 and 4. The specific ROIs used were: ischaemic core, early and late infarct growth, radiographic recovery, diffusion lesion pseudonormalization. A further ROI was defined for this Chapter: peri-infarct. Peri-infarct ROIs were generated in ASL image space by dilating the final infarct mask using a 3×3×3 kernel centered on each voxel of the final infarct mask. The final infarct mask was subtracted from the dilated mask to leave the peri-infarct ROI. This tissue represents regions likely to have abnormal perfusion, but survive, and are not defined by the ASL signal itself.

All between scan time point registration was performed using non-linear registration warps generated by registration of the structural images.[131] Within scan time point registration was achieved using a rigid body registration.[133] Masks were translated from native image space to the presenting structural image before registration into VEPCASL image space. These masks were then thresholded (0.5) and composite masks generated according to the definitions outlined in Chapters 3 and 4.

2.6. *Tissue type partial volume estimates*

Tissue segmentation of the presenting structural T1-weighted image was used to define grey and white matter partial volume estimates (PVEs).[146] PVEs were registered into perfusion image space allowing grey and white matter masks with differing PVE thresholds to be generated. Primary analyses were performed within grey matter masks with a default PVE of 0.5 at each time point. Further analyses were made within grey and white matter masks thresholded at PVEs of 0.7, and a PVE of 0.9 in white matter only, to allow effects of partial volume to be investigated. A maximum grey matter partial volume estimate of 0.7 was chosen because the thin cortices of stroke patients, relative to the voxel size, resulted in the exclusion of the majority of voxels if higher thresholds were used (Figure 5.1).

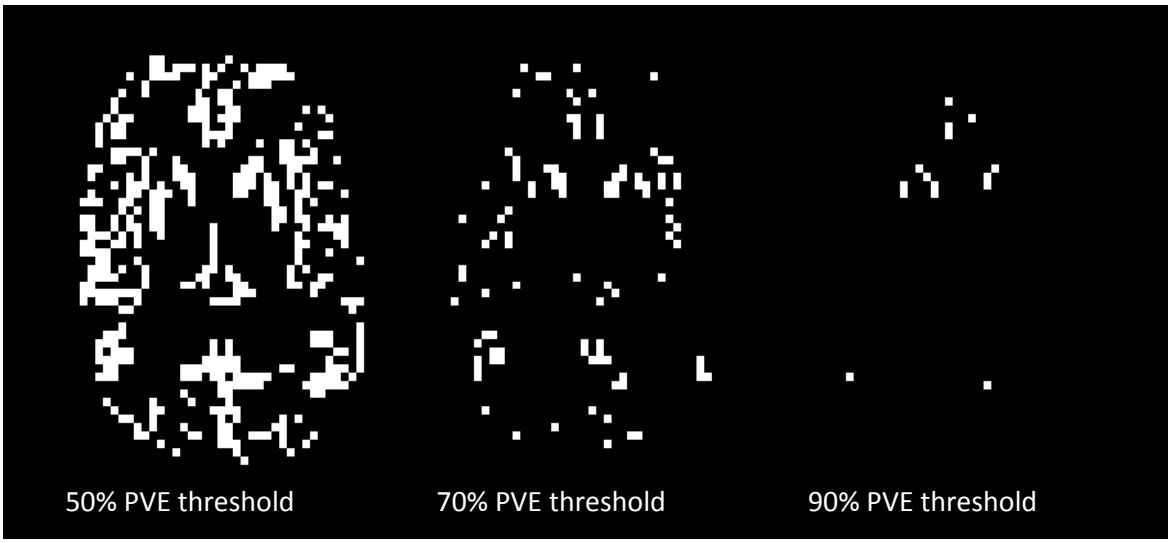

Figure 5. 1 – Binary images representing voxels from a single slice in ASL image space using increasing thresholds of partial volume estimates to define grey matter. PVE = partial volume estimate.

2.7. *Data extraction and analysis*

2.7.1. *Bolus arrival time*

To investigate the distribution of BATs within the presenting perfusion lesion, data were extracted from the acute arrival time maps. Data were only extracted where the variance estimate for the bolus arrival time was less than a threshold of 0.175s. This ensured that the BAT distribution represented only those voxels where there was a reasonable confidence about the BAT value. The proportion of voxels for which the BAT could be reliably estimated was recorded in addition to the mean BAT within those voxels. BAT cannot be estimated for those voxels where CBF is near 0 and where the arrival time delay is later than approximately 2.5s. This maximum arrival time delay is constrained by the maximum post labeling delay of 1.5s, the labeling period of 1.4s and the T1 decay of water (1.7s at 3.0T).[180] Histograms were generated to assess the BAT distribution of voxels.

2.7.2. *Cerebral blood flow*

Mean and standard deviations were extracted to generate both patient level and voxel level data within each of the defined ROIs. Repeatability within healthy volunteers and the contralateral hemispheres of patients was quantified using the coefficient of variation (mean ÷ standard deviation) and ANOVA. The acute scans were selectively used to minimize the inclusion of patients who had reperfused at the time of presenting imaging.

2.8. *Receiver operating characteristic curve analysis*

To investigate the utility of using VEPCASL to predict tissue at risk of infarction, ROC curve analyses were performed on the perfusion data to generate AUC values. Youden indices were calculated to estimate the optimum CBF thresholds to predict infarction. Analyses were performed to assess the ability of CBF to predict tissue viability, defined by the acute ADC lesion, and to predict tissue at risk, defined by the final infarct.

3. Results

3.1. *Patient details and data quality*

The patient demographics and data quality are presented in Table 5.1. 32 patients were prospectively enrolled in this study and underwent VEPCASL imaging, of which 2 had no identifiable lesion on the presenting DWI and transient neurological symptoms so were excluded from further analysis. Of 100 VEPCASL datasets, 23 were discarded due to motion corruption. Motion affected scans at all time points with the exception of the 1 month scans. Representative perfusion images are presented in Figure 5.2.

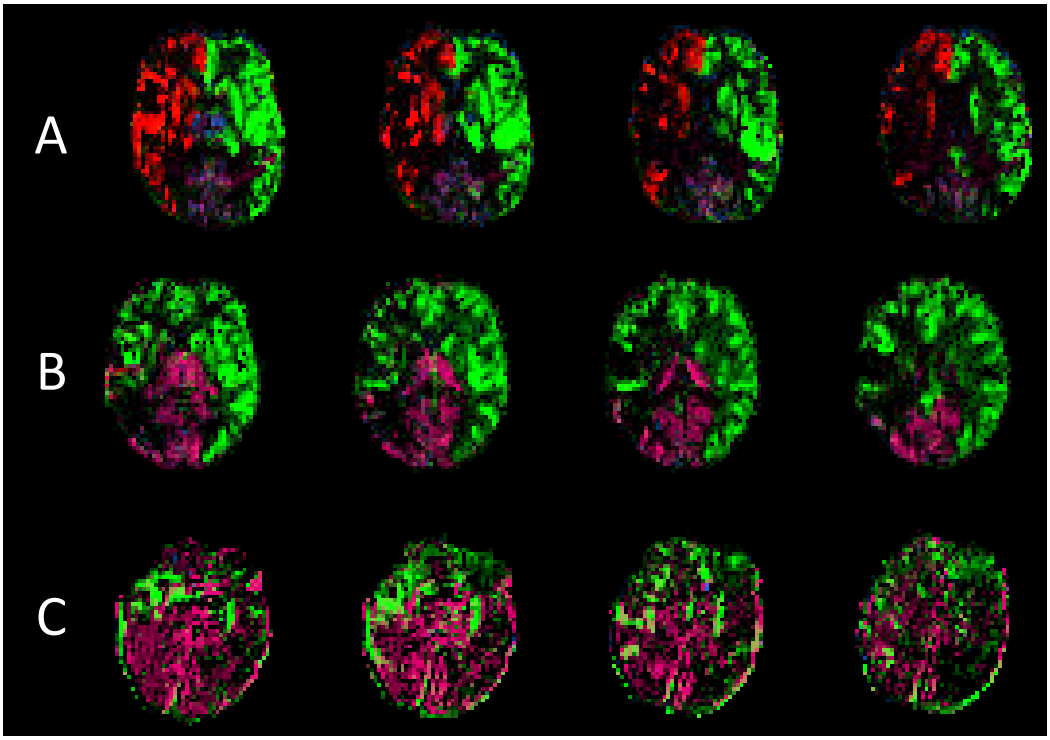

Figure 5. 2 - Representative VEPCASL perfusion images from three patients. A: perfusion deficit in the territory of the right internal carotid artery (red); B: perfusion deficit in the right hemisphere, but supplied by the left internal carotid artery; C: corrupt perfusion data (excluded)

Patient number	Hemisphere	Sex	Age	NIHSS at presentation	Thrombolysed	Time to presenting scan (hh:mm)	Presenting scan	2 hour scan	24 hour scan	1 week scan	1 month scan
3	L	F	84	3	N	03:25	N	G	G	G	G
4	L	M	92	25	Y	02:50	B	B	G	B	N
5	R	M	64	3	N	01:41	G	B	G	G	G
7	L	F	86	27	N	03:09	G	G	G	B	G
9	L	F	88	25	N	02:15	B	G	N	N	N
10	R	F	94	15	N	03:20	G	G	G	N	G
12	R	F	70	19	Y	02:20	G	N	N	N	N
13	L	F	81	21	N	03:25	G	G	G	N	N
15	R	M	50	6	Y	03:49	G	G	G	G	G
16	L	M	95	19	Y	04:14	G	N	N	G	G
17	L	F	91	10	N	04:53	N	N	N	G	G
18	L	F	53	13	Y	02:48	N	G	G	G	G
19	R	M	57	7	N	01:43	G	G	G	G	G
20	R	M	86	2	N	01:46	G	G	G	N	N
23	R	F	92	25	N	02:32	B	B	B	B	N
25	L	F	68	23	Y	01:00	N	N	B	B	G
27	R	F	80	14	Y	09:50	G	N	B	N	G
30	L	M	80	3	N	11:06	G	N	G	G	G
33	L	F	76	10	Y	02:40	G	G	N	G	G
34	L	F	78	9	Y	02:50	B	B	B	N	N
35	R	F	66	2	N	16:03	G	N	N	N	G
37	L	F	56	7	Y	01:35	G	G	N	N	G
41	L	M	71	8	Y	14:36	G	N	G	N	G
43	L	M	48	3	N	16:10	G	N	N	G	G
44	L	F	103	18	Y	03:10	G	N	B	N	N
45	L	M	82	13	Y	03:00	G	B	B	B	N
50	L	F	76	25	Y	02:40	B	N	N	N	N
51	L	F	76	11	N	11:25	G	N	G	G	G
52	R	F	77	2	N	02:15	N	G	B	B	N
53	L	M	56	24	N	06:45	G	N	G	G	G

Good	20	12	14	12	19
Bad	5	5	7	6	0
Total	25	17	21	18	19
Proportion discarded	20%	29%	33%	33%	0%

Table 5. 1 – Patient demographics and data quality. G = good quality; B = bad quality; N = data not available; NIHSS = National Institute for Health Stroke Scale.

3.2. *CBF in healthy volunteers*

71 of 72 healthy volunteer datasets were of sufficient quality for inclusion in the analysis. The average grey matter perfusion was 62 ± 15 ml/100g/min (mean ± standard deviation). Coefficients of variation between measures at the same scan time point was

8.5%, between scan time points was 9.7% and between individuals was 15.9%. Two-way ANOVA demonstrated a significant variation in CBF measurements between both the individual and the scan time ($p<0.0001$). Data are presented in Figure 5.3.

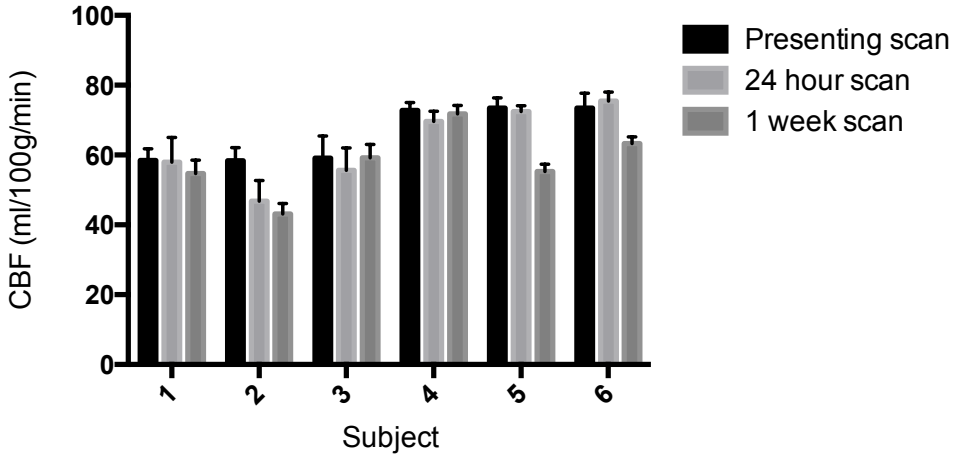

Figure 5. 3 –Cerebral blood flow (CBF) variation seen within and between healthy individuals

3.3. *Bolus arrival time in healthy volunteers*

Distribution of bolus arrival times in the ROIs of healthy volunteers is presented in Figure 5.4. Median bolus arrival time was 1.1s with 99% of voxels having an arrival time of less than 2s. Bolus arrival time could be estimated with confidence in 89% of voxels.

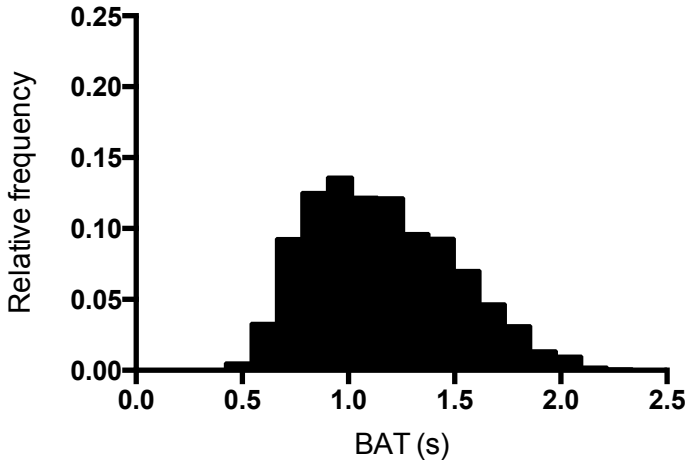

Figure 5. 4 – Bolus arrival time (BAT) distribution in the healthy volunteer ROIs

3.4. *CBF in the contralateral hemisphere of patients*

Within the contralateral ROIs of patients the mean CBF was 54ml/100g/min (± 43ml/100g/min, n = 8522). The coefficient of variation was 25% between patients and 16% between time points. For patients with both presenting and 24 hour scans, two-way ANOVA demonstrated a significant interaction between the patient and the contralateral CBF values (p= 0.02), but not between the scan time and CBF (p=0.12). CBF values from the contralateral hemisphere are presented in Figure 5.5. There was no effect of tPA infusion on contralateral CBF.

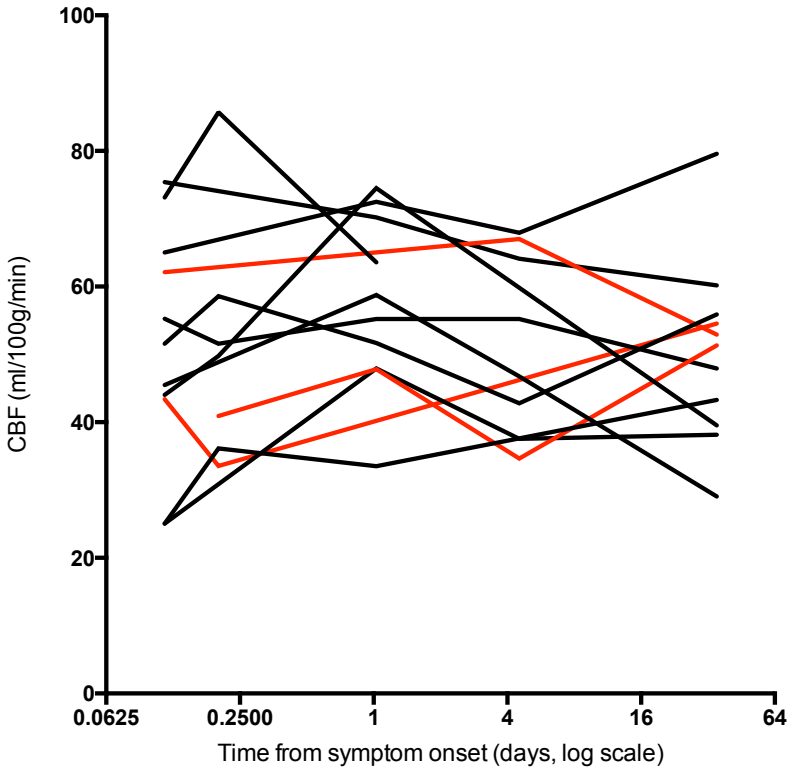

Figure 5. 5 – Contralateral cerebral blood flow (CBF) values over time in individual patients. Red lines = patients infused with tPA acutely.

3.5. *Bolus arrival time in patients*

The distribution of arrival times can be seen in Figure 5.6. Using a BAT variance threshold of 0.175s estimates of perfusion were made in 74% of voxels within the contralateral ROI and to 41% within the presenting perfusion deficit. The median arrival time in the contralateral hemisphere voxels was 1.1s (mean ± standard deviation; 1.22s ± 0.30s, n = 6305) and in the perfusion deficit was 1.3s (1.44s, SD ± 0.29s, n = 4458) (unpaired t-test, $p < 0.0001$).

An analysis with a much lower BAT variance threshold was used (0.04s) to assess whether model priors were overly influencing the BAT estimate. This produced a similar distribution of BATs to the higher threshold (Fig 5.6), although only in a small subset of voxels (6%).

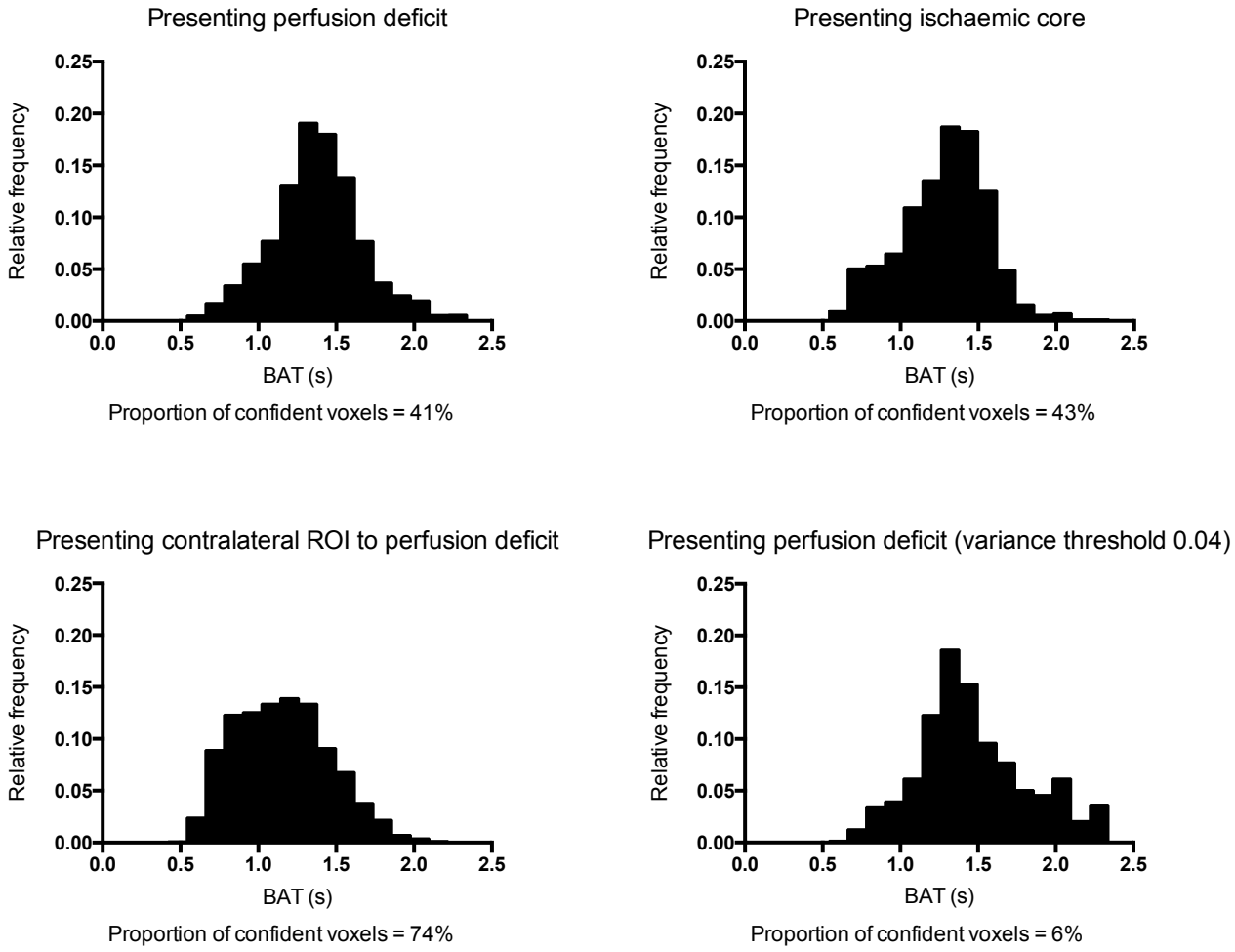

Figure 5. 6 – Distribution of bolus arrival times (BAT) in the perfusion deficit and mirrored contralateral region (top left and bottom left). Distributions in the ischaemic core (top right) and using a stricter BAT variance threshold in the perfusion deficit (bottom right).

3.6. *CBF in the ischaemic hemisphere of patients*

Within the cerebral grey matter, a graduated severity of hypoperfusion was seen within 6 hours of stroke onset (Figure 5.7, top panel). Ischaemic core had the lowest perfusion at presentation (mean ± SD, 14 ± 16 ml/100g/min, n = 732), followed by regions of early (21 ± 28 ml/100g/min, n = 2139) and then late infarct growth (25 ± 35, n = 830; ANOVA, $p < 0.0001$ for ischaemic hemisphere ROIs). Mean CBF in the peri-infarct region (28 ± 33 ml/100g/min, n = 2186) was less than the contralateral region (51 ± 43 ml/100g/min, n = 7145; t-test, $p < 0.0001$) but not as severely hypoperfused as ROIs that infarcted.

At a patient level, mean CBF values showed a similar pattern to voxel level data, although this did not reach statistical significance (ANOVA, p = 0.1 for ipsilateral ROIs). There were a range of CBF values for each ROI definition at a patient level and considerable overlap between the ipsilateral ROIs values (Figure 5.7, bottom panel).

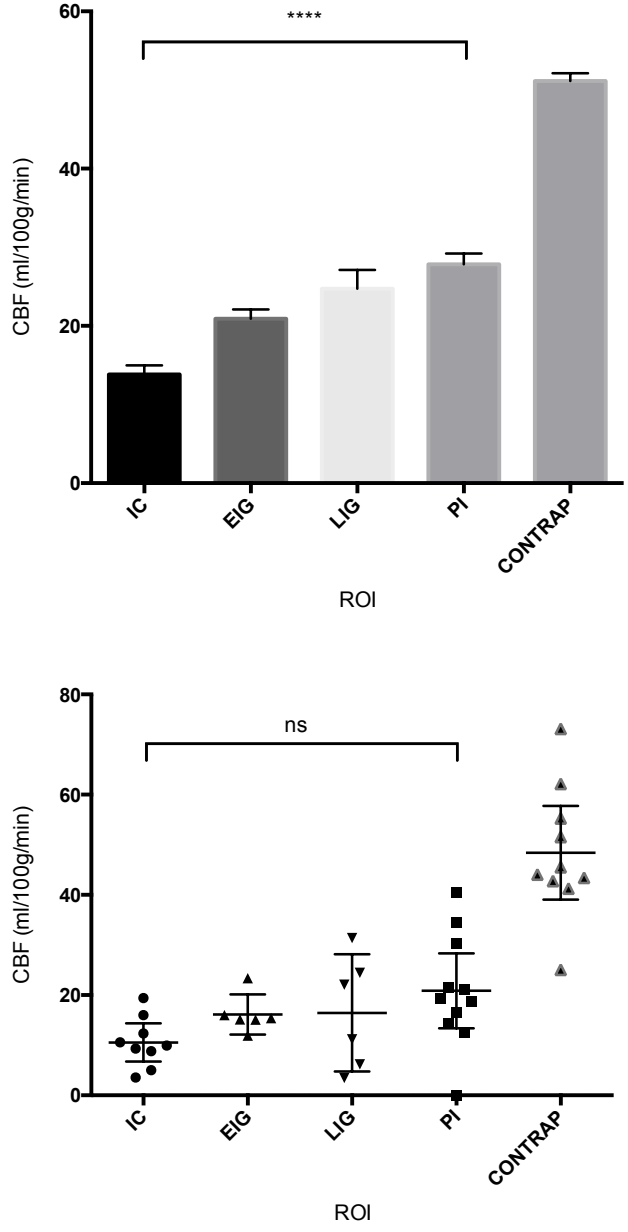

Figure 5. 7 - Top panel: voxelwise mean CBF in grey matter regions of interest in the acute (<6 hours) presenting scans. Bottom panel: Patient level data for the same regions of interest at the same time point. IC = ischaemic core; EIG = early ischaemic growth; LIG = late ischaemic growth; PI = peri-infarct; CONTRAP = ROI contralateral to the perfusion deficit. Grey matter partial volume estimate threshold = 0.5

Exploration of the CBF values within the presenting ADC lesion can be seen in Figure 5.8. Regions of diffusion lesion pseudonormalization had a lower CBF than the ischaemic core as a whole (7 ± 9ml/100g/min, n = 74; t-test, $p < 0.0001$). In the radiographic reversal tissue there were wide confidence estimates, even at the voxel level, due to the relatively small volumes of grey matter this represents.

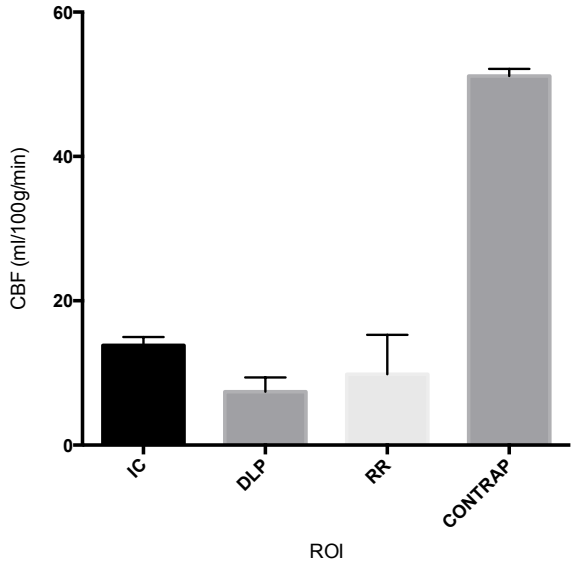

Figure 5. 8 - Voxelwise mean CBF in grey matter regions of interest within the ischaemic core in the acute (<6 hours) presenting scans. IC = ischaemic core; DLP = diffusion lesion pseudonormalization; RR = radiographic recovery; CONTRAP = mirrored perfusion deficit. Grey matter partial volume estimate threshold=0.5

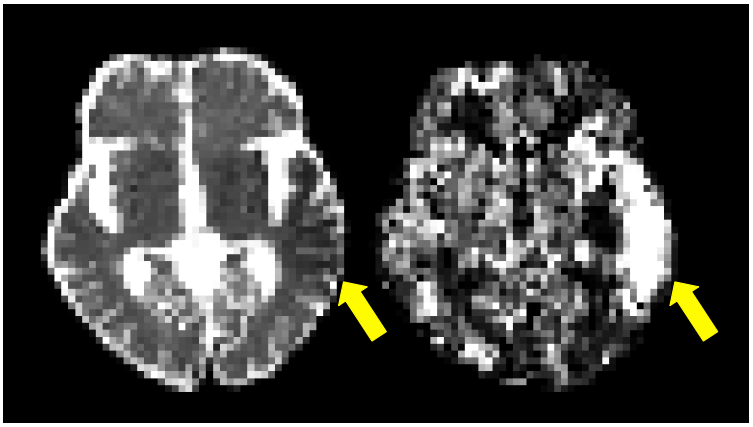

Figure 5. 9 – An example of hyperaemia in the infarct core of a patient at 1 week. Presenting apparent diffusion coefficient image (left) registered to 1 week total CBF map (right). Yellow arrow indicated location of ischaemic core.

3.7. *Contrast-to-noise*

The weighted mean acute contrast-to-noise ratio (CNR) for CBF within the final infarct was 1.03.

3.8. *Serial CBF measures*

Within both ischaemic core and regions of infarct growth there was heterogeneity in the degree and rate of reperfusion (Figure 5.9, 5.10 and 5.11). In early and late infarct growth there were regions that reperfused to varying degrees and regions that appear to suffer a delayed persistent hypoperfusion. This variation is not a reflection of global changes as demonstrated by the relatively stable contralateral CBF values (Figure 5.5). By 1 month all ROIs in the infarct growth ROIs demonstrate reduced perfusion.

3.1. *Receiver operating characteristic curve analysis*

ROC curve analysis for presenting and acute perfusion generated AUCs of 0.69 and 0.70 respectively for predicting final infarct. Performance was better for defining the presenting ADC lesion at with AUCs of 0.72 and 0.74 respectively. The Youden index identified an optimum CBF threshold of 26ml/100g/min for final infarct and 24ml/100g/min for presenting ADC lesion regardless of whether acute or all presenting perfusion data were used. Graphs summarizing the ROC curve analysis of acute perfusion data can be seen in Figure 5.12.

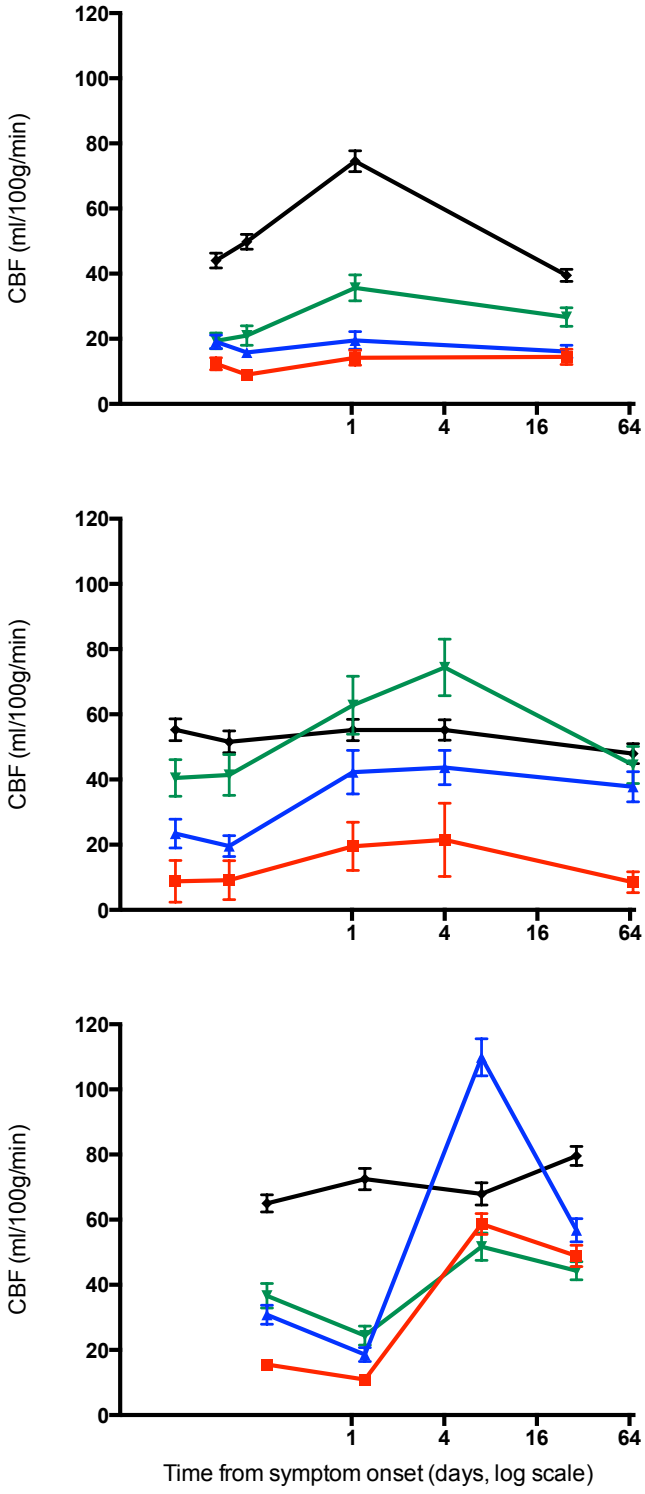

Figure 5. 10 - Example perfusion dynamics from 3 patients (7, 19 and 53). IC = ischaemic core; IG = infarct growth; PI = peri-infarct; CONTRAP = mirrored perfusion deficit.

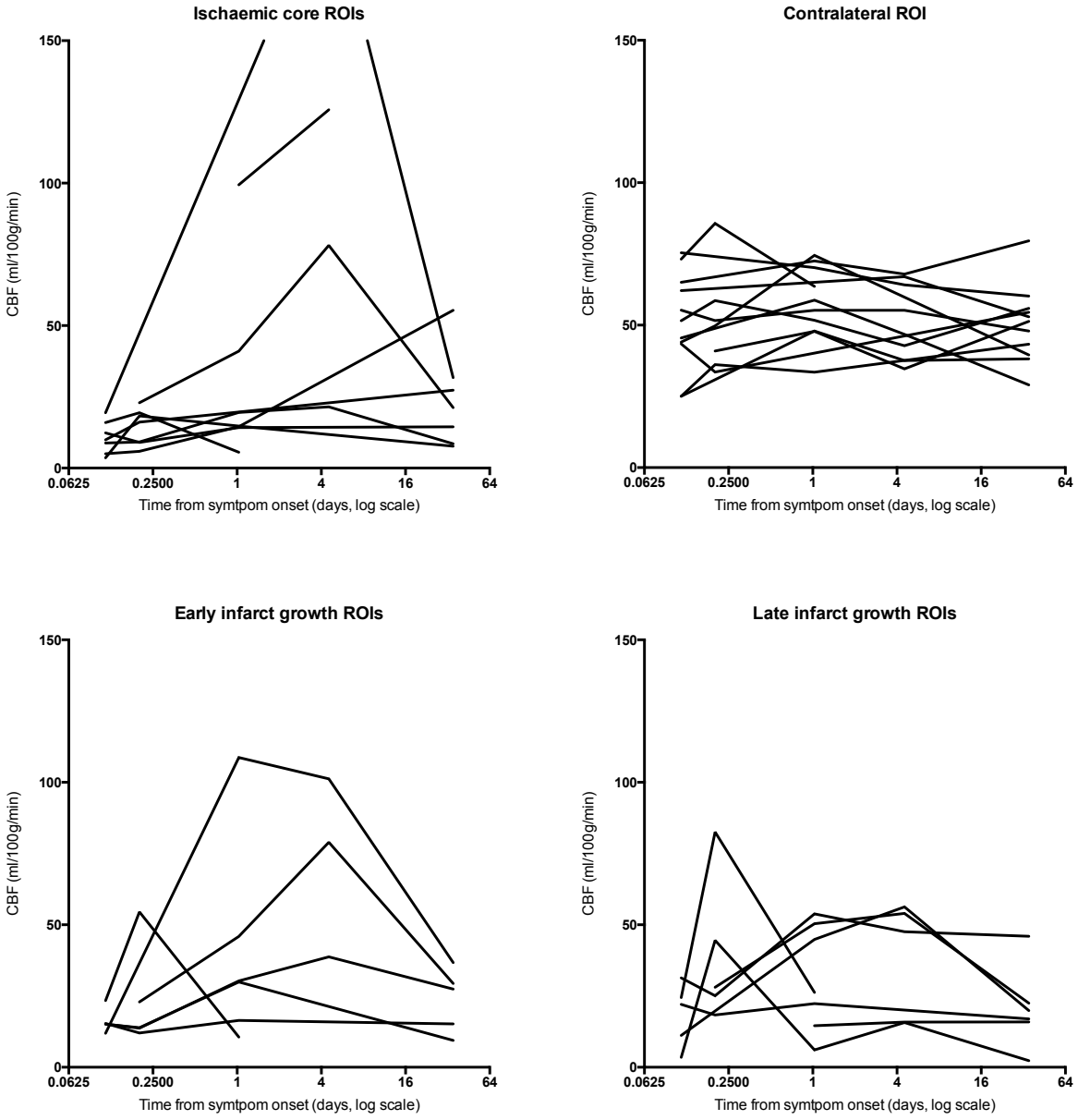

Figure 5. 11 – Serial perfusion measurements from individual patients arranged by ROI.

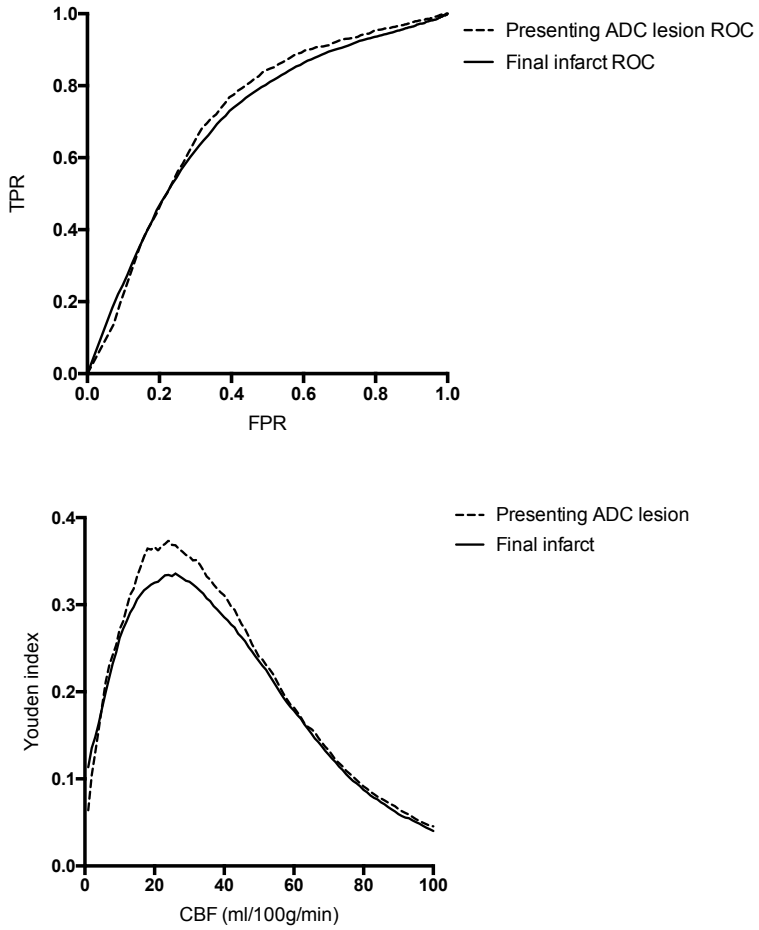

Figure 5. 12 – Top panel: receiver operating characteristics (ROC) curves for predicting presenting infarct (defined by the ADC lesion) and final infarct using acute CBF. Bottom panel: Youden analysis using acute perfusion to predict presenting infarct and final infarct. TPR = true positive rate; FPR = false positive rate; ADC = apparent diffusion coefficient; CBF = cerebral blood flow.

3.2. *White matter perfusion*

CBF values obtained from white matter ROIs acutely can be seen in Figure 5.13. There is significant difference in the level of perfusion both between ischaemic and contralateral ROIs, and between ischaemic core and infarct growth, but the absolute values are higher than those quoted in the literature for the contralateral "healthy" hemisphere white matter (15-30ml/100g/min).[87] Examination of the patient level data revealed that an individual outlier did not drive this.

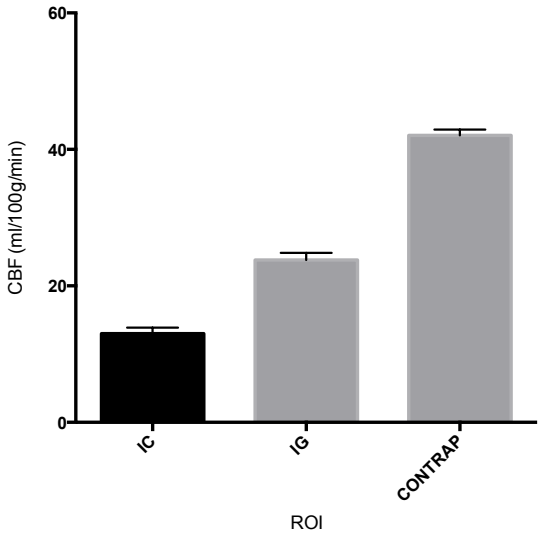

Figure 5. 13 - Voxelwise mean CBF in white matter regions of interest in the acute (<6 hours) presenting scans. IC = ischaemic core; IG = ischaemic growth; CONTRAP = ROI contralateral to the perfusion deficit. White matter partial volume estimate threshold = 0.5

3.1. *Effects of partial volume*

The effect of the PVE threshold on CBF quantification can be seen in Figure 5.14. Although the grey matter PVE threshold was not raised above 0.7, increasing the threshold to this value does not appear to change the CBF estimates significantly. Increasing the PVE threshold in white matter brings CBF values closer to, but still higher than, a level which would be expected in the non-ischaemic white matter.[87]

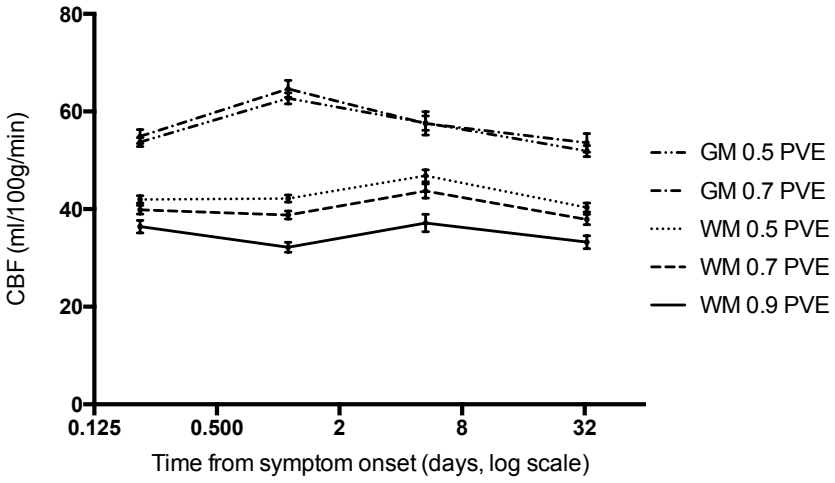

Figure 5. 14 – The effect of different partial volume estimate (PVE) thresholds over time. GM = grey matter; WM = white matter; CBF = cerebral blood flow.

4. Discussion

This Chapter demonstrates that multiple PLD VEPCASL can serially measure absolute grey matter perfusion in stroke patients. Acutely the mean CBF values in patients are consistent with values derived using preclinical and radioisotope based imaging techniques.[19, 169, 181] CBF measured with VEPCASL can distinguish the severity of ischaemia between tissue of different fate and estimate BAT. However, VEPCASL is susceptible to motion artefact and only 80% of presenting images were of adequate quality, compared to 90% in DSC-PWI studies in similar patients.[182]

4.1. *Non-ischaemic CBF*

Grey matter CBF values obtained from healthy volunteers and the contralateral hemispheres in patients are consistent with those obtained using radioisotopes, such as $^{15}O_2$ and ^{15}O water PET,[183-186] or Xenon clearance.[187, 188] The normal value of grey matter CBF is around 40-80ml/100g/min and is known to fall with age and cerebrovascular disease, which may explain the contralateral variability between individuals seen in the patient cohort.[185, 186] There was no significant variability in the contralateral hemisphere of patients related to scan time, which might have been expected if there was significant diaschisis. The between patient variability supports the use of relative CBF to measure contrast within an individual, but suggests that comparisons of relative CBF between patients may be less robust. Overall, the coefficients of variation were less than those for measuring cerebral blood volume using dynamic susceptibility contrast MRI in healthy volunteers,[189] and within the recommended limits for ASL studies (less than 20%).[190]

The BATs measured in the ischaemic and contralateral regions of patients also support the validity of these perfusion measurements. In those voxels where perfusion is

sufficient to estimate BAT, the distribution is within a time frame where multiple PLD ASL can reliably measure CBF. Where the measured CBF is too low to assess BAT, this may represent genuine low flow or flow with a delayed arrival time. However, the distribution of those voxels that can be measured would suggest that arrival time is not the limiting factor in the majority. The distribution of arrival times measured provides justification for the recommendations of the International Society for Magnetic Resonance in Medicine Perfusion Study Group consensus statement in choosing 2.0s as an appropriate single post labeling delay for ASL studies in "adult clinical patients".[82]

In white matter, the inherently low signal to noise ratio of ASL techniques would be expected to result in difficulty detecting a contrast between ischaemic and non-ischaemic tissue.[86] However, the issue in this analysis was an overestimation of CBF, which is likely to be explained by the disproportionate effect that partial volumes of grey matter will have on white matter measurements, errors of registration, and misclassification of tissue type.[86] Increasing the PVE threshold to define tissue type improved the mean contralateral white matter CBF measurement to a level more consistent with normal perfusion, but did not correct it completely. The higher than expected acute white matter CBF values are likely to reflect measurement error. Genuinely high perfusion, as part of an acute global compensatory response, is less likely because the CBF values are sustained for the whole month following stroke onset, well beyond the natural history of any acute hypertensive response.[191]

4.2. *Ischaemic CBF*

When using the pooled voxel level data acutely, grey matter perfusion was lowest in the ischaemic core, and in particular in the regions of diffusion lesion pseudonormalization. This degree of hypoperfusion is consistent with the findings from Chapter 4, which

suggested that normalization of diffusion characteristics by 24 hours was a marker of severe ischaemia and tissue death, with rapid progression to vasogenic oedema and tissue necrosis, rather than tissue level recovery. Early infarct growth ROIs had lower perfusion than late infarct growth, and both were more hypoperfused than the peri-infarct tissue.

Perfusion dynamics, such as delayed hypoperfusion at 24 hours, explained infarct growth or tissue survival in some, but not all patients. Regions of late infarct growth, apparently escaping infarction at 24 hours, showed delayed or ongoing hypoperfusion only in a subset of patients. This observation would support the hypothesis that the tissue injury represented by late infarct growth is not all viable penumbra at 24 hours that goes on to infarct. It is explained by either a second episode of low perfusion in some patients and the delayed radiographic appearance of injury in others.

The hypothesis of delayed radiographic appearance of injury, rather than late infarction of viable tissue is supported by the underestimation of final infarction using the 24 hour trace DWI documented in Chapter 4, and also the observation of diffusion lesion growth in patients with proven recanalisation.[192] Pathophysiological processes with a delayed influence on the T2-weighted signal might explain apparently delayed late infarct growth despite often normal perfusion. Narrow therapeutic windows for reperfusion therapies would not support the widespread presence of ischaemic penumbra at 24 hours, and therefore the potential for genuine infarct growth. This may underlie observations of apparent penumbral "mismatch" tissue well beyond 4.5 hours,[73, 193, 194] which has prompted several imaging based trials,[110, 116, 195-197] none of which have been translated into routine clinical practice.

The optimum CBF threshold for identifying tissue at risk was similar to that in the published literature.[80, 169-171] There is little robust data for the CBF threshold for the presenting infarction,[198] but it is surprising that in this analysis it was similar to the tissue at risk CBF threshold. This may be a consequence of reperfusion in regions of ADC lesion prior to the time of the presenting scan, either as a result of auto-recanalization or thrombolysis treatment. Alternatively, at the time of presenting imaging in this study the threshold for infarction may have risen to a similar level to the threshold for tissue at risk. Given the median onset to scan time of 3 hours this would be consistent with experimental data.[166, 168] Other explanations would include noise, delayed signal not being distinguished from low flow, partial volume effects on the infarct ROIs leading to a higher CBF value in some of these voxels, and partial volume effects outside the lesions erroneously reducing CBF values in some normally perfused voxels. Regardless of the explanation, the ROC curve analysis in this Chapter highlights the challenge of using presenting CBF alone to define tissue state and supports the need for complementary imaging techniques to improve tissue definition.

At the patient level, a similar pattern of mean acute CBF values was seen to the voxelwise values, reinforcing a graduated degree of hypoperfusion from ischaemic core through to apparently less severely ischaemic tissue. However, there is a variation in the degree of hypoperfusion between patients in the ROIs. Regions with similar degrees of hypoperfusion have different reperfusion dynamics, but nonetheless have similar fates. Conversely tissues with different fates can have similar levels of initial hypoperfusion and reperfusion dynamics.

Knowledge of CBF is clearly not sufficient to predict tissue outcome and other factors have a role in determining tissue fate. These factors are likely to include prior or

subsequent fluctuations in perfusion that are not captured by the imaging schedule. In addition to the degree and duration of ischaemia, the susceptibility of the tissue will have a role in determining its fate.[161, 199] Factors determining susceptibility might include prior exposure to ischaemia,[200] variations in metabolically demanding injurious processes,[13] intrinsic differences in regions of the brain,[201] and other factors relating to the individual, such as micro RNA expression or immune responses.[202-204]

4.3. *Limitations*

This study is limited in its ability to validate the accurate measurement of CBF using VEPCASL in stroke patients, as there is no comparator against which to assess it. However, there is no clinically relevant gold standard and similar values were generated to those obtained using autoradiographic approaches and preclinical models. The dropout rate is similar to other studies of acute stroke although the corruption of a proportion of data secondary to motion is greater than for DSC-PWI and simpler ASL sequences.[182, 205] Dropout rate and missing data may introduce a bias into the results, as these missing data are more likely to be patients with a poor clinical outcome.

Any ASL study in cerebrovascular disease has inherent limitations. The distinction of late arriving blood from voxels with truly low CBF is not possible and limited by the lack of angiographic data. However, using this multiple PLD technique does increase confidence in CBF values given the distribution of the BATs that appear within detectable time frames. The lower signal to noise ratio of ASL demands larger voxel sizes or extended scanning times, but the latter is not practical in acute patient studies. The larger voxel sizes (approximately 9 times the volume of the DWI voxels) exacerbate the effects of partial volume, both in terms of defined ROIs, and grey and white matter differentiation. Changing the PVE thresholds used did not significantly

alter the grey matter perfusion estimates in this study, but partial volume effects are likely to contribute to the challenges of measuring white matter CBF using ASL. DSC-PWI uses intravenous contrast and hence generates greater contrast to noise ratios, allowing shorter imaging times and smaller voxels to be acquired.

In this Chapter, the relationship of tissue perfusion and tissue outcome has been explored. However, the analysis is limited by the lack of angiographic data describing vessel patency at each time point. Such data would enhance the analyses as it would not only increase confidence in the CBF quantification, but allow the relationship between recanalization and reperfusion to be explored. The effect of collateral circulation could also be investigated using the vessel encoding. VEPCASL would allow absolute CBF values to be measured over time to better explore the mechanisms underlying the heterogeneity of reperfusion dynamics.

Finally, larger scale studies would allow the exploration of cerebral perfusion using VEPCASL in subgroups of homogeneous patients to explore the patient factors that might interact with hypoperfusion in the individual.

5. Conclusions

Multiple PLD VEPCASL is an appealing technique for the investigation of stroke pathophysiology and can be used to measure serial cerebral perfusion. VEPCASL can measure differences in absolute CBF within the grey matter of the affected hemisphere and this analysis has demonstrated degrees of hypoperfusion that correlate with tissue fate. Although CBF explained some of the tissue fate there was heterogeneity of acute hypoperfusion and subsequent perfusion dynamics at the level of the individual patients. This lack of consistency means that knowledge of CBF alone did not predict viability or risk of infarction with confidence. Other factors play a role in determining tissue

outcome, which may explain the historical difficulty of selecting patients for treatments using perfusion-weighted imaging alone.

Chapter 6: Serial pH-Weighted Imaging In Acute Stroke: Amide Proton Transfer MRI

1. Introduction

The original concept of the ischaemic penumbra suggested that concurrent imaging of regional CBF and metabolism would be required to identify tissue at risk that may benefit from intervention.[18] While there have been major technological advances in acute stroke imaging since this was proposed, the search for robust evidence to support individual imaging-guided treatment decisions is ongoing (Chapter 2).[58, 206] A contributing factor may be that, aside from PET imaging, the development of metabolic imaging markers has been limited when compared to the focus on methods to assess perfusion.

Amide proton transfer (APT) MRI, a chemical exchange saturation transfer (CEST) imaging technique, can be used to generate a pH-weighted signal through the assessment of the base-catalysed and, hence, pH-dependent transfer of protons between intracellular amide groups and water (Chapter 1).[67] It has been proposed that pH-weighted imaging may improve the delineation of tissue at risk by separating benign oligaemia from an acidotic ischaemic penumbra.[207]

1.1. *pH changes in ischaemia*

The majority of research into cerebral acid-base physiology has been in the preclinical setting. In these models the normal intracellular pH is around 7.0 – 7.25, depending on the technique used,[164, 208-211] with significant buffering by protein and phosphate to maintain pH at a constant level.[212, 213] In ischaemia both acidosis and alkalosis have been described depending on the nature of the metabolic disturbance.

1.1.1. *Acidosis*

During ischaemia, intracellular generation of protons, and therefore acidosis, occurs predominantly as a result of ATP hydrolysis, although there are also contributions from carbon dioxide production and incomplete oxidation of fuels.[16] Under normal conditions the proton concentration is maintained by synthesis of new ATP molecules, but imbalance of ATP utilization and synthesis leads to disruption of intracellular pH. At CBF levels of around 20ml/100g/min, energy reserves are no longer sufficient to maintain ATP and anaerobic glycolysis is required. Anaerobic glycolysis itself does not generate net hydrogen ions, only lactate, but the concomitant ATP hydrolysis leads to a lactic acidosis (Figure 6.1).[16, 214]

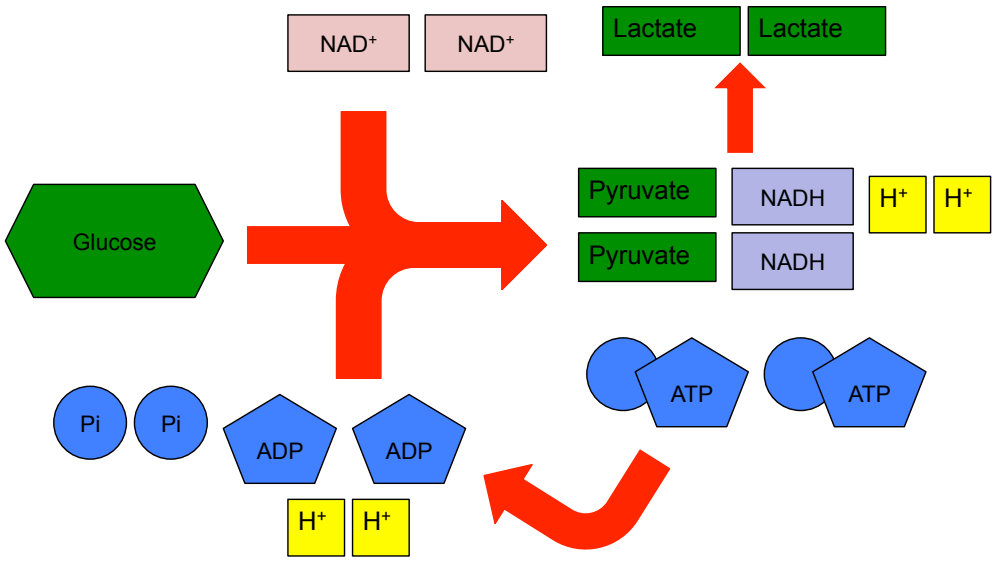

Figure 6. 1 - Anaerobic glycolysis. ADP = adenosine diphosphate, ATP = adenosine triphosphate, NAD+/NADH = nicotinamide adenine dinucleotide, Pi = inorganic phosphate.

The theoretical maximum pH change under physiologically reproducible conditions of ischaemia and hyperglycaemia is 0.9 pH units and experimental evidence supports this assertion, although the absolute values measured depend on the technique and model used.[164, 208-211, 213, 215, 216] Hyperglycaemia drives acidosis in ischaemia by provision of the substrate for anaerobic glycolysis. In the context of hyperglycaemia, lactate is

higher in experimental models of cerebral ischaemia,[217] and this correlates with poorer outcome of the tissue in patients.[94] Physiological variables that affect the response of intracellular pH to ischaemia include hypoglycaemia and hypothermia, both of which moderate the degree of acidosis.[217, 218] Acidosis progresses over the duration of ischaemia and has been observed as soon as 15 minutes following the onset of hypoperfusion.[217, 219]

Acutely, acidosis is an appealing biomarker of ischaemic metabolic stress and tissue at risk because it correlates well with the severity of hypoperfusion in controlled experimental models,[164] and occurs before irreversible injury.[19] As such it has been hypothesised that pH-weighted imaging could add complementary information to perfusion- and diffusion-weighted imaging.[207] Pre-clinical studies using pH-weighted imaging from APT MRI have supported the potential of acidosis as a biomarker of the ischaemic penumbra.[220-222] In these models of focal cerebral ischaemia acidosis predicts final infarction and appears to allow discrimination of penumbral tissue from benign oligaemia.[222]

1.1.2. *Alkalosis*

In experimental models alkalosis has been observed following transient cerebral ischaemia.[208, 219, 223-225] As CBF drops to levels where there is insufficient metabolic substrate for oxidative phosphorylation, ATP levels are maintained by phosphocreatine reserves, PCr, and the creatine phosphokinase reaction:

$$PCr + ADP + H^+ \leftrightarrow ATP + Cr$$

This reaction reduces the concentration of hydrogen ions and hence raises the intracellular pH.[16, 164] Following the extrusion of protons from the cell and buffering

during acidosis, restitution of ATP levels and the utilisation of the remaining protons (via creatine phosphokinase, adenylate cyclase and oxidative phosphorylation pathways) may also result in an intracellular alkalosis. This is supported by the observation that alkalosis occurs following transient ischaemia,[219] and only in tissue that has been sufficiently ischaemic to produce lactate.[208] Recovery of ATP levels and alkalosis does not necessarily result in tissue survival, but is observed in tissue that goes on to infarct.[225] Delayed alkalosis has also been observed following chronic cerebral ischaemia (24 to 72 hours) and this is associated with delayed neuronal injury in these models.[223, 224]

1.2. *Mechanism of injury*

Direct injury of cells, secondary to intracellular acidosis and in the absence of ischaemia, depends on the degree and duration of acidosis: neurons and glia with an intracellular pH of 3.5 will die after 10 minutes, but a pH of 6.5 is sufficient to kill cells after 6 hours.[226-229] Direct effects of intracellular acidosis on protein structure are thought to mediate cellular injury and resemble the histological changes observed during ischaemia.[228, 230] The degree of acidosis that can cause direct injury requires both hyperglycaemia and complete ischaemia, and therefore acidosis is unlikely to be the primary mechanism to mediate cellular injury following ischaemia in most patients.[227]

Acidosis may exacerbate ischaemic injury at less severe degrees of acidosis than are required for direct injury by the activation of acid-sensing ion channels and the influx of calcium into cells.[231-233] Inhibition of such processes has been suggested as a neuroprotective target.[234, 235] For this reason, intracellular acidosis following bioenergetic failure may not only be a biomarker of metabolic stress, but also provide a therapeutic target.[234, 235]

In contrast, it is not clear whether alkalosis has a causal relationship with delayed cellular injury or is just a biomarker associated with it. Alkalosis has been observed in glial cells the context of cortical spreading depression without ischaemia.[135, 236] Alkalosis correlates with the degree of electrical activity, and although the mechanisms and implications are not well understood the contribution of spreading depolarizations to neuronal injury may explain the association of alkalosis with delayed ischaemic injury.[236, 237]

1.3. *Clinical studies*

Magnetic resonance spectroscopy (MRS) has been used to investigate the metabolism of human stroke within single voxels. Phosphorus MRS allows pH and concentrations of high energy phosphate to be measured in stroke, although without spatial resolution.[93, 238] Within the first 24 hours, acidosis has been observed within the ischaemic hemisphere, and is associated with a reduction in ATP and rise in phosphate.[93] This acidosis normalised over the first few days. At later time points following stroke onset (chronic ischaemia, 3 to 14 days) alkalosis has been measured with reductions in both phosphocreatine and ATP concentrations.[238]

Hydrogen MRS has been used to measure lactate in stroke using a multivoxel technique and with some spatial resolution (1cm^3 voxels).[92, 94] Lactate, which is not detected in health, has been measured both before and after the appearance of DWI changes although its relationship with pH has not always been clear in the experimental setting.[215]

Whilst MRS does not provide the clinically meaningful spatial resolution called for by Astrup *et al*.,[18] the chemical exchange saturation technique, APT MRI does give metabolic information with spatial resolution similar to perfusion imaging techniques.[67]

pH-weighted imaging using amide proton transfer has been developed for use in acute stroke and has demonstrated a contrast in signal between ischaemic and healthy tissue.[96, 239] However, in these studies the degree of metabolic disturbance and the association with tissue outcome has not been demonstrated.

1.4. *Aims*

In this Chapter, the model-based APT ratio (APTR*)[96, 97] was used to quantify the dynamics of pH-weighted signal within the first 24 hours. The potential of using pH-weighted imaging as a metabolic biomarker in acute human stroke was explored at a tissue and patient level.

The aims of this Chapter were:

- In health, to determine the repeatability of pH-weighted imaging between individuals and within individuals over time;
- To investigate the pattern of pH-weighted signal within the ischaemic hemisphere regions of interest;
- To investigate the temporal dynamics of the pH-weighted signal within regions of interest;
- To explore the additive value pH-weighted imaging may be able to provide as a metabolic biomarker.

2. Methods

2.1. *Healthy volunteers, patients and data quality*

Six healthy volunteers underwent four repeated CEST image acquisitions at 3 time points as described in Chapter 3. All patients recruited into the large volume imaging protocol were included in the qualitative assessment of patient data integrity. Patients were included in quantitative analyses if there was non-corrupt CEST data available and there were the required lesions with which to define the ROIs.

All images were inspected by a clinician (GH) and assessed for quality. Images were judged to be of good quality if there was an absence of artefact or significant uncorrected motion.

2.2. *Image acquisition*

pH-weighted images were acquired by estimating APT effect using single-slice CEST echo planar imaging (TR = 5000ms, TE = 28ms, voxel size = 3.0×3.0×5.0mm up to and including patient 12; TR = 5000ms, TE = 23ms, voxel size = 3.4×3.4×5.0mm from patient 13 onwards) localized to the lesion on DWI. The CEST preparation consisted of a 2s train of 50 Gaussian pulses (flip angle=184°, power= 0.55μT, duration=20ms, delay time=20ms) over 32 frequency offsets with a sampling schedule from -4.5 to 4.5ppm.[96, 240] Up to and including patient 12 had an evenly distributed sampling schedule (-4.5ppm to 4.5ppm with increments of 0.3ppm, and 300ppm). From patient 13 onwards an optimized sampling schedule was used with data collection focussed on the region of the z-spectrum relating to the APT effect (-300, -50, -30, -4.1, -3.8, -3.5, -3.2, -2.9, -0.9, -0.6, -0.3, 0, 0.3, 0.6, 0.9, 2.9, 3.1, 3.2, 3.3, 3.4, 3.4, 3.5, 3.5, 3.6, 3.6, 3.7, 3.8, 3.9, 4.1, 30, 50, 300ppm). Total acquisition time was 2 minutes 45 seconds.

2.3. *APTR**

APTR* is a metric combining the effect of amide-proton exchange rate, which is directly related to pH, and concentration of amide-bearing molecules. Low APTR* values represent intracellular acidosis. APTR* does not rely upon data from saturation frequencies on the opposite site of the water resonance as a reference unlike conventional APTR, avoiding changes that might occur in ischaemia unrelated to pH, such as B_0 inhomogeneity.[97] APTR* is more homogenous than APTR in healthy subjects, and in acute stroke patients is optimized to produce better contrast-to-noise ratio between ischaemic and normal tissue.[96]

APTR* is derived from model-based analysis of the APT z-spectrum and controls for the effects of B_0 inhomogeneity, T1 and T2. APTR* is calculated using the fitted model parameters from a 3-pool exchange model:

$$APTR^* = \frac{S_w(3.5ppm) - S_{w+a}(3.5ppm)}{M_{w0}}$$

Where S refers to the simulated signal at 3.5 ppm using the fitted model parameters, subscripts w and w+a refer to water pool and both water and amide pools, and M_{w0} is the fitted unsaturated signal. The 3-pool exchange model used for the data fitting was water, amide and asymmetry magnetization transfer. The third pool represents a combination of the saturation effect observed at the negative frequency offsets and the conventional magnetization transfer.[97, 98]

2.4. *Image processing*

Perfusion images were processed using a nonlinear fit to the general ASL kinetic model for all voxels within a brain mask to quantify CBF as described in Chapter 5.[177, 178]

Within and between scan registrations of image volumes was by means of rigid body and non-linear registration respectively as described in Chapter 4.[131, 133]

CEST imaging was retrospectively motion corrected using the in-built MATLAB tool before pH-weighted signal was quantified using APTR*.[96, 97] The unprocessed CEST image was registered to the corresponding structural T1-weighted image slice, to which it was aligned at time of acquisition, using the 2D registration schedule within FSL.[131] Accuracy of registration was checked by a clinician (GH). The registration matrix was inverted, and the masks and image slices were registered from structural to CEST image space.

2.5. *Regions of interest*

Volunteer and patient regions of interest (ROIs) used in this analysis are described in Chapters 3 and 4. The specific patient ROIs used in this analysis are ischaemic core, early and late infarct growth, radiographic recovery, diffusion lesion pseudonormalization, and oligaemic regions. Oligaemic regions are those within the presenting perfusion deficit (as defined in Chapter 5) that survive. Whichever was larger of the contralateral perfusion deficit and contralateral final infarct was used as the contralateral ROI.

Grey and white matter partial volume estimates were generated from the T1-weighted structural image and the appropriate slice selected.[146] Masks were translated from native image space to the presenting structural image before registration into CEST image space. These masks were then thresholded and composite masks were generated according to the definitions outlined in Chapter 3 and 4.

2.6. *Data extraction and analysis*

Absolute APTR* was extracted from the healthy volunteer and contralateral patient ROIs to determine the variability of the normal signal within and between individuals. Repeatability was quantified using the coefficient of variation (standard deviation ÷ mean). Relative APTR* was used as the pH-weighted signal in the ischaemic hemisphere rather than absolute APTR* to minimise the effect of individual variability on the results.[96] Voxel-wise analysis used the pooled weighted mean of acute relative APTR* within each ROI mask. Patient level data were also extracted and presented for each ROI with the associated confidence estimates. Serial data were extracted over the first 24 hours to estimate the dynamics of relative APTR*. Statistical tests used were unpaired t-tests for direct comparison between the means in the ROIs and ANOVA for multiple ROI comparisons.

Perfusion data were registered to CEST image space for data extraction. CBF values were extracted within a grey matter mask. For investigation of the effect of reperfusion on pH-weighted signal patients were designated as reperfusing if the CBF in the ischaemic ROI was greater than 25ml/100g/min by 24 hours (threshold obtained from Chapter 5).

3. Results

3.1. *Patient details and data quality*

The patient details and demographics can be seen in Table 6.1. 32 patients were prospectively enrolled in this study and underwent CEST imaging, of which 2 had no identifiable lesion on the presenting DWI and transient neurological symptoms so were excluded from further analysis. The artefacts observed were most commonly due to motion (in particular through plane motion, which cannot be corrected retrospectively),

but also included significant partial volume contamination where the selected slice was juxtaposed to a fissure, and fat ringing. This latter artefact was minimized in patient 16 onwards by use of water excitation rather than fat suppression in the CEST pulse sequence.

Patient number	Hemisphere	Sex	Age	NIHSS at presentation	Thrombolysed	Time to presenting scan (hh:mm)	Presenting scan	2 hour scan	24 hour scan
3	L	F	84	3	N	03:25	G	G	G
4	L	M	92	25	Y	02:50	G	G	G
5	R	M	64	3	N	01:41	G	G	G
7	L	F	86	27	N	03:09	G	G	G
9	L	F	88	25	N	02:15	B	B	N
10	R	F	94	15	N	03:20	B	B	B
12	R	F	70	19	Y	02:20	B	N	N
13	L	F	81	21	N	03:25	G	G	G
15	R	M	50	6	Y	03:49	B	B	B
16	L	M	95	19	Y	04:14	G	G	N
17	L	F	91	10	N	04:53	G	G	G
18	L	F	53	13	Y	02:48	G	G	B
19	R	M	57	7	N	01:43	G	G	G
20	R	M	86	2	N	01:46	G	G	G
23	R	F	92	25	N	02:32	B	B	B
25	L	F	68	23	Y	01:00	B	N	B
27	R	F	80	14	Y	09:50	G	N	G
30	L	M	80	3	N	11:06	G	N	B
33	L	F	76	10	Y	02:40	G	G	N
34	L	F	78	9	Y	02:50	G	G	G
35	R	F	66	2	N	16:03	B	N	N
37	L	F	56	7	Y	01:35	G	G	N
41	L	M	71	8	Y	14:36	G	N	G
43	L	M	48	3	N	16:10	G	N	N
44	L	F	103	18	Y	03:10	G	N	G
45	L	M	82	13	Y	03:00	G	B	G
50	L	F	76	25	Y	02:40	B	N	N
51	L	F	76	11	N	11:25	G	N	G
52	R	F	77	2	N	02:15	B	B	B
53	L	M	56	24	N	06:45	G	N	G

Good	21	13	15
Bad	9	6	7
Total	30	19	22
Proportion discarded	30%	32%	32%

Table 6. 1 - Demographic data and scan quality. G = good quality, B = bad quality, N = data unavailable, NIHSS = National Institute for Health Stroke Scale

Representative APTR* images can be seen in Figure 6.2.

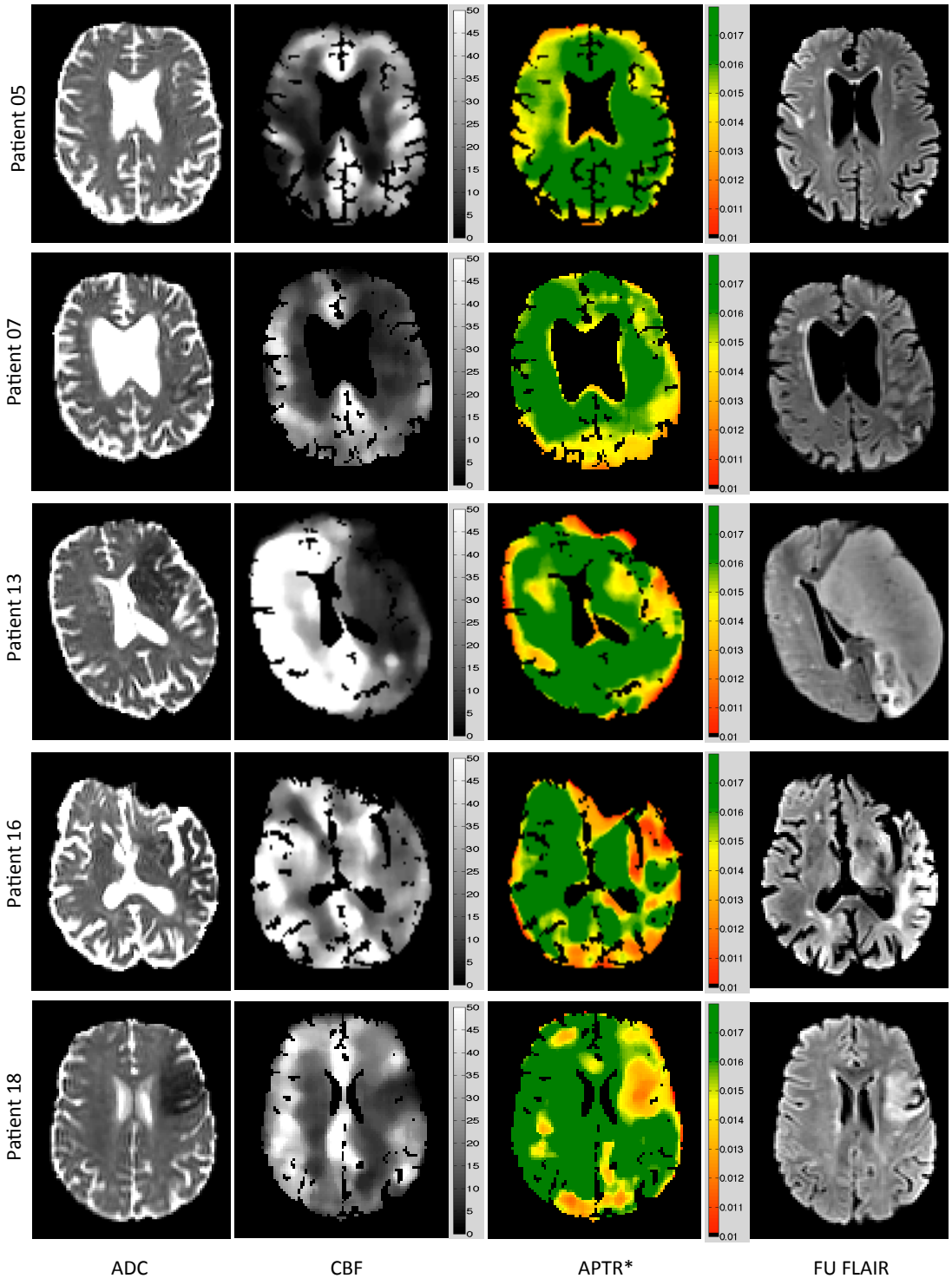

Figure 6. 2 - Representative data from 5 patients. ADC = apparent diffusion coefficient; CBF = cerebral blood flow (scale = ml/100g/min); APTR* = model-based amide proton transfer ratio; FU FLAIR = follow up T2-weighted FLAIR imaging. Adapted from Harston *et al.* 2015.[241]

3.2. *pH-weighted signal in healthy volunteers*

All APTR* images in the healthy volunteers were of sufficient quality for inclusion in the analysis. Within the healthy volunteers there was a coefficient of variation between scans 24 hours apart of 6.1%, and between different volunteers it was 5.0%. Two-way ANOVA of the absolute APTR* data demonstrated a significant variation between volunteers ($p = 0.002$), but not between time points ($p = 0.3$). Data are presented in Figure 6.3.

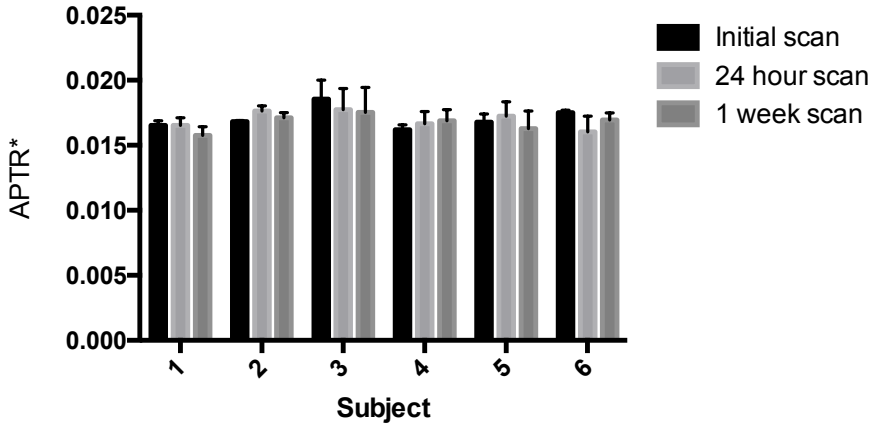

Figure 6. 3 - Normal modified amide proton transfer ratio (APTR*) variation seen within and between individuals

There was a small but statistically significant difference between grey and white matter APTR* values (Table 6.2).

	Mean	SD	Mean difference (GM - WM)	Paired t-test (GM, WM)
All tissue	0.0169	0.00108		
GM	0.0168	0.00106	-2.1%	0.002
WM	0.0172	0.00118		

Table 6. 2 – Mean model-based amide proton transfer ratio (APTR*) in grey matter (GM) and white matter (WM)

3.3. *pH-weighted signal in the contralateral hemispheres of patients*

In the contralateral ROIs of patients the absolute APTR* coefficient of variation between subjects was 8.0%. Within subject variability between presenting and 24 hour scan times had a coefficient of variation of 9.9%. There was no significant variation in contralateral APTR* between patients or scan times (two-way ANOVA, $p = 0.4$ and $p = 0.4$).

3.4. *pH-weighted signal in the ischaemic hemisphere of patients*

Acutely, tissue in the ischaemic core, infarct growth and oligaemic ROIs all demonstrated a reduced weighted mean APTR* (acidosis) relative to the contralateral hemisphere (Figure 6.4, left panel). Ischaemic core tissue has the lowest relative APTR* value (mean ± SD = 0.87 ± 0.20, n = 382) followed by infarct growth (0.93 ± 0.25, n = 875) and then oligaemia (0.98 ± 0.19, n = 1087). These varied significantly (ANOVA, $p < 0.0001$, individual t-test <0.0001 for each comparison). There was no difference in relative APTR* between early and late infarct growth ($p = 0.6$).

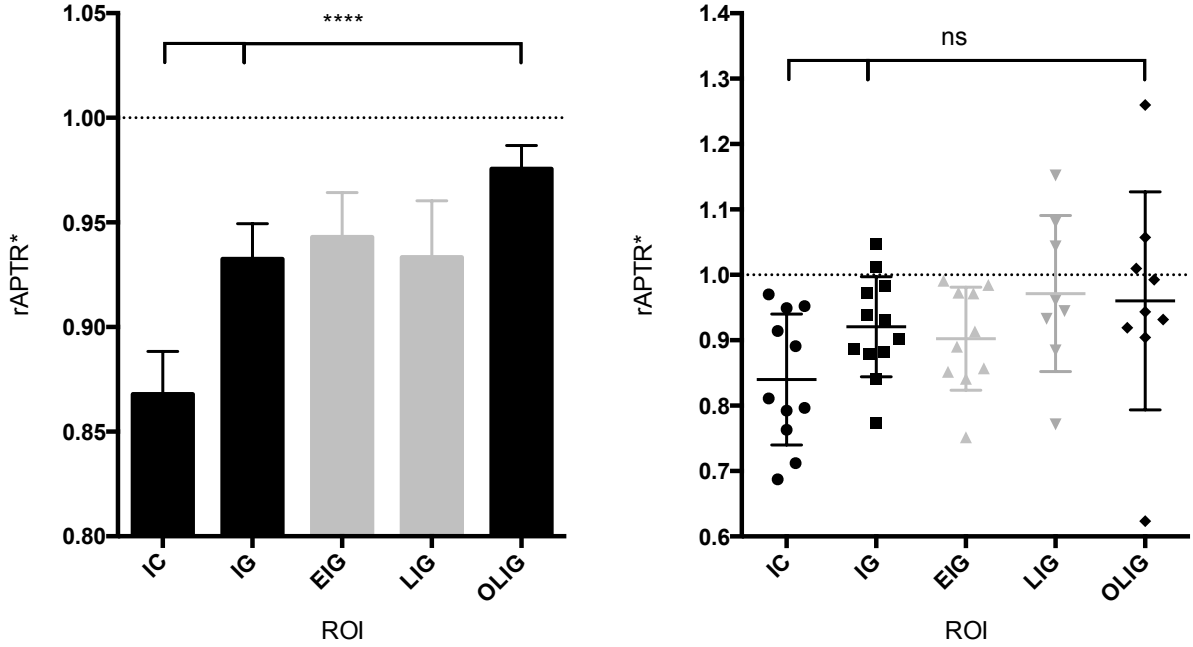

Figure 6. 4 - Left: voxelwise mean relative amide proton transfer ratio (APTR*, error bar = 95% confidence interval) in regions of interest (ROI). Right: patient level APTR* data (error bar = standard deviation). IC = ischaemic core; IG = infarct growth; EIG = early IG; LIG = late IG; OLIG = oligaemic tissue. **** = p<0.0001, ns = not significant (ANOVA).

At a patient level the mean values in the ROIs demonstrated a similar pattern, but the differences failed to reach statistical significance (ANOVA, p = 0.07). Within each ROI there was a range of relative APTR* values with considerable overlap between ROIs (Figure 6.4, right panel).

Using pooled voxel data, within the ischaemic core there was no difference in the relative APTR* between radiographic recovery (0.81 ± 0.26, n = 35) and the ischaemic core (p = 0.1), but there was a significant difference between the tissue of diffusion lesion pseudonormalization (0.80 ± 0.12, n = 60) and the ischaemic core as a whole, with diffusion lesion pseudonormalization having a lower relative APTR* and hence a more acidotic signal (p = 0.02) (Figure 6.5).

3.5. *Contrast-to-noise*

The weighted mean acute contrast-to-noise ratio (CNR) for APTR* within the final infarct was 0.43.

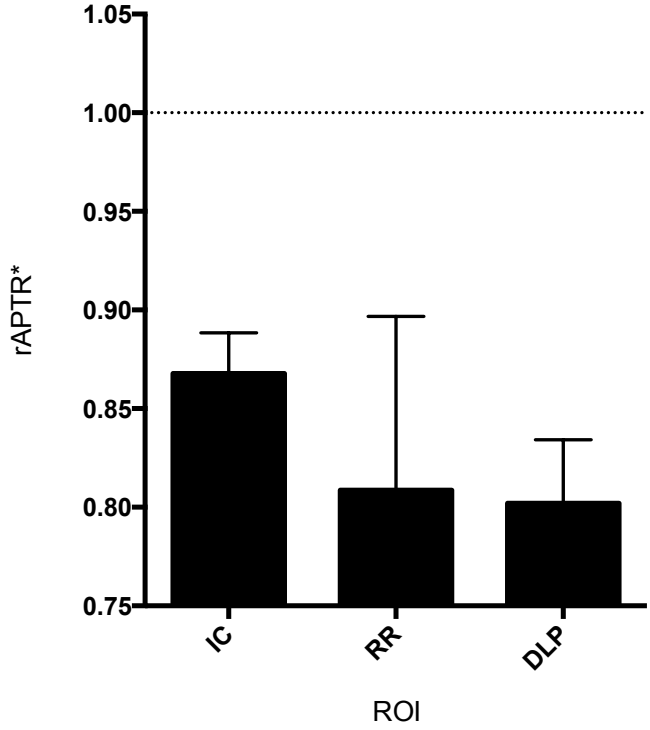

Figure 6. 5 - Voxelwise mean relative amide proton transfer ratio (APTR*, error bar = 95% confidence interval) in regions of interest within the presenting ADC lesion. IC = ischaemic core; RR = radiographic reversal; DLP = diffusion lesion pseudonormalization.

3.6. *pH-weighted signal in the ischaemic grey and white matter*

Grey and white matter responses to ischaemia follow a similar pattern to each other, although the values in white matter are lower than in grey matter in ischaemic core and oligaemic ROIs ($p = 0.008$ and 0.007 respectively) (Figure 6.6). The reduced number of voxels in this analysis generated wider confidence intervals than the combined data, which made it difficult to estimate early and late infarct growth values with accuracy.

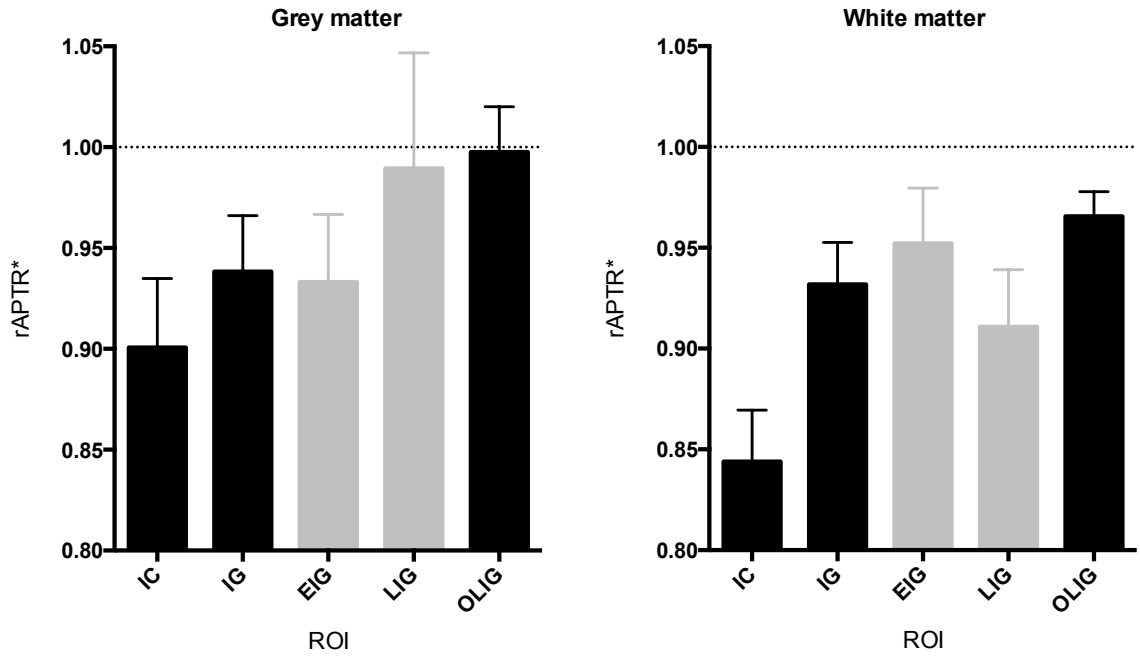

Figure 6. 6 – Voxelwise mean relative amide proton transfer ratio (APTR*) in ROIs restricted to grey and white matter. IC = ischaemic core; IG = infarct growth; EIG = early IG; LIG = late IG; OLIG = oligaemic tissue.

3.7. *Cerebral blood flow*

The pooled mean CBF in the same 2D ROIs used for APTR* analysis, but restricted to the grey matter can be seen in Figure 6.7. The CBF differs significantly between ischaemic core and infarct growth ($p = 0.01$), but is lower in oligaemic tissue than in the infarct growth ROIs.

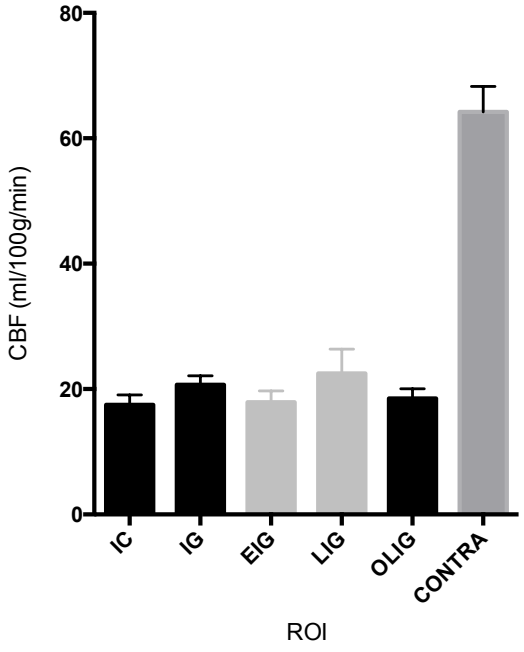

Figure 6. 7 – Voxelwise grey matter cerebral blood flow (CBF, error bars = 95% confidence interval).). IC = ischaemic core; IG = infarct growth; EIG = early IG; LIG = late IG; OLIG = oligaemic tissue; CONTRA = contralateral ROI.

3.8. *Serial pH-weighted imaging analysis*

Serial data within individual patient ROIs can be seen in Figure 6.8. There is a marked heterogeneity of relative APTR* dynamics over time in all ROIs. Within the ischemic core the majority of relative APTR* values remain low until at least the 24 hour scan time. There is one exception (patient 19), who had a transient alkalosis at the 2 hour scan. This patient had also had an unusual clinical presentation: he presented with stable mild symptoms, but deteriorated clinically between the 2 and 24 hour scan times (NIHSS: 2 at presentation, 2 at +2 hour scan, 10 at 24 hour scan). Tissue within the early infarct growth ROIs demonstrates a similar distribution of relative APTR* dynamics to ischaemic core, but with a less severely acidotic signal. Within the late infarct growth ROIs there are several patients who demonstrate elevated APTR* (alkalotic signal) both early and at 24 hours. Oligaemic tissue has predominantly normal relative APTR* over time with a few of individuals who have abnormal relative APTR*

early, all of which normalize by 24 hours. Attempts to categorize the patients by reperfusion status did not explain the dynamics of the relative APTR* signal (Figure 6.9).

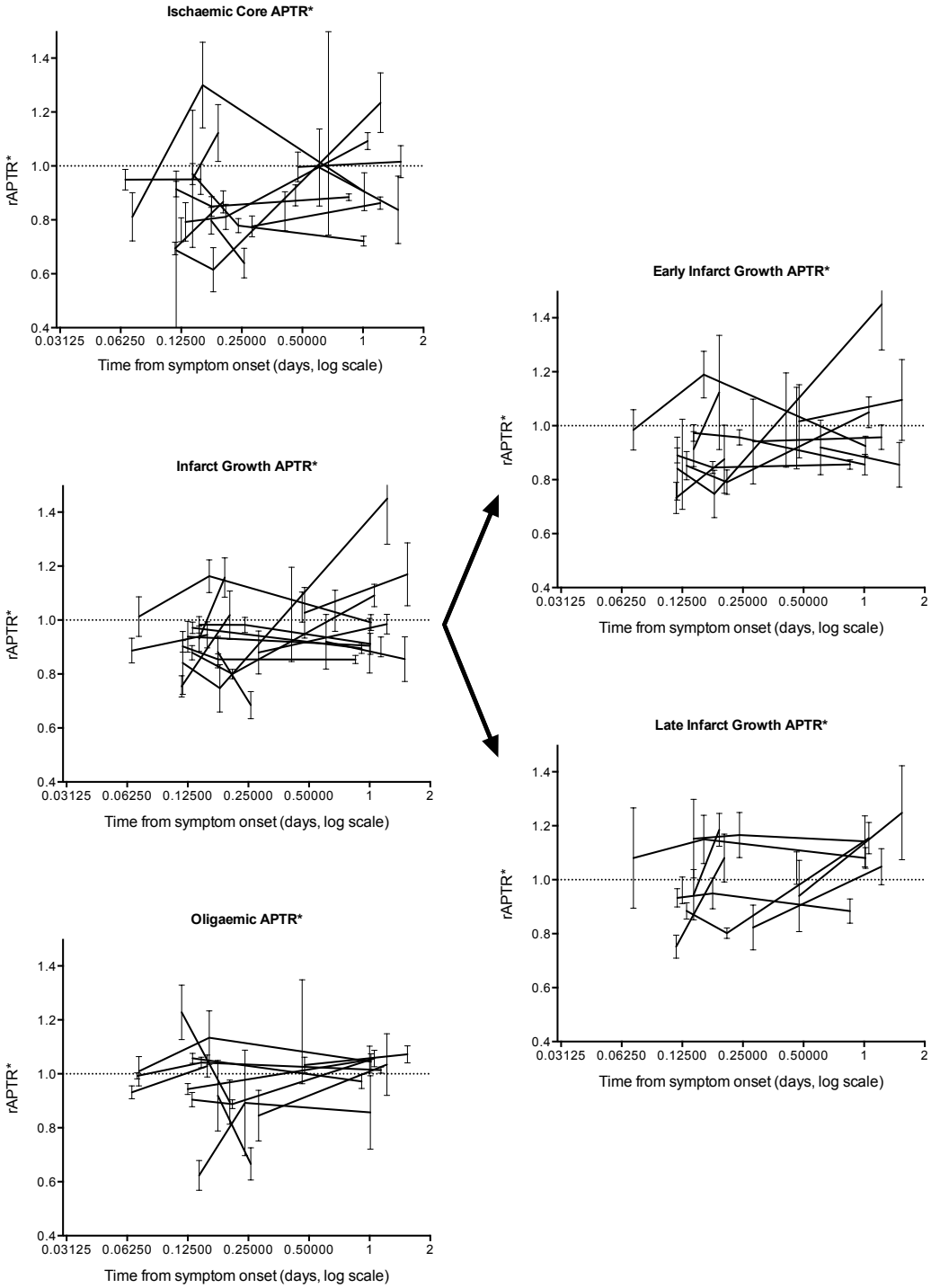

Figure 6. 8– Serial relative amide proton transfer ratio (APTR*, error bars = 95% confidence intervals) over time in individual patients divided into regions of interest.

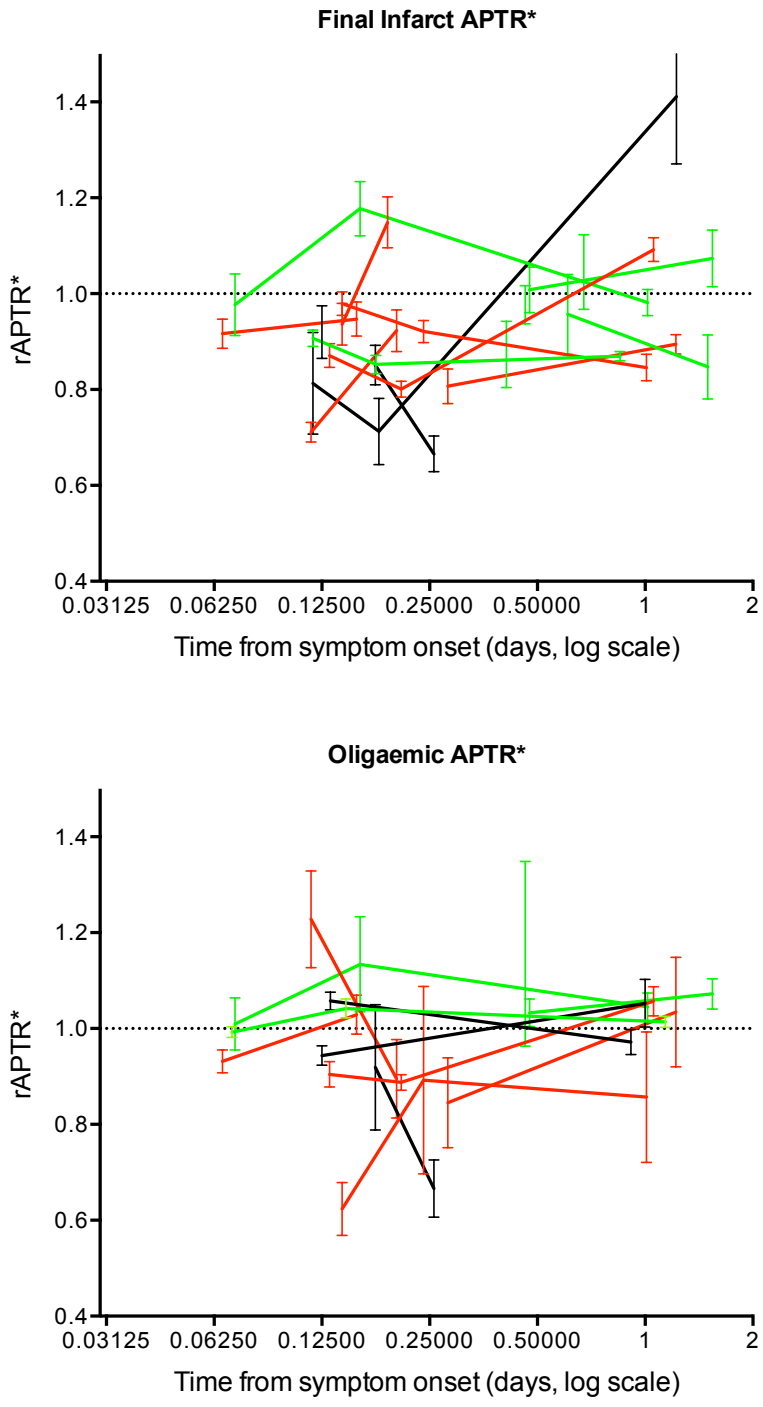

Figure 6. 9 - Serial relative amide proton transfer ratio (APTR*, error bars = 95% confidence intervals) over time in individual patients divided into tissue that survives (oligaemic) and tissue that infarcts (final infarct). Green lines = reperfusion, red lines = no reperfusion, black lines = reperfusion status unknown.

4. Discussion

These data establish the proof of principle that pH-weighted imaging can provide complementary metabolic information in the context of acute ischaemic stroke. This Chapter builds on previous work to optimise the generation of a pH-weighted signal to show that intracellular pH at presentation is significantly associated with final tissue outcome.[96, 239, 242, 243] pH-weighted imaging provides complementary information to existing perfusion and DWI sequences in a clinical setting and the dynamics of this metabolic biomarker may give insight into the pathophysiology of acute stroke.

4.1. *Repeatability*

The data from healthy volunteers and contralateral hemispheres of patients show that APTR* gives repeatable values within individuals with a variation at least as good as CBF (Chapter 5). Although the variation in APTR* seen between the contralateral hemisphere of patients is greater than between healthy volunteers, it is still comparable to CBF variations. The increased variability in patients may be due to the influence of partial volume effects at the surface of the brain secondary to a greater degree of atrophy in the patient cohort. APTR* is particularly sensitive to effects of partial volume because of the low amide concentration in cerebrospinal fluid.

Despite the relatively good repeatability of absolute APTR* within and between patients the low CNR made relative APTR* preferable for pooled analysis and comparisons over time. Although the contralateral hemisphere can exhibit abnormal blood flow (diaschisis) following stroke this is not thought to be pathological and no evidence of this was seen in Chapter 5.[244-246] Therefore, diaschisis is unlikely to cause the critical metabolic disruption required to produce an abnormal pH in the contralateral hemisphere.

4.2. *Ischaemia*

The acute data show a biologically plausible signal of intracellular acidosis associated with final tissue outcome. The ischaemic core is more acidotic than tissue that is subsequently recruited to the final infarct. Tissue within the oligaemic ROI that ultimately does not infarct is significantly less acidotic than either ischaemic core or infarct growth. Interestingly, between early and late infarct growth there was no difference in mean relative APTR*, supporting the hypothesis that the injury that becomes apparent after 24 hours is due to radiographic insensitivity of trace DWI at 24 hours to infarction, rather than the presence of persisting ischaemic penumbra at this time point.

pH-weighted MRI provides an insight into ADC lesion reversal, which has variously been reported at 0 to 83% of the presenting ADC lesion.[142] Within the ADC lesion there were few voxels that were defined as radiographic reversal (i.e. genuine recovery) and so confident estimation of the signal in these ROIs was not possible. However, regions of diffusion lesion pseudonormalization demonstrated a more severe acidosis than the ischaemic core as a whole. This supports the observation of lower perfusion in this region (Chapter 5) and suggests a more severe metabolic stress that leads to early necrosis and cell lysis, vasogenic oedema, and the resulting reduction in barriers to diffusion by 24 hours.[111] This would corroborate the PET imaging finding that there is heterogeneity of metabolism within the ADC lesion and that this appears to be linked to ADC reversal.[157]

There is variability in the degree of APTR* abnormality in ROIs at the level of the individual patient, comparable to that seen with measures of CBF. There are several explanations for this. Firstly, the variety of pathophysiological processes that mediate

cell death may have different metabolic effects, but share the same ultimate radiographic fate. Secondly, the ROIs within individuals may have different responses to ischaemia or resilience to metabolic disturbance. Finally, noise at the level of the individual may explain some of the variation especially when the ROIs contain few voxels. The variability in the ischaemic regions makes the use of pH-weighted imaging alone to define tissue state unrealistic, but rather supports its integration with other imaging modalities in the investigation of stroke pathophysiology.

Comparison of relative APTR* with CBF in the ROIs supports the additive role of pH-weighted imaging as a metabolic biomarker. Whilst ischaemic core is both less well perfused and more acidotic than infarct growth, it is APTR* and not CBF that distinguishes viable from non-viable tissue within the perfusion deficit. This comparison does adversely penalise the ability of CBF to distinguish this tissue (oligaemic tissue by definition has low CBF and some of the infarct growth voxels may have early reperfusion), but nonetheless it highlights the potential value of using a metabolic biomarker in addition to perfusion data. Furthermore, for tissue where CBF is difficult to measure reliably, i.e. white matter, pH-weighted imaging can provide useful information about tissue fate.[82, 86]

In healthy volunteers it was confirmed that there is little difference between healthy grey and white matter APTR* values,[96] and importantly the data in patients showed that there was a similar pattern of pH-weighted signal responses to ischaemia. Grey matter and white matter have different constituent cells and metabolism, which would explain the slightly different magnitudes of response in different ROIs.

4.3. *Dynamic pH-weighted signal changes*

The serial measurements of relative APTR* in individuals reflected the heterogeneity and graduated severity of acidosis seen in the acute data, but also showed several temporal patterns that are worth examining. The ischaemic core ROIs were predominantly acidotic acutely, with a heterogeneous response by 24 hours. Given that this tissue was infarcted at presentation the subsequent metabolic pattern would not have affected the outcome. The severe and persistent acidosis in many of the ischaemic core ROIs is consistent with ATP hydrolysis following energy failure in cells.

Infarct growth ROIs were less severely acidotic acutely than infarct core, and the majority of regions demonstrated disrupted metabolism, either an acidosis or an alkalosis, at 24 hours. Whether this was an acidosis or alkalosis was associated with the timing of appearance of radiographic injury, i.e. early or late infarct growth. Late infarct growth ROIs tended to be alkalotic at 24 hours and were often also alkalotic at the 2 hour imaging time. In contrast, early infarct growth regions were more commonly acidotic over the 24 hours. This difference in pH dynamics is likely to reflect different pathophysiological mechanisms of tissue injury, which underlie the different timings of infarction defined on conventional imaging. The association of alkalosis with delayed appearance of tissue injury is consistent with the preclinical data that showed alkalosis in tissue that was less severely ischaemic than infarct core, but nonetheless went on to infarct.[225]

The oligaemic ROIs were either of normal pH or acidotic acutely, and all had normal pH-weighted signal by 24 hours, demonstrating recovery of metabolism in tissue that survives. Oligaemic ROIs represent both benign oligaemia and ischaemic penumbra. ROIs consisting of predominantly benign oligaemia may explain those regions showing

persistently normal metabolism over 24 hours, and those consisting of salvaged penumbra may explain the regions with abnormal metabolism acutely that recovers by 24 hours.

The effect of reperfusion on pH-weighted signal dynamics is not clear from these data. Categorizing patients by reperfusion status does not reliably bring out any patterns. This may be due to a combination of the dynamic nature of perfusion, and different perfusion thresholds and mechanisms of injury in different tissues. Reperfusion may even exacerbate injury and metabolic stress in some instances.[21] Finally, the heterogeneity of perfusion dynamics demonstrated in Chapter 5 means that creating binary groups according to reperfusion status is probably an oversimplification of the pathology of stroke.

4.4. *Limitations*

pH-weighted imaging does not require contrast (e.g. gadolinium) or exogenous stimulus (e.g. inhaled gases), can derive a signal from both grey and white matter, and appears to add a metabolic dimension to conventional MRI techniques. However, further work is required to develop this technique and explore its interpretation.

The sequence used in this study generates a single slice image, but 3D sequences would allow extensive investigation of the signal in different tissues remote from the plane of the diffusion lesion. 3D imaging would improve image registration, and would be a prerequisite for clinical use. Developing the sequence and postprocessing techniques might improve the signal to noise ratio, allowing smaller voxels and therefore fewer artefacts from the effects of partial volume. Like other MRI techniques the CEST sequence is susceptible to motion. Although these artefacts could be corrected post hoc

if a 3D sequence were employed, a prospective motion correction strategy would be preferable.

pH-weighted imaging generates a relatively low ischaemic contrast-to-noise ratio compared to CBF, similar in magnitude to the variability between scan times and patients. For this reason a relative pH-weighted signal was used in this analysis, but if noise could be reduced then absolute APTR* could be used for comparison. This would be of use in defining regions by pH-weighted signal at presentation rather than defining ROIs using other modalities. Additionally, better understanding of certain physiological parameters (e.g. amide proton concentration) would mean that an absolute pH value could be generated from the APTR* value.[96] This would allow comparison with preclinical models that use invasive measures of pH, and improved definition of the physiological processes that the pH-weighted signal is identifying.

In this analysis the variations in the rate of APT were assumed to be predominantly due to differences in pH. Care was taken to interpret the signal under conditions where this assumption is likely to hold true (i.e. acutely after ischaemic onset and using APTR* as a quantification metric).[96, 97] However, at later time points the assumption that APTR* is solely pH dependent becomes less valid. T1 and T2 effects are likely to increasingly influence APTR* despite the modeling, and the concentration of amide may change (although this is known to be constant in the first few hours following ischaemia).[67] Future, larger studies will allow the interaction of the pH-weighted signal with physiological (e.g. glucose, temperature), treatment, and imaging (e.g. perfusion dynamics) parameters to be investigated.

5. Conclusions

Measuring amide proton transfer allows the exploration of serial pH-weighted signal in acute stroke within different tissue types. pH-weighted imaging may have a role in improving the imaging definition of ischaemic penumbra, and may also be useful in understanding regional vulnerability and secondary injury, addressing an unmet need of MRI biomarkers in acute stroke.[206] In addition, given that pH is a physiological parameter that can be manipulated, pH-weighted imaging has the potential to meet the criteria of a Treatment-Relevant Acute Imaging Target.[58] These data strongly support the further investigation of pH-weighted imaging in patients with acute ischaemic stroke. pH-weighted imaging may fulfil the criteria of a clinically pragmatic metabolic imaging biomarker to complement perfusion imaging in the identification of the ischaemic penumbra.[18]

Chapter 7: Summary and Conclusions

The broad aim of this thesis was to investigate the pathophysiology of acute ischaemic stroke using serial MRI measurements in a cohort of patients. A combination of structural, perfusion and metabolic MRI biomarkers were used to rigorously characterize the pathophysiological processes at a tissue level over time.

1. Summary

In Chapter 2, studies using imaging biomarkers in acute stroke trials were systematically reviewed to determine the state of imaging biomarkers and what insight they have provided in the past. It was shown that there has been varied and inconsistent use of imaging modality, timing, thresholds, and definitions, when using imaging biomarkers as treatment modifiers or to assess efficacy. No imaging biomarker has consistently been shown to select patients that might benefit from intervention in randomized trials, leaving time from onset as the only consistent treatment modifier used in clinical practice.[55] When penumbral biomarkers have been used to select patients, perfusion imaging alone has been used to identify the tissue at risk threshold, without reference to metabolism as originally called for by Astrup *et al.*[18]

In Chapter 4 the framework within which imaging biomarkers would be assessed was developed. Optimum methodology for defining infarction was determined and the timing of the appearance of infarction was explored using conventional MRI techniques. ROIs were defined to interpret the serial data in the subsequent Chapters. Using these ROIs the natural history of the diffusion-weighted imaging signal, specifically ADC, was interrogated. It was shown that diffusion signal changes at different times reflect different processes. Normalization of ADC at 24 hours was shown to be a pseudonormalization rather than tissue recovery. In Chapter 5 and 6 this

diffusion lesion pseudonormalization ROI was shown to be more severely hypoperfused and more acidotic acutely, thus likely to represent more severe ischaemia than the remainder of the ischaemic core. Other ROIs defined in this Chapter included early and late infarct growth. It was shown that trace DWI at 24 hours does not represent the final infarction and that approximately half of the total infarct growth occurs after 24 hours.

In Chapter 5, CBF was measured using multiple post labeling delay (PLD) vessel-encoded pseudocontinuous arterial spin labeling (VEPCASL). This perfusion imaging technique allowed serial measures of CBF to be taken and the arrival times of the blood to be calculated. Calculating the arrival time of blood supported the validity of using ASL to measure perfusion in stroke and provided evidence for the use of a 2.0s single post labeling delay in imaging patients.[82] Acutely, the degree of hypoperfusion correlated with the severity of ischaemic injury. However, the subsequent dynamics of perfusion were heterogeneous, and tissue fate within individuals could not be explained by CBF dynamics alone.

In Chapter 6, the use of pH-weighted imaging, using amide proton transfer, was explored. Acutely, pH-weighted imaging demonstrated a biologically plausible graduated intracellular acidosis across ROIs, and unlike CBF there was a consistent signal in both grey and white matter. The observed acidosis reflected preclinical data and clinical MRI spectroscopy studies that have demonstrated an acidosis acutely following ischaemia. The serial pH-weighted signal also provided an insight into the pathophysiology of the different ROIs. The ischaemic core was most severely acidotic acutely, which often persisted at 24 hours. Infarct growth was less severely acidotic acutely and tended to be either alkalotic or acidotic at 24 hours. Subdividing infarct growth into early and late showed that late infarct growth ROIs were often alkalotic,

particularly at 24 hours. This is consistent with preclinical data that has shown an association of delayed injury with intracellular alkalosis.[223, 224, 247] Oligaemic tissue, that by definition survives, consistently had normal pH, and by inference metabolism, at 24 hours even if there had been an acidosis acutely.

2. General considerations

2.1. *MRI biomarkers in acute stroke*

As discussed in Chapter 1, imaging biomarkers can be used either as a research tool to investigate pathophysiology, identify treatment targets and assess efficacy in proof of principle studies, or as a clinical tool to guide treatment decisions, inform prognosis and assess efficacy of interventions. This thesis shows that serial MRI has the potential to provide a wealth of biological information, non-invasively, regarding the physical and biological properties of the brain following acute stroke. Specifically, the results support the use of serial, multimodal image acquisition to interrogate the pathophysiological processes and add dimensions to the assessment of tissue state.

2.1.1. *Penumbral imaging*

pH-weighted imaging can provide a metabolic perspective to complement perfusion and diffusion-weighted imaging. Such an approach resonates with the original definition of the ischaemic penumbra,[18] and these results should encourage the development of other metabolically derived signals in stroke imaging research. Perfusion imaging at a single time point provides a snapshot of a dynamic process and it is inherently limited without insight into the preceding severity and duration of hypoperfusion. Even with serial data perfusion is not sufficient to explain tissue outcome. Metabolic imaging may add to perfusion imaging by providing information about the ischaemic stress a region of tissue has experienced, reflecting the accrued metabolic stress of the cells. For example,

severely hypoperfused tissue with normal metabolism might reflect tissue with a brief reversible ischaemia, whereas mildly hypoperfused tissue with severe metabolic disruption may represent tissue with prolonged ischaemia that is less likely to recover. Metabolic imaging may also identify delayed injurious processes (for example by finding alkalotic regions), identifying treatment targets amenable to intervention beyond the acute time point. The findings in this thesis would suggest that metabolic imaging may improve definition of ischaemic penumbra acutely, and highlight ongoing injury that might be amenable to intervention.

2.1.2. *Infarct definition*

Metabolic imaging could refine the definition of the ischaemic core. In Chapter 4, some of the limitations of diffusion-weighted imaging are identified. Diffusion changes represent distinct biological processes at different time points, and even within the same patient diffusion characteristics can have different implications in remote regions. In common with some other studies the results do not support the presence of clinically significant volumes of brain with restricted diffusion that can survive.[111, 143] However, the results do challenge whether restricted diffusion, with or without T2-weighted signal change (i.e. trace DWI), is sufficient to define infarction. The apparent infarct growth of the trace DWI lesion beyond 24 hours may reflect either ongoing injurious processes or a delayed appearance of radiographic injury even at 24 hours. Whilst DWI techniques appear to be reasonably specific in defining infarction, it should not be assumed that DWI is completely sensitive. Metabolic imaging may be able to identify regions of brain beyond the restricted diffusion that are also ischaemic core.

The pH-weighted signal in the ischaemic core was severely acidotic acutely and within the region of diffusion lesion pseudonormalization the acidosis was particularly

pronounced. Diffusion lesion pseudonormalization is likely to be explained by both necrosis and vasogenic oedema. Proactively investigating the early dynamic metabolism of the ischaemic core could provide insight into the likelihood of developing malignant oedema. Treatments aimed at alleviating the metabolic stresses that result in oedema would not only offset the need for surgical decompression, but may also help prevent subacute clinical deterioration in those patients with smaller infarcts.

2.1.3. *Heterogeneity*

There is marked heterogeneity of pathophysiology between and within patients. Although patterns can be seen at a tissue level acutely, between patients the individual data are heterogeneous and the temporal dynamics are diverse. Within individual patients, there are multiple regions with distinct perfusion and metabolic profiles that result in discrete patterns of ischaemic injury. This observation may underlie the difficulty of trying to group patients for treatment using what are likely to be oversimplifications of the range of pathophysiological processes observed. Such an observation suggests the need for more complex imaging stratification, a move that is likely delay times to treatment initiation and make it even harder to observe treatment benefits.

2.1.4. *Clinical use*

To use MRI in routine clinical practice for acute stroke requires not only that the sequences are capable of selecting patients who benefit from intervention, but also that the sequences generate interpretable 3D imaging, without significant data loss from artefact, in a short period of time. Given the imperative for prompt treatment, for MRI to become clinically useful in selecting patients it must be much quicker in both acquisition and processing. The sequences investigated as part of this thesis do not

currently meet these criteria. Specific challenges to overcome prior to clinical use are discussed below and include contrast-to-noise ratios and susceptibility to artefact.

2.2. *Technical considerations*

2.2.1. *Contrast-to-noise ratios*

In order to be used clinically, ROIs defined using imaging biomarkers need to be created *a priori.* In this thesis, the biomarkers under investigation have been framed according to the tissue outcome, in order to study their biological properties. However, if the biomarkers are to be used *a priori* adequate CNR is required to define tissue regions. In Chapter 3, ROIs were defined on follow up imaging using conventional MRI sequences (T2-weighted FLAIR and trace DWI) and these had CNRs in the range of 1.9 to 7.0. Although the inter-rater agreements were generally good, even with these CNRs there was some disagreement between raters. For CBF and APTR* acutely, the CNRs were 1.03 and 0.43 respectively, much lower than those of the follow up imaging. Whilst VEPCASL generated a greater CNR than APT, this is limited to grey matter analysis, which further limits its utility in *a priori* tissue definition.

Low CNRs are an inherent limitation to using either ASL or APT MRI as a clinically useful treatment modifier. Both techniques rely on small signals: for ASL this is a 1-2% signal change due to the influx of radiolabelled blood and for APT this is a small diminution in the water signal from a rate change in exchange between amide groups and water. This leaves little scope for enhancing the signal. Minimizing noise is equally challenging because this would require longer imaging times or larger voxels, neither of which are clinically pragmatic.

2.2.2. *Motion artefact*

The longer the duration of a scan the less tolerable it is to an acutely unwell patient and the greater the risk of motion artefact. MRI takes longer to acquire than CT imaging and therefore is susceptible to motion artefact in a patient cohort. *Post hoc* motion correction can reduce the data loss due to motion, and such techniques were employed for the sequences used in this thesis. However, not all motion can be corrected, and approximately 20% of the acute VEPCASL and APT data were lost because of motion. This occurred despite efforts to optimize the scanning environment to minimize motion, including attention to patient comfort and direct supervision of the patient during the scan. Scanning times were kept to a minimum, but short scanning times reduce signal to noise ratios and require larger voxels, thus exacerbating the problems of partial volume.

2.2.3. *Effects of partial volume*

Partial volume effects occur when multiple categories of tissue exist in a single voxel. The voxel is ascribed one tissue type, but other less prevalent types within the voxel will still influence the signal within it. This contamination may be from tissue with a different fate or from tissues with different properties, such as grey and white matter, and CSF. The greater the volume of each voxel, the greater the likelihood of partial volume contamination. In patients, the effects of partial volume are particularly pronounced with regards to grey and white matter: with age and cerebrovascular disease there is cortical thinning resulting in fewer voxels with predominantly grey matter content. Generating smaller voxels takes more time or leads to a reduction in the signal-to-noise ratio. Both of these are detrimental to the study design and so a compromise must be reached.

2.2.4. *Spatial resolution*

In all imaging studies spatial resolution is restricted to the macroscopic scale and it is not possible to discern responses of different cell types to ischaemia using MRI. Mean measurements are taken for each voxel as a whole and there is no capacity to dissect the responses of different cell types. This results in voxels, and the clusters of voxels that form the ROIs, being assigned to a single category, but they may represent different proportions of cell types and fates. For example, selective neuronal loss is known to occur outside the macroscopic infarct and has been identified using flumazenil PET scanning.[36, 160] In this study, such a tissue fate would have been labeled as surviving tissue.

There is evidence from experimental literature that there is a microscopic spatial heterogeneity of pathophysiology, not related to cell type, below the resolution of MRI.[32, 209] This level of spatial detail can only be explored in preclinical models, but it is important to account for this when interpreting clinical data. Further subtlety may be lost by the effects of partial volume that can lead to underestimation of a signal in a small region. Aside from the limitations of individual imaging biomarkers spatial resolution is an inherent limitation of using MRI to investigate pathophysiology.

2.3. *Study limitations*

These data are potentially subject to bias from patient dropout and loss to follow up. Despite best efforts to ensure all patients could return for follow up, death, clinical deterioration, and patient preference all accounted for some loss of follow up data. Patients with more severe strokes are less likely to return for imaging and, therefore, those with follow up data are a biased group.

The number of patients in this study precluded the incorporation of patient level factors into the interpretation of the data. Clinical factors such as sex, blood pressure, and diabetes mellitus have not been used in the analysis, as the sample size is too small to generate meaningfully sized subgroups. Larger studies would permit this level of analysis.

In order to draw conclusions data were pooled into subgroups such as the acute data (within 6 hours of symptom onset). Whilst this creates homogeneous grouping it is unlikely that the degree and duration of ischaemia for all patients will have been similar. It is impossible to know the fluctuations in perfusion prior to arrival at hospital or the exact time of onset for every patient. This may account for some of the variability between patients in addition to other factors such as sex, genetic profile and prior exposure to ischaemia.

3. Future work

In addition to the requirements for validating the findings of this thesis in an independent cohort and investigating the characteristics in larger groups, there are several specific areas that are worth further study.

3.1. *Clinical correlation*

The analyses in this thesis are tissue based, using a framework defined by presenting and follow up imaging. As recruitment continues and patient numbers increase it will be important to investigate the patient factors that influence the biomarkers, and to correlate the changes in the imaging biomarkers with clinically meaningful outcomes. Such analyses would allow the evaluation of the imaging biomarkers as surrogates that have the potential to inform clinical or research practice.[51]

3.2. *Motion correction*

Motion artefact affects all imaging modalities, but is a particular problem in MRI due to the long imaging times and the sensitivity to noise. *Post hoc* techniques can correct for some of this error, but other data are lost. Prospective motion correction is an appealing strategy to correct for motion as the data is acquired.[248] This would be of particular benefit in 2D image acquisition, for which through plane movement cannot be corrected retrospectively.

3.3. *Oedema*

In Chapter 3, optimal image registration was achieved using non-linear registration algorithms to correct for distortions due to oedema. Using this technique the degree of distortion relative to presentation was estimated. Such an approach might provide useful information to quantify oedema at 24 hours and predict the likelihood of clinical deterioration in the context of malignant middle cerebral artery syndrome. This information could be tested in helping clinical decision making surrounding hemicraniectomy, and would meet the definition of a TRAIT, were it to be validated prospectively.

3.4. *Arterial spin labeling*

In Chapter 5, the relationship of CBF to tissue outcome was investigated. At a patient level, there was heterogeneity of the reperfusion dynamics that suggested a more complex relationship of reperfusion with vessel status than a binary recanalization versus no recanalization. If angiographic data was acquired serially, VEPCASL could be used to explore the factors that influence microvascular perfusion following recanalization, including the effect of collateral blood flow from the other vascular territories of the main feeding vessels. Further, by labeling inflowing blood distal to the

Circle of Willis more subtle collateral blood flow dynamics could be described. Other aspects of VEPCASL development might include improvements in signal generation in the white matter, which has recently been developed in healthy volunteers.[87]

3.5. *Chemical exchange saturation transfer*

In order to develop the CEST sequence for pH-weighted imaging several improvements are required. Firstly, it is necessary to develop a 3D sequence rather than the 2D slice used in this thesis. This would necessitate longer image acquisition times, but these would be in the region of 5 minutes and therefore remain clinically pragmatic. Improvements in CNR are also required if tissue is to be defined by its metabolic profile *a priori.* Although improvement in contrast might be possible were the spectral resolution to be improved, there is a biological limit to the contrast seen. Noise reduction in the sequence and minimization of artefact would also increase the CNR. Strategies to achieve this would include use of higher magnetic field strengths, incorporation prospective motion correction, and development of the model analysis for APTR* to better model the non-APT mediated effects on the observed signal. Were these developments to be successfully implemented, APTR* could meet the criteria for a TRAIT, with potential to act as a biomarker for both acute and delayed ischaemic injury.

Another area that warrants further work is exploration of signal remote from the APT effect in the CEST z-spectrum, such as the nuclear Overhauser enhancement effect that may provide information regarding changes in protein structures within the cells.[249] Such information would allow insight into mechanisms of cell injury and infarction in acute stroke.

4. Closing remarks

The work in this thesis is the first attempt to use serial perfusion imaging, using ASL-derived absolute CBF, and metabolic imaging, using APT-derived pH-weighted imaging, to explore the dynamics of the pathophysiology of acute stroke in patients. This approach is akin to that proposed by Astrup *et al*., in the original definition of the ischaemic penumbra.[18] The complexity and heterogeneity of the pathophysiological processes have been highlighted, and the potential utility of using pH-weighted imaging to elucidate these processes, in addition to perfusion imaging, has been demonstrated. Better understanding of the pathophysiology of acute stroke has the potential to identify novel treatment targets, improve the definition of pathologies within individual patients, and to select patients who will benefit from an intervention. This work represents a proof of concept that requires development and validation in independent cohorts of patients, but nonetheless provides some explanation for the challenges of using imaging biomarkers patients with acute ischaemic stroke.

Appendix A: Example Search Strategy used in Chapter 2

Example search strategy (MEDLINE via Ovid)

1. Randomized Controlled Trials as Topic/
2. randomized controlled trial/
3. Random Allocation/
4. Double Blind Method/
5. Single Blind Method/
6. clinical trial/
7. clinical trial, phase i.pt.
8. clinical trial, phase ii.pt.
9. clinical trial, phase iii.pt.
10. clinical trial, phase iv.pt.
11. controlled clinical trial.pt.
12. randomized controlled trial.pt.
13. multicenter study.pt.
14. clinical trial.pt.
15. exp Clinical Trials as topic/
16. or/1-15
17. (clinical adj trial$).tw.
18. ((singl$ or doubl$ or treb$ or tripl$) adj (blind$3 or mask$3)).tw.
19. PLACEBOS/
20. placebo$.tw.
21. randomly allocated.tw.
22. (allocated adj2 random$).tw.
23. or/17-22
24. 16 or 23
25. case report.mp.
26. letter/
27. historical article/
28. or/25-27
29. 24 not 28
30. exp Tomography, Emission Computed/ or exp Magnetic Resonance Imaging/ or brain imaging.af.
31. (ct or dwi).af.
32. imaging.af.
33. (perfusion or diffusion).af.
34. magnetic resonance imag$.af.
35. mri.af.
36. computed tomograph$.af.
37. pet.af.
38. spect.af.
39. exp Tomography, X-Ray Computed/
40. or/30-39
41. Cerebrovascular disorders/
42. exp Brain ischemia/
43. Carotid artery diseases/ or Carotid artery thrombosis/
44. stroke/ or exp brain infarction/
45. exp Hypoxia-ischemia, brain/
46. Cerebral arterial diseases/ or Intracranial arterial diseases/
47. exp Intracranial embolism/ and thrombosis/
48. (stroke$ or apoplex$ or cerebral vasc$ or cerebrovasc$ or cva or transient isch?emic attack$ or tia$).mp.
49. (brain or cerebr$ or cerebell$ or vertebrobasil$ or hemispher$ or intracran$ or intracerebral or infratentorial or supratentorial or middle cerebr$ or mca$ or anterior circulation).mp.
50. (isch?emi$ or infarct$ or thrombo$ or emboli$ or occlus$ or hypoxi$).mp.
51. 49 and 50
52. 41 or 42 or 43 or 44 or 45 or 46 or 47 or 48 or 51
53. 29 and 40 and 52
54. limit 53 to (english language and humans and yr="1995 -Current" and "all adult (19 plus years)")

Appendix B: Studies included in Chapter 2

1. Randomised controlled trial of streptokinase, aspirin, and combination of both in treatment of acute ischaemic stroke. Multicentre Acute Stroke Trial--Italy (MAST-I) Group. Lancet. 1995;346(8989):1509-1514.
2. Hacke W, Kaste M, Fieschi C, et al. Intravenous thrombolysis with recombinant tissue plasminogen activator for acute hemispheric stroke. The European Cooperative Acute Stroke Study (ECASS). JAMA. 1995;274(13):1017-1025.
3. Infeld B, Davis SM, Donnan GA, et al. Streptokinase increases luxury perfusion after stroke. Stroke. 1996;27(9):1524-1529.
4. Generalized efficacy of t-PA for acute stroke. Subgroup analysis of the NINDS t-PA Stroke Trial. Stroke. 1997;28(11):2119-2125.
5. Chen ZM. CAST: Randomised placebo-controlled trial of early aspirin use in 20,000 patients with acute ischaemic stroke. Lancet. 1997;349(9066):1641-1649.
6. Clark WM, Warach SJ, Pettigrew LC, Gammans RE, Sabounjian LA. A randomized dose-response trial of citicoline in acute ischemic stroke patients. Citicoline Stroke Study Group. Neurology. 1997;49(3):671-678.
7. De Deyn PP, De Reuck J, Deberdt W, Vlietinck R, Orgogozo JM, Raoult B. Treatment of acute ischemic stroke with piracetam. Stroke. 1997;28(12):2347-2352.
8. del Zoppo GJ, Higashida RT, Furlan AJ, Pessin MS, Rowley HA, Gent M. PROACT: a phase II randomized trial of recombinant pro-urokinase by direct arterial delivery in acute middle cerebral artery stroke. PROACT Investigators. Prolyse in Acute Cerebral Thromboembolism. Stroke. 1998;29(1):4-11.
9. Hacke W, Kaste M, Fieschi C, et al. Randomised double-blind placebo-controlled trial of thrombolytic therapy with intravenous alteplase in acute ischaemic stroke (ECASS II). Second European-Australasian Acute Stroke Study Investigators. Lancet. 1998;352(9136):1245-1251.
10. Yasaka M, O'Keefe GJ, Chambers BR, et al. Streptokinase in acute stroke: Effect on reperfusion and recanalization. Neurology. 1998;50(3):626-632.
11. Berrouschot J, Barthel H, Koster J, et al. Extracorporeal rheopheresis in the treatment of acute ischemic stroke: A randomized pilot study. Stroke. 1999;30(4):787-792.
12. Clark WM, Williams BJ, Selzer KA, Zweifler RM, Sabounjian LA, Gammans RE. A randomized efficacy trial of citicoline in patients with acute ischemic stroke. Stroke. 1999;30(12):2592-2597.
13. Clark WM, Wissman S, Albers GW, Jhamandas JH, Madden KP, Hamilton S. Recombinant tissue-type plasminogen activator (Alteplase) for ischemic stroke 3 to 5 hours after symptom onset. The ATLANTIS Study: a randomized controlled trial. Alteplase Thrombolysis for Acute Noninterventional Therapy in Ischemic Stroke. JAMA. 1999;282(21):2019-2026.
14. Furlan A, Higashida R, Wechsler L, et al. Intra-arterial prourokinase for acute ischemic stroke. The PROACT II study: a randomized controlled trial. Prolyse in Acute Cerebral Thromboembolism. JAMA. 1999;282(21):2003-2011.

15. Infeld B, Davis SM, Donnan GA, et al. Nimodipine and perfusion changes after stroke. Stroke. 1999;30(7):1417-1423.
16. Manelfe C, Larrue V, von Kummer R, et al. Association of hyperdense middle cerebral artery sign with clinical outcome in patients treated with tissue plasminogen activator. Stroke. 1999;30(4):769-772.
17. Ogawa A, Yoshimoto T, Kikuchi H, et al. Ebselen in acute middle cerebral artery occlusion: a placebo-controlled, double-blind clinical trial. Cerebrovasc Dis. 1999;9(2):112-118.
18. Pantano P, Caramia F, Bozzao L, Dieler C, von Kummer R. Delayed increase in infarct volume after cerebral ischemia: correlations with thrombolytic treatment and clinical outcome. Stroke. 1999;30(3):502-507.
19. Effect of intravenous recombinant tissue plasminogen activator on ischemic stroke lesion size measured by computed tomography. NINDS; The National Institute of Neurological Disorders and Stroke (NINDS) rt-PA Stroke Study Group. Stroke. 2000;31(12):2912-2919.
20. Broderick JP, Lu M, Kothari R, et al. Finding the most powerful measures of the effectiveness of tissue plasminogen activator in the NINDS tPA stroke trial. Stroke. 2000;31(10):2335-2341.
21. Fogelholm R, Erila T, Palomaki H, Murros K, Kaste M. Effect of nimodipine on final infarct volume after acute ischemic stroke. Cerebrovasc Dis. 2000;10(3):189-193.
22. Warach S, Pettigrew LC, Dashe JF, et al. Effect of citicoline on ischemic lesions as measured by diffusion-weighted magnetic resonance imaging. Citicoline 010 Investigators. Ann. Neurol. 2000;48(5):713-722.
23. Clark WM, Wechsler LR, Sabounjian LA, Schwiderski UE. A phase III randomized efficacy trial of 2000 mg citicoline in acute ischemic stroke patients. Neurology. 2001;57(9):1595-1602.
24. Derex L, Tomsick TA, Brott TG, et al. Outcome of stroke patients without angiographically revealed arterial occlusion within four hours of symptom onset. Am J Neuroradiol. 2001;22(4):685-690.
25. Diener HC, Ringelstein EB, von Kummer R, et al. Treatment of acute ischemic stroke with the low-molecular-weight heparin certoparin: results of the TOPAS trial. Therapy of Patients With Acute Stroke (TOPAS) Investigators. Stroke. 2001;32(1):22-29.
26. Grotta J, Trial I. Combination therapy stroke trial: Recombinant tissue-type plasminogen activator with/without lubeluzole. Cerebrovasc Dis. 2001;12(3):258-263.
27. Patel SC, Levine SR, Tilley BC, et al. Lack of clinical significance of early ischemic changes on computed tomography in acute stroke. JAMA. 2001;286(22):2830-2838.
28. Gilligan AK, Markus R, Read S, et al. Baseline blood pressure but not early computed tomography changes predicts major hemorrhage after streptokinase in acute ischemic stroke. Stroke. 2002;33(9):2236-2242.
29. Lyden P, Shuaib A, Ng K, et al. Clomethiazole acute stroke study in ischemic stroke (CLASS-I): Final results. Stroke. 2002;33(1):122-128.

30. Roberts HC, Dillon WP, Furlan AJ, et al. Computed tomographic findings in patients undergoing intra-arterial thrombolysis for acute ischemic stroke due to middle cerebral artery occlusion: results from the PROACT II trial. Stroke. 2002;33(6):1557-1565.
31. Hill MD, Rowley HA, Adler F, et al. Selection of acute ischemic stroke patients for intra-arterial thrombolysis with pro-urokinase by using ASPECTS. Stroke. 2003;34(8):1925-1931.
32. Wechsler LR, Roberts R, Furlan AJ, et al. Factors influencing outcome and treatment effect in PROACT II. Stroke. 2003;34(5):1224-1229.
33. Alexandrov AV, Molina CA, Grotta JC, et al. Ultrasound-enhanced systemic thrombolysis for acute ischemic stroke. N Engl J Med. 2004;351(21):2170-2178.
34. De Georgia MA, Krieger DW, Abou-Chebl A, et al. Cooling for Acute Ischemic Brain Damage (COOL AID): a feasibility trial of endovascular cooling. Neurology. 2004;63(2):312-317.
35. Abciximab Emergent Stroke Treatment Trial I. Emergency administration of abciximab for treatment of patients with acute ischemic stroke: results of a randomized phase 2 trial. Stroke. 2005;36(4):880-890.
36. Daffertshofer M, Gass A, Ringleb P, et al. Transcranial low-frequency ultrasound-mediated thrombolysis in brain ischemia: increased risk of hemorrhage with combined ultrasound and tissue plasminogen activator: results of a phase II clinical trial. Stroke. 2005;36(7):1441-1446.
37. Demchuk AM, Hill MD, Barber PA, Silver B, Patel SC, Levine SR. Importance of early ischemic computed tomography changes using ASPECTS in NINDS rtPA Stroke Study. Stroke. 2005;36(10):2110-2115.
38. Emsley HCA, Smith CJ, Georgiou RF, et al. A randomised phase II study of interleukin-1 receptor antagonist in acute stroke patients. J Neurol Neurosur Ps. 2005;76(10):1366-1372.
39. Hacke W, Albers G, Al-Rawi Y, et al. The Desmoteplase in Acute Ischemic Stroke Trial (DIAS): A phase II MRI-based 9-hour window acute stroke thrombolysis trial with intravenous desmoteplase. Stroke. 2005;36(1):66-73.
40. Levine SR, Broderick JP, Brott T, et al. Recombinant tissue plasminogen activator for minor strokes: The National Institute of Neurological Disorders and Stroke rt-PA Stroke Study experience. Ann Emerg Med. 2005;46(3):243-252.
41. Singhal AB, Banner T, Roccatagliata L, et al. A pilot study of normobaric oxygen therapy in acute ischemic stroke. Stroke. 2005;36(4):797-802.
42. Dzialowski I, Hill MD, Coutts SB, et al. Extent of early ischemic changes on computed tomography (CT) before thrombolysis: prognostic value of the Alberta Stroke Program Early CT Score in ECASS II. Stroke. 2006;37(4):973-978.
43. Els T, Oehm E, Voigt S, Klisch J, Hetzel A, Kassubek J. Safety and therapeutical benefit of hemicraniectomy combined with mild hypothermia in comparison with hemicraniectomy alone in patients with malignant ischemic stroke. Cerebrovasc Dis. 2006;21(1-2):79-85.

44. Furlan AJ, Eyding D, Albers GW, et al. Dose Escalation of Desmoteplase for Acute Ischemic Stroke (DEDAS): Evidence of safety and efficacy 3 to 9 hours after stroke onset. Stroke. 2006;37(5):1227-1231.
45. Hennerici MG, Kay R, Bogousslavsky J, Lenzi GL, Verstraete M, Orgogozo JM. Intravenous ancrod for acute ischaemic stroke in the European Stroke Treatment with Ancrod Trial: a randomised controlled trial. Lancet. 2006;368(9550):1871-1878.
46. Warach S, Kaufman D, Chiu D, et al. Effect of the glycine antagonist gavestinel on cerebral infarcts in acute stroke patients, a randomized placebo-controlled trial: The GAIN MRI substudy. Cerebrovasc Dis. 2006;21(1-2):106-111.
47. Shin DH, Moon GJ, Bang OY. Albumin therapy in acute stroke patients. J Neurol. 2007;254(7):870-878.
48. Vahedi K, Vicaut E, Mateo J, et al. Sequential-design, multicenter, randomized, controlled trial of early decompressive craniectomy in malignant middle cerebral artery infarction (DECIMAL Trial). Stroke. 2007;38(9):2506-2517.
49. Wong KS, Chen C, Ng PW, et al. Low-molecular-weight heparin compared with aspirin for the treatment of acute ischaemic stroke in Asian patients with large artery occlusive disease: a randomised study. Lancet Neurol. 2007;6(5):407-413.
50. Adams HP, Effron MB, Torner J, et al. Emergency Administration of Abciximab for Treatment of Patients With Acute Ischemic Stroke: Results of an International Phase III Trial. Stroke. 2008;39(1):87-99.
51. Alexandrov AV, Mikulik R, Ribo M, et al. A pilot randomized clinical safety study of sonothrombolysis augmentation with ultrasound-activated perflutren-lipid microspheres for acute ischemic stroke. Stroke. 2008;39(5):1464-1469.
52. Davis SM, Donnan GA, Parsons MW, et al. Effects of alteplase beyond 3 h after stroke in the Echoplanar Imaging Thrombolytic Evaluation Trial (EPITHET): a placebo-controlled randomised trial. Lancet Neurol. 2008;7(4):299-309.
53. Hacke W, Kaste M, Bluhmki E, et al. Thrombolysis with alteplase 3 to 4.5 hours after acute ischemic stroke. N Engl J Med. 2008;359(13):1317-1329.
54. Nichols C, Khoury J, Brott T, Broderick J. Intravenous recombinant tissue plasminogen activator improves arterial recanalization rates and reduces infarct volumes in patients with hyperdense artery sign on baseline computed tomography. J Stroke Cerebrovasc. 2008;17(2):64-68.
55. Ebinger M, Iwanaga T, Prosser JF, et al. Clinical-diffusion mismatch and benefit from thrombolysis 3 to 6 hours after acute stroke. Stroke. 2009;40(7):2572-2574.
56. Ehrenreich H, Weissenborn K, Prange H, et al. Recombinant human erythropoietin in the treatment of acute ischemic stroke. Stroke. 2009;40(12):e647-e656.
57. Hacke W, Furlan AJ, Al-Rawi Y, et al. Intravenous desmoteplase in patients with acute ischaemic stroke selected by MRI perfusion-diffusion weighted imaging or perfusion CT (DIAS-2): a prospective, randomised, double-blind, placebo-controlled study. Lancet Neurol. 2009;8(2):141-150.
58. Kidwell CS, Lees KR, Muir KW, et al. Results of the MRI substudy of the intravenous magnesium efficacy in stroke trial. Stroke. 2009;40(5):1704-1709.

59. Molina CA, Barreto AD, Tsivgoulis G, et al. Transcranial ultrasound in clinical sonothrombolysis (TUCSON) trial. Ann. Neurol. 2009;66(1):28-38.
60. Sen S, Huang DY, Akhavan O, Wilson S, Verro P, Solander S. IV vs. IA TPA in acute ischemic stroke with CT angiographic evidence of major vessel occlusion: a feasibility study. Neurocrit Care. 2009;11(1):76-81.
61. Teal P, Davis S, Hacke W, et al. A Randomized, Double-Blind, Placebo-Controlled Trial to Evaluate the Efficacy, Safety, Tolerability, and Pharmacokinetic/Pharmacodynamic Effects of a Targeted Exposure of Intravenous Repinotan in Patients With Acute Ischemic Stroke. Stroke. 2009;40(11):3518-3525.
62. Thijs VNS, Peeters A, Vosko M, et al. Randomized, placebo-controlled, dose-ranging clinical trial of intravenous microplasmin in patients with acute ischemic stroke. Stroke. 2009;40(12):3789-3795.
63. Chemmanam T, Campbell BC, Christensen S, et al. Ischemic diffusion lesion reversal is uncommon and rarely alters perfusion-diffusion mismatch. Neurology. 2010;75(12):1040-1047.
64. De Silva DA, Brekenfeld C, Ebinger M, et al. The benefits of intravenous thrombolysis relate to the site of baseline arterial occlusion in the Echoplanar Imaging Thrombolytic Evaluation Trial (EPITHET). Stroke. 2010;41(2):295-299.
65. McCormick M, Hadley D, McLean JR, Macfarlane JA, Condon B, Muir KW. Randomized, controlled trial of insulin for acute poststroke hyperglycemia. Ann Neurol. 2010;67(5):570-578.
66. Parsons MW, Christensen S, McElduff P, et al. Pretreatment diffusion- and perfusion-MR lesion volumes have a crucial influence on clinical response to stroke thrombolysis. J Cerebr Blood F Met. 2010;30(6):1214-1225.
67. Schabitz WR, Laage R, Vogt G, et al. AXIS: a trial of intravenous granulocyte colony-stimulating factor in acute ischemic stroke. Stroke. 2010;41(11):2545-2551.
68. Bi M, Ma Q, Zhang S, et al. Local mild hypothermia with thrombolysis for acute ischemic stroke within a 6-h window. Clin Neurol Neurosur. 2011;113(9):768-773.
69. Nagakane Y, Christensen S, Brekenfeld C, et al. EPITHET: Positive Result After Reanalysis Using Baseline Diffusion-Weighted Imaging/Perfusion-Weighted Imaging Co-Registration. Stroke. 2011;42(1):59-64.
70. Shuaib A, Bornstein NM, Diener H-C, et al. Partial aortic occlusion for cerebral perfusion augmentation: safety and efficacy of NeuroFlo in Acute Ischemic Stroke trial.[Erratum appears in Stroke. 2011 Nov;42(11):e632-3]. Stroke. 2011;42(6):1680-1690.
71. Michel P, Ntaios G, Reichhart M, et al. Perfusion-CT guided intravenous thrombolysis in patients with unknown-onset stroke: A randomized, double-blind, placebo-controlled, pilot feasibility trial. Neuroradiology. 2012;54(6):579-588.
72. Nagakane Y, Christensen S, Ogata T, et al. Moving beyond a single perfusion threshold to define penumbra: A novel probabilistic mismatch definition. Stroke. 2012;43(6):1548-1555.
73. Padma Srivastava MV, Bhasin A, Bhatia R, et al. Efficacy of minocycline in acute ischemic stroke: A single-blinded, placebo-controlled trial. Neurology India. 2012;60(1):23-28.

74. Parsons M, Spratt N, Bivard A, et al. A randomized trial of tenecteplase versus alteplase for acute ischemic stroke. N Engl J Med. 2012;366(12):1099-1107.
75. Rosso C, Corvol JC, Pires C, et al. Intensive versus subcutaneous insulin in patients with hyperacute stroke: Results from the randomized INSULINFARCT trial. Stroke. 2012;43(9):2343-2349.
76. Warach S, Al-Rawi Y, Furlan AJ, et al. Refinement of the magnetic resonance diffusion-perfusion mismatch concept for thrombolytic patient selection: insights from the desmoteplase in acute stroke trials. Stroke. 2012;43(9):2313-2318.
77. Broderick JP, Palesch YY, Demchuk AM, et al. Endovascular therapy after intravenous t-PA versus t-PA alone for stroke. N Engl J Med. 2013;368(10):893-903.
78. Ciccone A, Valvassori L, Nichelatti M, et al. Endovascular treatment for acute ischemic stroke. N Engl J Med. 2013;368(10):904-913.
79. Gui QF, Yang YM, Ying SH, Zhang MM. Xueshuantong improves cerebral blood perfusion in elderly patients with lacunar infarction. Neural Regen Res. 2013;8(9):792-801.
80. Kasner SE, Rose DZ, Skokan A, et al. Transcranial laser therapy and infarct volume. Stroke. 2013;44(7):2025-2027.
81. Kidwell CS, Jahan R, Gornbein J, et al. A trial of imaging selection and endovascular treatment for ischemic stroke. N Engl J Med. 2013;368(10):914-923.
82. Ringelstein EB, Thijs V, Norrving B, et al. Granulocyte colony-stimulating factor in patients with acute ischemic stroke results of the Ax200 for ischemic stroke trial. Stroke. 2013;44(10):2681-2687.
83. Hill MD, Demchuk AM, Goyal M, et al. Alberta stroke program early computed tomography score to select patients for endovascular treatment interventional management of stroke (IMS)-III trial. Stroke. 2014;45(2):444-449.
84. Hougaard KD, Hjort N, Zeidler D, et al. Remote ischemic perconditioning as an adjunct therapy to thrombolysis in patients with acute ischemic stroke: A randomized trial. Stroke. 2014;45(1):159-167.

Appendix C: Studies using Imaging as Eligibility Criteria

Author (year)	Intervention	No. of participants	Modality	Criterion
Hacke (1995)	Alteplase	620	CT	<1/3 MCA territory
Clark (1997)	Citicoline	259	CT	No evidence of cerebral oedema
De Deyn (1997)	Piracetam	927	CT	No mass effect with midline shift
Del Zoppo (1998)	IA pro-urokinase	46	CT	No mass effect with midline shift
			DSA	TIMI 0/1 (M1/M2)
Hacke (1998)	Alteplase	800	CT	<1/3 MCA territory
Berrouschot (1999)	Rheopheresis	33	CT	<1/3 MCA territory
			SPECT	Activity deficit
Clark (1999)	Citicoline	394	CT	No brainstem or cerebellar infarction
Clark (1999)	Alteplase	613	CT	<1/3 MCA territory
Furlan (1999)	IA pro-urokinase	180	CT	<1/3 MCA territory
			DSA	TIMI 0/1 (M1/M2 MCA)
Ogawa (1999)	Ebselen	105	CT	No low density
			DSA	M1 or M2 MCA occlusion
Warach (2000)	Citicoline	100	MRI	Requires >1ml, <66ml involving grey matter in MCA territory (DWI)
Clark (2001)	Citicoline	899	CT	No evidence of cerebral oedema
Diener (2001)	Certoparin	404	CT	<1/3 MCA territory
Grotta (2001)	Lubeluzole	89	CT	<1/3 MCA territory
Alexandrov (2004)	TCD	126	TCD	TIBI 0-3 (MCA)
AbESTT inv (2005)	Abciximab	400	CT	<1/2 MCA territory
Daffertshofer (2005)	TCD	26	MRI	DWI lesion present and exclude if complete MCA infarction
			MRA	Vascular obstruction on MRA
Hacke (2005)	Desmoteplase	104	MRI	<1/3 MCA territory (DWI)
			MRA	Exclude ICA occlusion without ipsilateral distal occlusion
			MRP	Diffusion-perfusion mismatch
Singhal (2005)	Normobaric oxygen	16	MRP	Diffusion-perfusion mismatch
Els (2006)	Hypothermia (HC pts)	25	MRP	Diffusion-perfusion mismatch
Furlan (2006)	Desmoteplase	37	MRP	Diffusion-perfusion mismatch
Hennerici (2006)	Ancrod	1222	CT	<1/3 MCA territory
Warach (2006)	Gavestinel	106	MRI	Requires >1.5cm diameter or >5ml (DWI)
Shin (2007)	Albumin	49	MRI	DWI lesion in MCA territory
Vahedi (2007)	Hemicraniectomy	38	MRI	Requires >145ml (DWI)
Wong (2007)	Heparin (nadroparin)	353	Carotid duplex / TCD / MRA	Moderate large artery occlusive disease
Adams (2008)	Abciximab	808	CT	<1/2 MCA territory
Alexandrov (2008)	Microspheres (with TCD)	15	TCD	TIBI 0-3 (MCA)
Davis (2008)	Alteplase	101	CT	<1/3 MCA territory
Hacke (2008)	Alteplase	821	CT	<1/3 MCA territory
Ehrenreich (2009)	EPO	522	MRI	DWI lesion and FLAIR negative
Hacke (2009)	Desmoteplase	193	MRI/CT	<1/3 MCA territory (DWI or CT)
			MRA/CTA	Exclude ICA occlusion
			MRP/CTP	Diffusion-perfusion mismatch

Author (year)	Intervention	No. of participants	Modality	Criterion
Kidwell (2009)	Magnesium	90	MRI	Requires >5ml, later 3ml (DWI)
Molina (2009)	TCD + microspheres	35	TCD	TIBI 0-3 (MCA/ACA/PCA/ICA/BA)
Sen (2009)	IA Alteplase	7	CT	<1/3 MCA territory
			CTA	Major vessel occlusion
Teal (2009)	Repinotan	681	CT	<1/3 MCA territory
Thijs (2009)	Microplasmin	40	CT	<1/3 MCA territory
			MRP	PWI >2cm diameter
Schabitz (2010)	G-CSF	44	MRI	<2/3 MCA (DWI) and non-lacunar infarct
			MRA	No carotid-T occlusion
			MRP	Diffusion-perfusion mismatch
Bi (2011)	Hypothermia	93	MRP	Diffusion-perfusion mismatch
Shuaib (2011)	NeuroFlo	515	CT	<1/3 MCA territory
Michel (2012)	IV tPA	12	CTP	Favorable CTP profile
			CTA	Occluded extracranial ICA
Parsons (2012)	Tenecteplase	75	CT	<1/3 MCA territory
			CTA	Vessel occlusion (ACA/MCA/PCA)
			CTP	Diffusion-perfusion mismatch
Rosso (2012)	IV insulin	180	MRI	DWI lesion present
Broderick (2013)	Endovascular treatment	656	CTA	M1/ICA/BA occlusion and NIHSS 8-9
Ciccone (2013)	Endovascular treatment	362	CT	Acute infarction
Gui (2013)	Xueshuantong	64	MRI	DWI lesion <2cm (lacunar infarct)
Hougaard (2014)	Remote Ischaemic Perconditioning	443	MRI	DWI lesion present
Kidwell (2013)	Embolectomy	118	MRA/CTA	Target occlusion
Ringelstein (2013)	G-CSF	328	MRI	DWI lesion >15ml
			MRI	<1/3 MCA territory
			MRI	No mass effect with midline shift
			MRI	Non-lacunar infarct
			MRA	No carotid T occlusion

Key: HC: hemicraniectomy; IA: intra-arterial; TCD: transcranial Doppler ultrasound; EPO: erythropoetin; G-CSF: granulocyte colony stimulating factor; CT(A/P): computed tomography (angiography/perfusion); DSA: digital subtraction angiography; SPECT: single photon emission CT; MRI/A/P: magnetic resonance imaging/angiography/perfusion; TIMI: thrombolysis in myocardial infarction score; MCA: middle cerebral artery; DWI: diffusion-weighted imaging; TIBI: thrombolysis in brain ischaemia; ACA: anterior cerebral artery; PCA: posterior cerebral artery; ICA: internal carotid artery; BA: basilar artery

Appendix D: Studies using Imaging to Assess Outcome

First author	Intervention	Modality	Measure	Timing	Imaging result	Prespecified
NINDS (2000)	Alteplase	CT	Lesion volume	3 months	Neg	N
		CT	Lesion volume	7-10 days	Neg	N
		CT	Lesion volume	24 hours	Pos	N
Alexandrov (2004)	TCD	TCD	Recanalization (TIBI 5)	2 hours	Pos	Y
Berrouschot (1999)	Rheopheresis	CT	Lesion volume	5 days	Neg	Y
		SPECT	Graded SPECT scale	6-8 hours	Neg	Y
		SPECT	Graded SPECT scale	5 days	Neg	Y
Chemmanam (2010)	Alteplase	MRI	% voxels with DWI reversal	3 months	Neg	N
Daffertshofer (2005)	TCD	MRA	Recanalization rate	6-24 hours	Neg	Y
		MRP	Perfusion deficit	6 hours	Neg	Y
		MRI	Lesion volume (DWI)	6 hours	Neg	Y
Davis (2008)	Alteplase	MRI	Geometric mean growth (exponential of mean log relative growth: day 90 T2 / baseline DWI)	3 months	Neg	Y
		MRI	Median relative growth (day 90 T2 / baseline DWI)	3 months	Neg	Y
		MRI	Median absolute growth (day 90 T2 - baseline DWI)	3 months	Neg	Y
		MRI	Mean difference in cube root volumes	3 months	Neg	Y
		MRI	Lesion growth >0% (T2 and baseline DWI)	3 months	Pos	Y
		MRA	Recanalization (>1 point increase in TIMI)	3 months	Neg	Y
		MRP	Reperfusion (>90% of initial deficit, Tmax+2s)	3 months	Pos	Y
De Georgia (2004)	Endovascular cooling	MRI	Lesion growth (day 3-5 DWI /baseline DWI)	3-5 days	Neg	Y
Del Zoppo	IA pro-urokinase	DSA	Recanalization (TIMI 2/3)	2 hours	Pos	Y

(1998)						
Demchuk (2005)	Alteplase	CT	Lesion volume	7-10 days	Neg	N
Diener (2001)	Certoparin	CT	No lesion	7-8 days	Neg	Y
		CT	Lesion volume	7-8 days	Neg	Y
Ebinger (2009)	Alteplase	MRI	Lesion growth (day 3-5 DWI - baseline DWI, median)	3-5 days	Pos	N
		MRI	Lesion growth (day 90 T2 - day 3-5 DWI, median)	90 days	Neg	N
		MRI	Lesion growth (day 90 T2 - baseline DWI, median)	90 days	Pos	N
Ehrenreich (2009)	EPO	MRI	Lesion volume (FLAIR)	7-8 days	Neg	Y
Emsley (2005)	IL-1 receptor antagonist	CT	Lesion volume	5-7 days	Neg	Y
Fogelholm (2000)	Nimodipine	CT	Lesion volume	3 weeks - 3 months (IQR)	Neg	N
Furlan (1999)	IA pro-urokinase	DSA	Recanalization (TIMI 3 or 2/3)	2 hours	Pos	Y
Furlan (2006)	Desmoteplase	MRP/MRA	Reperfusion (>30% reduction in MTT deficit volume) or TIMI 2/3	4-8 hours	Neg	Y
		MRI	Lesion growth (increase in T2-weighted lesion, median)	1 month	Neg	N
Gui (2013)	Xueshuantong	MRP	Change in rCBV	1 month	Neg	Y
		MRP	Change in rCBF	1 month	Neg	Y
		MRP	Change in rMTT	1 month	Neg	Y
Hacke (2005)	Desmoteplase	MRP/MRA	Reperfusion (>30% reduction in MTT deficit volume) or TIMI 2/3	4-8 hours	Neg	Y
		MRI	Lesion growth (day 30 FLAIR - 24 hour DWI)	1 month	Not reported	Y
Hacke (2009)	Desmoteplase	MRI/CT	Lesion growth (day 30 -24 hour, various)	1 month	Neg	Y
Hennerici (2006)	Ancrod	CT	Lesion volume	7-10 days	Neg	Y
Hougaard (2014)	Remote Ischaemic Perconditioning	MRI	Penumbral salvage: (Baseline Tmax 6s volume - DWI lesion) - 1 month FLAIR	1 month	Neg	Y
		MRI	Lesion volume (FLAIR)	1 month	Neg	Y
		MRI	Infarct growth (1 month FLAIR - baseline DWI)	1 month	Neg	Y

		MRI	Baseline DWI volume	Presentation	Neg	Y
		MRI	Baseline PWI volume	Presentation	Neg	Y
Infeld (1996)	Streptokinase	SPECT	Hypoperfusion volume	3 months	Neg	Y
		SPECT	Hypoperfusion volume	1 day	Neg	Y
		SPECT	Early hypoperfusion volume change (24 hours - baseline)	3 months	Neg	Y
		SPECT	Late hypoperfusion volume change (3 months - 24 hours)	3 months	Neg	Y
		SPECT	Early hypoperfusion volume change (3 months - baseline)	3 months	Neg	Y
Infeld (1999)	Nimodipine	SPECT	Hypoperfusion volume	3 months	Neg	Y
		SPECT	Hypoperfusion volume	1 day	Neg	Y
		SPECT	Early hypoperfusion volume change (24 hours - baseline)	3 months	Neg	Y
		SPECT	Late hypoperfusion volume change (3 months - 24 hours)	3 months	Neg	Y
		SPECT	Early hypoperfusion volume change (3 months - baseline)	3 months	Neg	Y
Kasner (2013)	Transcranial laser therapy	MRI/CT	Lesion volume	5 days	Neg	N
		MRI/CT	ASPECTS	5 days	Neg	N
		MRI/CT	cortical ASPECTS	5 days	Neg	N
Kidwell (2009)	Magnesium	MRI	Median absolute growth (day 90 FLAIR - baseline DWI)	3 months	Neg	Y
		MRI	Median relative growth (day 90 FLAIR - baseline DWI)/baseline DWI	3 months	Neg	Y
		MRI	Lesion growth (>0% day 90 FLAIR and baseline DWI)	3 months	Neg	Y
Kidwell (2013)	Embolectomy	MRI/CT	Infarct volume (day 7)	7 days	Neg	Y
		MRI/CT	Infarct growth (day 7-day1)	7 days	Neg	Y
		MRI/CT	Reperfusion >90% (day 7)	7 days	Neg	Y
		MRI/CT	Recanalisation (day 7)	7 days	Neg	Y
Levine (2005)	Alteplase	CT	Lesion volume	7 days	Neg	N
Lyden (2002)	Clomethiazole	CT	Lesion volume	1 month	Neg	Y
McCormick (2010)	Insulin	MRI	Lesion growth (day 7 FLAIR - baseline DWI)	7 days	Neg	Y
		MRI	Lesion volume (FLAIR)	7 days	Neg	Y

		MRS	Lactate	3 days	Pos	Y
		MRS	Lactate	7 days	Neg	Y
Michel (2012)	IV tPA	MRI	Non-infarcted at-risk tissue (day 4)	4 days	Neg	Y
		CTA	Recanalization (24 hours)	24 hours	Neg	Y
Molina (2009)	TCD + microspheres	TCD	Complete recanalization	2 hours	Neg	Y
		TCD	Time to complete recanalization	2 hours	Neg	Y
Nagakane (2011)	Alteplase	MRI	Geometric mean lesion growth (day 90 T2 and baseline DWI)	3 months	Pos	N
		MRI	Median absolute growth (day 90 T2 and baseline DWI)	3 months	Pos	N
		MRI	Mean difference in cube root volumes (day 90 T2 and baseline DWI)	3 months	Neg	N
		MRI	Median difference in cube root volumes (day 90 T2 and baseline DWI)	3 months	Pos	N
		MRI	Growth >0% (day 90 T2 and baseline DWI)	3 months	Pos	N
		MRP	Reperfusion (>90% of initial deficit, Tmax+2s)	3-5 days	Pos	N
		MRP	Median percentage reperfusion	3-5 days	Pos	N
		MRA	Recanalization (>1 point increase on TIMI)	3-5 days	Neg	N
Nichols (2008)	Alteplase	CT	Median lesion volume	24 hours	Pos	N
		CT	Recanalization by resolution of HMCAS	24 hours	Pos	N
Ogawa (1999)	Ebselen	CT	Lesion volume	1 month	Neg	Y
Pantano (1999)	Alteplase	CT	Lesion growth (day 7- 24 hour)	7 days	Neg	N
		CT	Presence of any change (as a proportion, day 7- 24 hour)	7 days	Neg	N
Parsons (2012)	Tenecteplase	MRP/CTP	Reperfusion of initial deficit (%volume change of MTT defined tissue)	24 hours	Pos	Y
		MRI/CTP	Lesion growth (24hrs DWI - CTP)	24 hours	Pos	Y
		MRI/CTP	Lesion growth (90 day FLAIR - CTP)	3 months	Pos	Y
		MRA	Complete recanalization (TIMI 3)	24 hours	Neg	Y
		MRA	Complete or partial recanalization (improved TIMI)	24 hours	Pos	Y
		MRP	Volume reperfusion at 24 hours (MTT)	24 hours	Pos	N

		MRP	Penumbral salvage (24 hours)	24 hours	Pos	N
		MRP	Penumbral salvage (90 days)	3 months	Pos	N
Patel (2001)	Alteplase	CT	Lesion volume	3 months	Pos	N
Ringelstein (2013)	G-CSF	MRI	Lesion volume	1 month	Neg	Y
Roberts (2002)	IA pro-urokinase	CT	Lesion volume	24 hours	Pos	N
		CT	Lesion volume	7 days	Pos	N
Rosso (2012)	IV insulin	MRI	Mean infarct growth	1-3 days	Neg	Y
Schabitz (2010)	G-CSF	MRI	Lesion volume (unspecified modality)	3 months	Neg	Y
Sen (2009)	IA Alteplase	MRA	Recanalization (TIMI 2/3)	24 hours	Pos	Y
Shin (2007)	Albumin	MRI	Lesion growth ((Day 3-4 DWI - baseline DWI)/baseline DWI)	3-4 days	Neg	Y
Singhal (2005)	Normobaric oxygen	MRI	Lesion growth (4 hour DWI / baseline DWI)	4 hours	Pos	N
		MRI	Lesion growth (24 hour DWI / baseline DWI)	24 hours	Neg	N
		MRI	Lesion growth (7 days FLAIR / baseline DWI)	7 days	Neg	N
		MRI	Lesion growth (3 month FLAIR / baseline DWI)	3 months	Neg	Y
		MRP	Penumbral salvage: (baseline MTT volume - DWI volume)/(baseline MTT volume - baseline DWI volume)	4 hours	Pos	Y
		MRP	Penumbral salvage: (baseline MTT volume - DWI volume)/(baseline MTT volume - baseline DWI volume)	24 hours	Neg	N
		MRP	Penumbral salvage: (baseline MTT volume - DWI volume)/(baseline MTT volume - baseline DWI volume)	7 days	Neg	N
		MRP	Penumbral salvage: (baseline MTT volume - DWI volume)/(baseline MTT volume - baseline DWI volume)	3 months	Neg	N
		MRI	Temporary and sustained ADC reversal voxels	24 hours	Neg	N
		MRP	rCBV in affected volume	4 hours	Pos	Y
		MRP	rCBV in affected volume	24 hours	Pos	N

		MRP	rCBF in affected volume	4 hours	Pos	Y
		MRP	rCBF in affected volume	24 hours	Pos	N
		MRP	rMTT in affected volume	4 hours	Neg	Y
		MRP	rMTT in affected volume	24 hours	Neg	N
Srivastava (2012)	Minocycline	MRI	Infarct volume (day 30)	1 month	Neg	Y
		MRI	Infarct growth (1mo FLAIR - DWI)	1 month	Neg	Y
Thijs (2009)	Microplasmin	MRP	Reperfusion(>30% reduction in PWI or absence of PWI if <10ml)	4-12 hours	Neg	Y
		MRA	Improvement on MRA scale of 2 points	4-12 hours	Neg	Y
Warach (2000)	Citicoline	MRI	Lesion volume (week 12 T2 - baseline DWI)	3 months	Neg	Y
Warach (2006)	Gavestinel	MRI	Lesion growth (% change, 3 month DWI b0 and baseline DWI b1000)	3 months	Neg	Y
Yasaka (1998)	Steptokinase	SPECT	Reperfusion (binary and change in volume of hypoperfused tissue)	24 hours	Neg	Y
		TCD	Recanalization (operator assessment, no score)	7 days	Neg	Y

Key: IA: intra-arterial; EPO: erythropoetin; G-CSF: granulocyte colony stimulating factor; CT: computed tomography; MRI/A/P: magnetic resonance imaging/angiography/perfusion; DSA: digital subtraction angiography; SPECT: single photon emission CT; TCD: transcranial Doppler ultrasound; PWI: perfusion-weighted imaging; DWI: diffusion-weighted imaging; EIC :early ischaemic change; MCA: middle cerebral artery; TIMI: thrombolysis in myocardial infarction score; ASPECTS: Alberta Stroke Porgramme early CT score; HMCAS: hyperdense MCA sign; MTT: mean transit time; rMTT: relative MTT; rCBV: relative cerebral blood volume; rCBF: relative cerebral blood flow

Appendix E: Studies using Imaging to Define Subgroups

Author (year)	Intervention	Number of participants	Modality	Criterion	Subgroup size	Results different to primary analysis
MAST-I (1995)	Streptokinase	622	CT	No EIC	519	No
NINDS (1997)	Alteplase	624	CT	No EIC or thrombus identified	513	No
Broderick (2013)	Endovascular treatment	656	CT	ASPECTS 0-7	271	No
			CT	ASPECTS 8-10	378	No
			CTA	ICA/M1/BA occlusion	220	No
Chen (1997)	Aspirin	20655	CT	No EIC	2764	No
Davis (2008)	Alteplase	101	MRI	Lesion volume >5ml (DWI)	69	Yes
			MRP	20% PWI/DWI mismatch and PWI lesion-DWI lesion >10ml (Tmax+2s)	80	No
De Silva (2010)	Alteplase	87	MRA	MCA occlusion	32	Yes
			MRA	TIMI 0-1	49	No
			MRA	TIMI 2-3	38	No
			MRA	TIMI 0-2	54	No
			MRA	TIMI 3	33	No
Demchuk (2005)	Alteplase	608	CT	ASPECTS 8-10	402	No
			CT	ASPECTS 0-7	201	Yes (although same trend)
			CT	ASPECTS 3-7	185	No
			CT	ASPECTS <3	16	Yes (although same trend)
Derex (2001)	Alteplase	35	DSA	No vessel occlusion	10	Not clear

Dzialowski (2006)	Alteplase	788	CT	ASPECTS >7	557	No
			CT	ASPECTS <8	231	No
Gilligan (2002)	Streptokinase	270	CT	No EIC	94	No
			CT	Lesion <1/3 of vascular territory	82	No
			CT	Lesion >1/3 vascular territory	94	No
Hacke (2009)	Desmoteplase	193	MRA/CTA	TIMI 0-1	53	No
Hill (2003)	IA pro-urokinase	180	CT	ASPECTS 0-7	88	Yes (negative)
Hill (2014)	Endovascular treatment	656	CT	ASPECTS 8-10	378	No
			CT	ASPECTS 0-7	278	No
			CT	ASPECTS 0-4	92	No
			CT/angio	ASPECTS 8-10 and ICA/MCA occlusion	144	No
			CT/angio	ASPECTS 0-7 and ICA/MCA occlusion	128	No
			CT/angio	ASPECTS 0-4 and ICA/MCA occlusion	40	No
Kasner (2013)	Transcranial laser therapy	640	MRI/CT	Involvment of cortex	463	No
Kidwell (2009)	Magnesium	90	MRI	Lacunar stroke (DWI lesion <1.5ml, deep location)	15	No
			MRI	Baseline DWI >3ml	73	No
			MRP	20% PWI/DWI mismathch (Tmax+2s)	44	No
			MRP	20% PWI/DWI mismatch (Tmax+2s) and DWI >3ml	40	No
Kidwell (2013)	Embolectomy	118	CTP/MRP	Infarct/PWI <70% and core less than 90ml	68	No
			CTP/MRP	Non-penumbral	50	No
Levine (2005)	Alteplase	624	CT	Composite of NIHSS<2 and no EIC	28	No

Manelfe (1999)	Alteplase	603	CT	HMCAS	107	Yes
McCormick (2010)	Insulin	40	MRA	Intracranial vessel occlusion	11	Yes
Nagakane (2011)	Alteplase	101	MRI	Lesion volume >5ml (DWI)	69	Yes
			MRP	20% PWI/DWI mismatch and PWI lesion-DWI lesion >10ml (Tmax+2s, co-registered)	80	Yes
Nagakane (2012)	Alteplase	101	MRP	Severity weighted mismatch	61	No
Nichols (2008)	Alteplase	624	CT	HMCAS	79	Not clear
Ogawa (1999)	Ebselen	105	DSA	Persistent complete occlusion of M1 after thrombolysis	45	Yes
			DSA	Persistent complete occlusion of M1 or M2 after thrombolysis	70	Yes
			DSA	Recanalisation of M1 and M2 after thrombolysis	13	No
Pantano (1999)	Alteplase	450	CT at 24hrs	No EIC	87	Not done
			CT at 24hrs	Subcortical lesion	106	Not done
			CT at 24hrs	Cortical lesion	123	Not done
			CT at 24hrs	Mixed lesion	134	Not done
Parsons (2010)	Alteplase	98	MRP	20% PWI/DWI mismatch (Tmax+2s)	85	No
			MRP	PWI lesion <190ml, DWI lesion <25ml (Tmax+2s)	37	No
			MRP	PWI lesion 20-190ml, DWI lesion <25ml (Tmax+2s)	30	Yes
			MRP	PWI lesion <190ml, DWI lesion <18ml (Tmax+2s)	31	Yes, using mRS 0-1, no using mRS 0-2
			MRP	PWI lesion 20-190ml, DWI lesion <18ml (Tmax+2s)	24	Yes
			MRP	20% PWI/DWI mismatch (Tmax+2s), ICA occlusion excluded	65	No

			MRA	Lesion volume <25ml (DWI) and ICA occlusion excluded	47	Yes, using mRS 0-1, no using mRS 0-2
			MRP	PWI lesion >20ml, DWI lesion <25ml (Tmax+2s), ICA occlusion excluded	40	Yes, using mRS 0-1, no using mRS 0-2
			MRA	Lesion volume <18ml (DWI) and ICA occlusion excluded	39	Yes, using mRS 0-1, no using mRS 0-2
			MRP	PWI lesion >20ml, DWI lesion <18ml (Tmax+2s)	32	Yes
			MRP	20% PWI/DWI mismatch (Tmax+8s)	62	No
			MRP	PWI lesion <150ml, DWI lesion <25ml (Tmax+8s)	52	No
			MRP	PWI lesion 10-150ml, DWI lesion <25ml (Tmax+8s)	40	Yes, using mRS 0-1, no using mRS 0-2
			MRP	PWI lesion <150ml, DWI lesion <18ml (Tmax+8s)	43	No
			MRP	PWI lesion 10-150ml, DWI lesion <18ml (Tmax+8s)	33	Yes, using mRS 0-1, no using mRS 0-2
Patel (2001)	Alteplase	616	CT	Lesion volume >1/3 MCA	84	Yes
			CT	Lesion volume <1/3 MCA	110	Yes
			CT	No EIC	422	No
Roberts (2002)	IA urokinase	162	CT	No EIC	53	No
			CT	Lesion volume <20ml	77	No
			CT	Lesion volume 20-40ml	14	No
			CT	Lesion volume 40-60ml	7	No
			CT	Lesion volume >60ml	8	No
			DSA	No collaterals	50	No
			DSA	Collaterals	111	Yes
Rosso (2012)	IV insulin	180	MRA	Recanalization	70	Yes, negative
			MRA	Partial recanalization	50	Yes, negative

			MRA	No recanalization	34	Yes, negative
Warach (2012)	Desmotoplase	122	MRP	Mismatch volume <60ml	45	No
			MRP	Mismatch volume >60ml	66	No
Weschler (2003)	IA urokinase	180	CT	Lesion volume >5.25ml as part of a multimodal risk score	Variable	No
Yasaka (1998)	Steptokinase	37	SPECT	Perfusion deficit (12% drop c.f. contralateral)	22	No
			TCD	Vessel occlusion	16	No

Key: IA: intra-arterial; MRA: MRI: angiography; MRP: MRI perfusion; PWI: perfusion-weighted imaging; EIC :early ischaemic change; TIMI: thrombolysis in myocardial infarction score; ASPECTS: Alberta Stroke Programme early CT score; HMCAS: hyperdense MCA sign

References

1. Lee S, Shafe AC, Cowie MR. UK stroke incidence, mortality and cardiovascular risk management 1999-2008: time-trend analysis from the General Practice Research Database. *BMJ Open* 2011;1:e000269

2. Saka O, McGuire A, Wolfe C. Cost of stroke in the United Kingdom. *Age Ageing* 2009;38:27-32

3. Wardlaw JM, Murray V, Berge E, et al. Recombinant tissue plasminogen activator for acute ischaemic stroke: an updated systematic review and meta-analysis. *Lancet* 2012;379:2364-2372

4. Berkhemer OA, Fransen PS, Beumer D, et al. A randomized trial of intraarterial treatment for acute ischemic stroke. *N Engl J Med* 2015;372:11-20

5. Vahedi K, Hofmeijer J, Juettler E, et al. Early decompressive surgery in malignant infarction of the middle cerebral artery: a pooled analysis of three randomised controlled trials. *Lancet Neurol* 2007;6:215-222

6. Middleton S, McElduff P, Ward J, et al. Implementation of evidence-based treatment protocols to manage fever, hyperglycaemia, and swallowing dysfunction in acute stroke (QASC): a cluster randomised controlled trial. *Lancet* 2011;378:1699-1706

7. Neuhaus AA, Rabie T, Sutherland BA, et al. Importance of Preclinical Research in the Development of Neuroprotective Strategies for Ischemic Stroke. *JAMA Neurol* 2014 Mar 3. [Epub ahead of print]

8. O'Collins VE, Macleod MR, Donnan GA, et al. 1,026 experimental treatments in acute stroke. *Ann Neurol* 2006;59:467-477

9. Fisher M, Albers GW. Advanced imaging to extend the therapeutic time window of acute ischemic stroke. *Ann Neurol* 2013;73:4-9

10. Muir KW, Buchan A, von Kummer R, et al. Imaging of acute stroke. *The Lancet Neurology* 2006;5:755-768

11. Stroke Therapy Academic Industry R, II. Recommendations for clinical trial evaluation of acute stroke therapies. *Stroke* 2001;32:1598-1606

12. Stroke Therapy Academic Industry R. Recommendations for standards regarding preclinical neuroprotective and restorative drug development. *Stroke* 1999;30:2752-2758

13. Dirnagl U, Iadecola C, Moskowitz MA. Pathobiology of ischaemic stroke: an integrated view. *Trends Neurosci* 1999;22:391-397

14. Sudlow CL, Warlow CP. Comparable studies of the incidence of stroke and its pathological types: results from an international collaboration. International Stroke Incidence Collaboration. *Stroke* 1997;28:491-499

15. Adams HP, Jr., Bendixen BH, Kappelle LJ, et al. Classification of subtype of acute ischemic stroke. Definitions for use in a multicenter clinical trial. TOAST. Trial of Org 10172 in Acute Stroke Treatment. *Stroke* 1993;24:35-41

16. Erecinska M, Silver IA. ATP and brain function. *J Cereb Blood Flow Metab* 1989;9:2-19

17. Leithner C, Royl G. The oxygen paradox of neurovascular coupling. *J Cereb Blood Flow Metab* 2014;34:19-29

18. Astrup J, Siesjo BK, Symon L. Thresholds in cerebral ischemia - the ischemic penumbra. *Stroke* 1981;12:723-725

19. Hossmann KA. Viability thresholds and the penumbra of focal ischemia. *Ann Neurol* 1994;36:557-565

20. Hossmann KA. The two pathophysiologies of focal brain ischemia: implications for translational stroke research. *J Cereb Blood Flow Metab* 2012 Jan 11. [Epub ahead of print]

21. Eltzschig HK, Eckle T. Ischemia and reperfusion--from mechanism to translation. *Nat Med* 2011;17:1391-1401

22. Branston NM, Symon L, Crockard HA, et al. Relationship between the cortical evoked potential and local cortical blood flow following acute middle cerebral artery occlusion in the baboon. *Exp Neurol* 1974;45:195-208

23. Branston NM, Strong AJ, Symon L. Extracellular potassium activity, evoked potential and tissue blood flow. Relationships during progressive ischaemia in baboon cerebral cortex. *J Neurol Sci* 1977;32:305-321

24. Astrup J, Symon L, Branston NM, et al. Cortical evoked potential and extracellular K+ and H+ at critical levels of brain ischemia. *Stroke* 1977;8:51-57

25. Sharbrough FW, Messick JM, Jr., Sundt TM, Jr. Correlation of continuous electroencephalograms with cerebral blood flow measurements during carotid endarterectomy. *Stroke* 1973;4:674-683

26. Baron JC, Delattre JY, Bories J, et al. Comparison study of CT and positron emission tomographic data in recent cerebral infarction. *AJNR Am J Neuroradiol* 1983;4:536-540

27. Baron JC, Bousser MG, Rey A, et al. Reversal of focal "misery-perfusion syndrome" by extra-intracranial arterial bypass in hemodynamic cerebral ischemia. A case study with 15O positron emission tomography. *Stroke* 1981;12:454-459

28. Ackerman RH, Correia JA, Alpert NM, et al. Positron imaging in ischemic stroke disease using compounds labeled with oxygen 15. Initial results of clinicophysiologic correlations. *Arch Neurol* 1981;38:537-543

29. Marchal G, Rioux P, Serrati C, et al. Value of acute-stage positron emission tomography in predicting neurological outcome after ischemic stroke: further assessment. *Stroke* 1995;26:524-525

30. Marchal G, Serrati C, Rioux P, et al. PET imaging of cerebral perfusion and oxygen consumption in acute ischaemic stroke: relation to outcome. *Lancet* 1993;341:925-927

31. Baron JC, von Kummer R, del Zoppo GJ. Treatment of acute ischemic stroke. Challenging the concept of a rigid and universal time window. *Stroke* 1995;26:2219-2221

32. del Zoppo GJ, Sharp FR, Heiss WD, et al. Heterogeneity in the penumbra. *J Cereb Blood Flow Metab* 2011;31:1836-1851

33. Guadagno JV, Warburton EA, Jones PS, et al. The diffusion-weighted lesion in acute stroke: heterogeneous patterns of flow/metabolism uncoupling as assessed by quantitative positron emission tomography. *Cerebrovasc Dis* 2005;19:239-246

34. Heiss WD. The ischemic penumbra: correlates in imaging and implications for treatment of ischemic stroke. The Johann Jacob Wepfer award 2011. *Cerebrovasc Dis* 2011;32:307-320

35. Nicoli F, Lefur Y, Denis B, et al. Metabolic counterpart of decreased apparent diffusion coefficient during hyperacute ischemic stroke: a brain proton magnetic resonance spectroscopic imaging study. *Stroke* 2003;34:e82-87

36. Carrera E, Jones PS, Morris RS, et al. Is neural activation within the rescued penumbra impeded by selective neuronal loss? *Brain* 2013;136:1816-1829

37. Baron JC. Mapping the ischaemic penumbra with PET: a new approach. *Brain* 2001;124:2-4

38. Serena J, Leira R, Castillo J, et al. Neurological deterioration in acute lacunar infarctions: the role of excitatory and inhibitory neurotransmitters. *Stroke* 2001;32:1154-1161

39. Del Bene A, Palumbo V, Lamassa M, et al. Progressive lacunar stroke: review of mechanisms, prognostic features, and putative treatments. *Int J Stroke* 2012;7:321-329

40. Yamada M, Yoshimura S, Kaku Y, et al. Prediction of neurologic deterioration in patients with lacunar infarction in the territory of the lenticulostriate artery using perfusion CT. *AJNR Am J Neuroradiol* 2004;25:402-408

41. Wardlaw JM, Smith C, Dichgans M. Mechanisms of sporadic cerebral small vessel disease: insights from neuroimaging. *Lancet Neurol* 2013;12:483-497

42. Zaidi SF, Aghaebrahim A, Urra X, et al. Final Infarct Volume Is a Stronger Predictor of Outcome Than Recanalization in Patients With Proximal Middle Cerebral Artery Occlusion Treated With Endovascular Therapy. *Stroke* 2012;43:3238-3244

43. Cho TH, Nighoghossian N, Mikkelsen IK, et al. Reperfusion within 6 hours outperforms recanalization in predicting penumbra salvage, lesion growth, final infarct, and clinical outcome. *Stroke* 2015;46:1582-1589

44. Tsai JP, Albers GW. Reperfusion versus recanalization: the winner is. *Stroke* 2015;46:1433-1434

45. Bai J, Lyden PD. Revisiting cerebral postischemic reperfusion injury: new insights in understanding reperfusion failure, hemorrhage, and edema. *Int J Stroke* 2015;10:143-152

46. Kloner RA. No-reflow phenomenon: maintaining vascular integrity. *J Cardiovasc Pharmacol Ther* 2011;16:244-250

47. Neher JJ, Emmrich JV, Fricker M, et al. Phagocytosis executes delayed neuronal death after focal brain ischemia. *Proc Natl Acad Sci U S A* 2013;110:E4098-4107

48. Hussein HM, Georgiadis AL, Vazquez G, et al. Occurrence and predictors of futile recanalization following endovascular treatment among patients with acute ischemic stroke: a multicenter study. *AJNR Am J Neuroradiol* 2010;31:454-458

49. Molina CA. Futile recanalization in mechanical embolectomy trials: a call to improve selection of patients for revascularization. *Stroke* 2010;41:842-843

50. European Society of Radiology. White paper on imaging biomarkers. *Insights into imaging* 2010;1:42-45

51. Lassere MN, Johnson KR, Boers M, et al. Definitions and validation criteria for biomarkers and surrogate endpoints: development and testing of a quantitative hierarchical levels of evidence schema. *J Rheumatol* 2007;34:607-615

52. Svensson S MDBLJ. Surrogate outcomes in clinical trials: A cautionary tale. *JAMA internal medicine* 2013;173:611-612

53. Wardlaw JM. Surrogate outcomes: a cautionary note. *Stroke* 2009;40:1029-1031

54. Tzoulaki I, Siontis KC, Evangelou E, et al. Bias in associations of emerging biomarkers with cardiovascular disease. *JAMA internal medicine* 2013;173:664-671

55. Emberson J, Lees KR, Lyden P, et al. Effect of treatment delay, age, and stroke severity on the effects of intravenous thrombolysis with alteplase for acute ischaemic stroke: a meta-analysis of individual patient data from randomised trials. *Lancet* 2014;384:1929-1935

56. Jauch EC, Saver JL, Adams HP, Jr., et al. Guidelines for the early management of patients with acute ischemic stroke: a guideline for healthcare professionals from the American Heart Association/American Stroke Association. *Stroke* 2013;44:870-947

57. National Institute for Health and Care Excellence. Diagnosis and initial management of acute stroke and transient ischaemic attack (TIA). London, UK: NICE; 2008

58. Wintermark M, Albers GW, Broderick JP, et al. Acute Stroke Imaging Research Roadmap II. *Stroke* 2013;44:2628-2639

59. Campbell BC, Tu HT, Christensen S, et al. Assessing response to stroke thrombolysis: validation of 24-hour multimodal magnetic resonance imaging. *Arch Neurol* 2012;69:46-50

60. Parsons M, Spratt N, Bivard A, et al. A randomized trial of tenecteplase versus alteplase for acute ischemic stroke. *N Engl J Med* 2012;366:1099-1107

61. Parsons MW, Pepper EM, Chan V, et al. Perfusion computed tomography: prediction of final infarct extent and stroke outcome. *Ann Neurol* 2005;58:672-679

62. Fiebach JB, Schellinger PD, Jansen O, et al. CT and diffusion-weighted MR imaging in randomized order: diffusion-weighted imaging results in higher accuracy and lower interrater variability in the diagnosis of hyperacute ischemic stroke. *Stroke* 2002;33:2206-2210

63. Mitomi M, Kimura K, Aoki J, et al. Comparison of CT and DWI findings in ischemic stroke patients within 3 hours of onset. *J Stroke Cerebrovasc Dis* 2014;23:37-42

64. Lansberg MG, Albers GW, Beaulieu C, et al. Comparison of diffusion-weighted MRI and CT in acute stroke. *Neurology* 2000;54:1557-1561

65. Minematsu K, Li L, Fisher M, et al. Diffusion-weighted magnetic resonance imaging: rapid and quantitative detection of focal brain ischemia. *Neurology* 1992;42:235-240

66. Buxton RB, Frank LR, Wong EC, et al. A general kinetic model for quantitative perfusion imaging with arterial spin labeling. *Magn Reson Med* 1998;40:383-396

67. Zhou J, Payen JF, Wilson DA, et al. Using the amide proton signals of intracellular proteins and peptides to detect pH effects in MRI. *Nat Med* 2003;9:1085-1090

68. Ogawa S, Lee TM, Kay AR, et al. Brain magnetic resonance imaging with contrast dependent on blood oxygenation. *Proc Natl Acad Sci U S A* 1990;87:9868-9872

69. Radda GK. The use of NMR spectroscopy for the understanding of disease. *Science* 1986;233:640-645

70. Le Bihan D, Mangin JF, Poupon C, et al. Diffusion tensor imaging: concepts and applications. *J Magn Reson Imaging* 2001;13:534-546

71. Lansberg MG, Thijs VN, O'Brien MW, et al. Evolution of Apparent Diffusion Coefficient, Diffusion-weighted, and T2-weighted Signal Intensity of Acute Stroke. *AJNR Am J Neuroradiol* 2001;22:637-644

72. Buxton RB. Quantifying CBF with arterial spin labeling. *J Magn Reson Imaging* 2005;22:723-726

73. Markus HS. Cerebral perfusion and stroke. *J Neurol Neurosurg Psychiatry* 2004;75:353-361

74. Zaharchuk G, Bammer R, Straka M, et al. Improving dynamic susceptibility contrast MRI measurement of quantitative cerebral blood flow using corrections for partial volume and nonlinear contrast relaxivity: A xenon computed tomographic comparative study. *J Magn Reson Imaging* 2009;30:743-752

75. Kiselev VG. On the theoretical basis of perfusion measurements by dynamic susceptibility contrast MRI. *Magn Reson Med* 2001;46:1113-1122

76. Ostergaard L, Johannsen P, Host-Poulsen P, et al. Cerebral blood flow measurements by magnetic resonance imaging bolus tracking: comparison with [(15)O]H2O positron emission tomography in humans. *J Cereb Blood Flow Metab* 1998;18:935-940

77. van Osch MJ, van der Grond J, Bakker CJ. Partial volume effects on arterial input functions: shape and amplitude distortions and their correction. *J Magn Reson Imaging* 2005;22:704-709

78. Latchaw RE, Yonas H, Hunter GJ, et al. Guidelines and recommendations for perfusion imaging in cerebral ischemia: A scientific statement for healthcare professionals by the writing group on perfusion imaging, from the Council on Cardiovascular Radiology of the American Heart Association. *Stroke* 2003;34:1084-1104

79. Kane I, Carpenter T, Chappell F, et al. Comparison of 10 different magnetic resonance perfusion imaging processing methods in acute ischemic stroke: effect on lesion size, proportion of patients with diffusion/perfusion mismatch, clinical scores, and radiologic outcomes. *Stroke* 2007;38:3158-3164

80. Dani KA, Thomas RG, Chappell FM, et al. Computed tomography and magnetic resonance perfusion imaging in ischemic stroke: definitions and thresholds. *Ann Neurol* 2011;70:384-401

81. Calamante F, Christensen S, Desmond PM, et al. The physiological significance of the time-to-maximum (Tmax) parameter in perfusion MRI. *Stroke* 2010;41:1169-1174

82. Alsop DC, Detre JA, Golay X, et al. Recommended implementation of arterial spin-labeled perfusion MRI for clinical applications: A consensus of the ISMRM perfusion study group and the European consortium for ASL in dementia. *Magn Reson Med* 2014 Apr 8. [Epub ahead of print]

83. Alsop DC, Detre JA. Reduced transit-time sensitivity in noninvasive magnetic resonance imaging of human cerebral blood flow. *J Cereb Blood Flow Metab* 1996;16:1236-1249

84. Zaharchuk G. Arterial Spin Labeling for Acute Stroke: Practical Considerations. *Transl Stroke Res* 2012;3:228-235

85. Maleki N, Dai W, Alsop DC. Optimization of background suppression for arterial spin labeling perfusion imaging. *MAGMA* 2012;25:127-133

86. van Gelderen P, de Zwart JA, Duyn JH. Pittfalls of MRI measurement of white matter perfusion based on arterial spin labeling. *Magn Reson Med* 2008;59:788-795

87. Wu WC, Lin SC, Wang DJ, et al. Measurement of cerebral white matter perfusion using pseudocontinuous arterial spin labeling 3T magnetic resonance imaging--an experimental and theoretical investigation of feasibility. *PLoS One* 2013;8:e82679

88. Robertson CA, McCabe C, Gallagher L, et al. Stroke penumbra defined by an MRI-based oxygen challenge technique: 1. Validation using [14C]2-deoxyglucose autoradiography. *J Cereb Blood Flow Metab* 2011;31:1778-1787

89. Robertson CA, McCabe C, Gallagher L, et al. Stroke penumbra defined by an MRI-based oxygen challenge technique: 2. Validation based on the consequences of reperfusion. *J Cereb Blood Flow Metab* 2011;31:1788-1798

90. Dani KA, Santosh C, Brennan D, et al. T2*-weighted magnetic resonance imaging with hyperoxia in acute ischemic stroke. *Ann Neurol* 2010;68:37-47

91. Wise RG, Harris AD, Stone AJ, et al. Measurement of OEF and absolute CMRO2: MRI-based methods using interleaved and combined hypercapnia and hyperoxia. *Neuroimage* 2013;83:135-147

92. Dani KA, An L, Henning EC, et al. Multivoxel MR spectroscopy in acute ischemic stroke: comparison to the stroke protocol MRI. *Stroke* 2012;43:2962-2967

93. Levine SR, Helpern JA, Welch KM, et al. Human focal cerebral ischemia: evaluation of brain pH and energy metabolism with P-31 NMR spectroscopy. *Radiology* 1992;185:537-544

94. Parsons MW, Barber PA, Desmond PM, et al. Acute hyperglycemia adversely affects stroke outcome: a magnetic resonance imaging and spectroscopy study. *Ann Neurol* 2002;52:20-28

95. van Zijl PC, Yadav NN. Chemical exchange saturation transfer (CEST): what is in a name and what isn't? *Magn Reson Med* 2011;65:927-948

96. Tee YK, Harston GW, Blockley N, et al. Comparing different analysis methods for quantifying the MRI amide proton transfer (APT) effect in hyperacute stroke patients. *NMR Biomed* 2014;27:1019-1029

97. Chappell MA, Donahue MJ, Tee YK, et al. Quantitative Bayesian model-based analysis of amide proton transfer MRI. *Magn Reson Med* 2013;70:556-567

98. Hua J, Jones CK, Blakeley J, et al. Quantitative description of the asymmetry in magnetization transfer effects around the water resonance in the human brain. *Magn Reson Med* 2007;58:786-793

99. Sun PZ, Zhou J, Huang J, et al. Simplified quantitative description of amide proton transfer (APT) imaging during acute ischemia. *Magn Reson Med* 2007;57:405-410

100. Wintermark M, Sanelli PC, Albers GW, et al. Imaging recommendations for acute stroke and transient ischemic attack patients: A joint statement by the American Society of Neuroradiology, the American College of Radiology, and the Society of NeuroInterventional Surgery. *AJNR Am J Neuroradiol* 2013;34:E117-127

101. Vahedi K, Vicaut E, Mateo J, et al. Sequential-design, multicenter, randomized, controlled trial of early decompressive craniectomy in malignant middle cerebral artery infarction (DECIMAL Trial). *Stroke* 2007;38:2506-2517

102. Parsons MW, Christensen S, McElduff P, et al. Pretreatment diffusion- and perfusion-MR lesion volumes have a crucial influence on clinical response to stroke thrombolysis. *J Cerebr Blood F Met* 2010;30:1214-1225

103. Nagakane Y, Christensen S, Brekenfeld C, et al. EPITHET: Positive Result After Reanalysis Using Baseline Diffusion-Weighted Imaging/Perfusion-Weighted Imaging Co-Registration. *Stroke* 2011;42:59-64

104. Barber PA, Demchuk AM, Zhang J, et al. Validity and reliability of a quantitative computed tomography score in predicting outcome of hyperacute stroke before thrombolytic therapy. ASPECTS Study Group. Alberta Stroke Programme Early CT Score. *Lancet* 2000;355:1670-1674

105. Purushotham A, Campbell BC, Straka M, et al. Apparent diffusion coefficient threshold for delineation of ischemic core. *Int J Stroke* 2015;10:348-353

106. Coutts SB, Simon JE, Tomanek AI, et al. Reliability of assessing percentage of diffusion-perfusion mismatch. *Stroke* 2003;34:1681-1683

107. von Kummer R, Meyding-Lamade U, Forsting M, et al. Sensitivity and prognostic value of early CT in occlusion of the middle cerebral artery trunk. *AJNR Am J Neuroradiol* 1994;15:9-15; discussion 16-18

108. Patel SC, Levine SR, Tilley BC, et al. Lack of clinical significance of early ischemic changes on computed tomography in acute stroke. *JAMA* 2001;286:2830-2838

109. Hougaard KD, Hjort N, Zeidler D, et al. Remote ischemic perconditioning as an adjunct therapy to thrombolysis in patients with acute ischemic stroke: A randomized trial. *Stroke* 2014;45:159-167

110. Davis SM, Donnan GA, Parsons MW, et al. Effects of alteplase beyond 3 h after stroke in the Echoplanar Imaging Thrombolytic Evaluation Trial (EPITHET): a placebo-controlled randomised trial. *Lancet Neurol* 2008;7:299-309

111. Inoue M, Mlynash M, Christensen S, et al. Early diffusion-weighted imaging reversal after endovascular reperfusion is typically transient in patients imaged 3 to 6 hours after onset. *Stroke* 2014;45:1024-1028

112. Neumann AB, Jonsdottir KY, Mouridsen K, et al. Interrater agreement for final infarct MRI lesion delineation. *Stroke* 2009;40:3768-3771

113. Gonzalez RG, Schaefer PW, Buonanno FS, et al. Diffusion-weighted MR imaging: diagnostic accuracy in patients imaged within 6 hours of stroke symptom onset. *Radiology* 1999;210:155-162

114. Gonzalez RG. Low signal, high noise and large uncertainty make CT perfusion unsuitable for acute ischemic stroke patient selection for endovascular therapy. *J Neurointerv Surg* 2012;4:242-245

115. Ay H, Arsava EM, Vangel M, et al. Interexaminer difference in infarct volume measurements on MRI: a source of variance in stroke research. *Stroke* 2008;39:1171-1176

116. Kidwell CS, Jahan R, Gornbein J, et al. A trial of imaging selection and endovascular treatment for ischemic stroke. *N Engl J Med* 2013;368:914-923

117. Powers WJ. Intravenous thrombolysis of basilar artery thrombosis. *Ann Neurol* 2014;75:456-457

118. Tissue plasminogen activator for acute ischemic stroke. The National Institute of Neurological Disorders and Stroke rt-PA Stroke Study Group. *N Engl J Med* 1995;333:1581-1587

119. Lansberg MG, Straka M, Kemp S, et al. MRI profile and response to endovascular reperfusion after stroke (DEFUSE 2): a prospective cohort study. *Lancet Neurol* 2012;11:860-867

120. Simonsen CZ, Sorensen LH, Karabegovic S, et al. MRI before intraarterial therapy in ischemic stroke: feasibility, impact, and safety. *J Cereb Blood Flow Metab* 2014;34:1076-1081

121. Wisco D, Uchino K, Saqqur M, et al. Addition of hyperacute MRI aids in patient selection, decreasing the use of endovascular stroke therapy. *Stroke* 2014;45:467-472

122. Yoo AJ, Verduzco LA, Schaefer PW, et al. MRI-based selection for intra-arterial stroke therapy: value of pretreatment diffusion-weighted imaging lesion volume in selecting patients with acute stroke who will benefit from early recanalization. *Stroke* 2009;40:2046-2054

123. Broderick JP, Palesch YY, Demchuk AM, et al. Endovascular therapy after intravenous t-PA versus t-PA alone for stroke. *N Engl J Med* 2013;368:893-903

124. Rothwell PM. Treating individuals 2. Subgroup analysis in randomised controlled trials: importance, indications, and interpretation. *Lancet* 2005;365:176-186

125. Tomsick T. TIMI, TIBI, TICI: I came, I saw, I got confused. *AJNR Am J Neuroradiol* 2007;28:382-384

126. Kessler LG, Barnhart HX, Buckler AJ, et al. The emerging science of quantitative imaging biomarkers terminology and definitions for scientific studies and regulatory submissions. *Statistical methods in medical research* 2014 Jun 11. [Epub ahead of print]

127. Merino JG, Lattimore SU, Warach S. Telephone Assessment of Stroke Outcome Is Reliable. *Stroke* 2005;36:232-233

128. Harston GW, Sheehan M, Kennedy J. Emergency medicine research: rites, rituals and consent. *Emergency medicine journal : EMJ* 2014;31:90-91

129. Smith SM, Jenkinson M, Woolrich MW, et al. Advances in functional and structural MR image analysis and implementation as FSL. *Neuroimage* 2004;23 Suppl 1:S208-219

130. Woolrich MW, Jbabdi S, Patenaude B, et al. Bayesian analysis of neuroimaging data in FSL. *Neuroimage* 2009;45:S173-186

131. Jenkinson M, Beckmann CF, Behrens TE, et al. FSL. *Neuroimage* 2012;62:782-790

132. Desikan RS, Segonne F, Fischl B, et al. An automated labeling system for subdividing the human cerebral cortex on MRI scans into gyral based regions of interest. *Neuroimage* 2006;31:968-980

133. Jenkinson M, Bannister P, Brady M, et al. Improved optimization for the robust and accurate linear registration and motion correction of brain images. *Neuroimage* 2002;17:825-841

134. Jenkinson M, Smith S. A global optimisation method for robust affine registration of brain images. *Medical image analysis* 2001;5:143-156

135. Lo EH. Experimental models, neurovascular mechanisms and translational issues in stroke research. *Br J Pharmacol* 2008;153 Suppl 1:S396-405

136. Ma H, Zavala JA, Teoh H, et al. Penumbral mismatch is underestimated using standard volumetric methods and this is exacerbated with time. *J Neurol Neurosurg Psychiatry* 2009;80:991-996

137. Lo EH. A new penumbra: transitioning from injury into repair after stroke. *Nat Med* 2008;14:497-500

138. Greve DN, Fischl B. Accurate and robust brain image alignment using boundary-based registration. *Neuroimage* 2009;48:63-72

139. Kawano H, Hirano T, Nakajima M, et al. Diffusion-Weighted Magnetic Resonance Imaging May Underestimate Acute Ischemic Lesions: Cautions on Neglecting a Computed Tomography–Diffusion-Weighted Imaging Discrepancy. *Stroke* 2013;44:1056-1061

140. Quast MJ, Huang NC, Hillman GR, et al. The evolution of acute stroke recorded by multimodal magnetic resonance imaging. *Magn Reson Imaging* 1993;11:465-471

141. Knight RA, Dereski MO, Helpern JA, et al. Magnetic resonance imaging assessment of evolving focal cerebral ischemia. Comparison with histopathology in rats. *Stroke* 1994;25:1252-1261

142. Kranz PG, Eastwood JD. Does diffusion-weighted imaging represent the ischemic core? An evidence-based systematic review. *AJNR Am J Neuroradiol* 2009;30:1206-1212

143. Sakamoto Y, Kimura K, Shibazaki K, et al. Early ischaemic diffusion lesion reduction in patients treated with intravenous tissue plasminogen activator: infrequent, but significantly associated with recanalization. *Int J Stroke* 2013;8:321-326

144. de Crespigny A. Editorial comment--Mismatch or misconception? *Stroke* 2003;34:1683-1685

145. Smith SM, Brady JM. SUSAN - A new approach to low level image processing. *Int J Comput Vision* 1997;23:45-78

146. Zhang Y, Brady M, Smith S. Segmentation of brain MR images through a hidden Markov random field model and the expectation-maximization algorithm. *IEEE Trans Med Imaging* 2001;20:45-57

147. Mazziotta J, Toga A, Evans A, et al. A four-dimensional probabilistic atlas of the human brain. *J Am Med Inform Assn* 2001;8:401-430

148. Crum WR, Camara O, Rueckert D, et al. Generalised overlap measures for assessment of pairwise and groupwise image registration and segmentation. *Medical image computing and computer-assisted intervention : MICCAI International Conference on Medical Image Computing and Computer-Assisted Intervention* 2005;8:99-106

149. Klein A, Andersson J, Ardekani BA, et al. Evaluation of 14 nonlinear deformation algorithms applied to human brain MRI registration. *Neuroimage* 2009;46:786-802

150. Youden WJ. Index for rating diagnostic tests. *Cancer* 1950;3:32-35

151. Marks MP, Tong DC, Beaulieu C, et al. Evaluation of early reperfusion and i.v. tPA therapy using diffusion- and perfusion-weighted MRI. *Neurology* 1999;52:1792-1798

152. Eastwood JD, Engelter ST, MacFall JF, et al. Quantitative assessment of the time course of infarct signal intensity on diffusion-weighted images. *AJNR Am J Neuroradiol* 2003;24:680-687

153. Kidwell CS, Saver JL, Starkman S, et al. Late secondary ischemic injury in patients receiving intraarterial thrombolysis. *Ann Neurol* 2002;52:698-703

154. Simard JM, Kent TA, Chen M, et al. Brain oedema in focal ischaemia: molecular pathophysiology and theoretical implications. *Lancet Neurol* 2007;6:258-268

155. Fiehler J, Foth M, Kucinski T, et al. Severe ADC Decreases Do Not Predict Irreversible Tissue Damage In Humans. *Stroke* 2002;33:79-86

156. Campbell BC, Purushotham A, Christensen S, et al. The infarct core is well represented by the acute diffusion lesion: sustained reversal is infrequent. *J Cereb Blood Flow Metab* 2012;32:50-56

157. Guadagno JV, Warburton EA, Jones PS, et al. How affected is oxygen metabolism in DWI lesions?: A combined acute stroke PET-MR study. *Neurology* 2006;67:824-829

158. Dawson DA, Hallenbeck JM. Acute focal ischemia-induced alterations in MAP2 immunostaining: description of temporal changes and utilization as a marker for volumetric assessment of acute brain injury. *J Cereb Blood Flow Metab* 1996;16:170-174

159. Ejaz S, Williamson DJ, Ahmed T, et al. Characterizing infarction and selective neuronal loss following temporary focal cerebral ischemia in the rat: a multi-modality imaging study. *Neurobiol Dis* 2013;51:120-132

160. Baron JC. How healthy is the acutely reperfused ischemic penumbra? *Cerebrovasc Dis* 2005;20 Suppl 2:25-31

161. Heiss WD, Rosner G. Functional recovery of cortical neurons as related to degree and duration of ischemia. *Ann Neurol* 1983;14:294-301

162. Butcher K, Parsons M, Baird T, et al. Perfusion thresholds in acute stroke thrombolysis. *Stroke* 2003;34:2159-2164

163. Mies G, Auer LM, Ebhardt G, et al. Flow and neuronal density in tissue surrounding chronic infarction. *Stroke* 1983;14:22-27

164. Obrenovitch TP, Garofalo O, Harris RJ, et al. Brain tissue concentrations of ATP, phosphocreatine, lactate, and tissue pH in relation to reduced cerebral blood flow following experimental acute middle cerebral artery occlusion. *J Cereb Blood Flow Metab* 1988;8:866-874

165. Harris RJ, Symon L. Extracellular pH, potassium, and calcium activities in progressive ischaemia of rat cortex. *J Cereb Blood Flow Metab* 1984;4:178-186

166. Jones TH, Morawetz RB, Crowell RM, et al. Thresholds of focal cerebral ischemia in awake monkeys. *J Neurosurg* 1981;54:773-782

167. Tamura A, Graham DI, McCulloch J, et al. Focal cerebral ischaemia in the rat: 2. Regional cerebral blood flow determined by [14C]iodoantipyrine autoradiography following middle cerebral artery occlusion. *J Cereb Blood Flow Metab* 1981;1:61-69

168. Kaplan B, Brint S, Tanabe J, et al. Temporal thresholds for neocortical infarction in rats subjected to reversible focal cerebral ischemia. *Stroke* 1991;22:1032-1039

169. Baron JC. Perfusion thresholds in human cerebral ischemia: historical perspective and therapeutic implications. *Cerebrovasc Dis* 2001;11 Suppl 1:2-8

170. Bivard A, Krishnamurthy V, Stanwell P, et al. Arterial spin labeling versus bolus-tracking perfusion in hyperacute stroke. *Stroke* 2014;45:127-133

171. Bristow MS, Simon JE, Brown RA, et al. MR perfusion and diffusion in acute ischemic stroke: human gray and white matter have different thresholds for infarction. *J Cereb Blood Flow Metab* 2005;25:1280-1287

172. Simon JE, Bristow MS, Lu H, et al. A novel method to derive separate gray and white matter cerebral blood flow measures from MR imaging of acute ischemic stroke patients. *J Cereb Blood Flow Metab* 2005;25:1236-1243

173. Heiss WD, Grond M, Thiel A, et al. Tissue at risk of infarction rescued by early reperfusion: A positron emission tomography study in systemic recombinant tissue plasminogen activator thrombolysis of acute stroke. *J Cereb Blood Flow Metab* 1998;18:1298-1307

174. Traupe H, Kruse E, Heiss WD. Reperfusion of focal ischemia of varying duration: postischemic hyper- and hypo-perfusion. *Stroke* 1982;13:615-622

175. del Zoppo GJ, Hallenbeck JM. Advances in the vascular pathophysiology of ischemic stroke. *Thromb Res* 2000;98:73-81

176. Molina CA, Alvarez-Sabín J. Recanalization and Reperfusion Therapies for Acute Ischemic Stroke. *Cerebrovasc Dis* 2009;27:162-167

177. Okell TW, Chappell MA, Kelly ME, et al. Cerebral blood flow quantification using vessel-encoded arterial spin labeling. *J Cereb Blood Flow Metab* 2013;33:1716-1724

178. Chappell MA, Okell TW, Jezzard P, et al. A general framework for the analysis of vessel encoded arterial spin labeling for vascular territory mapping. *Magn Reson Med* 2010;64:1529-1539

179. Chappell MA, Okell TW, Payne SJ, et al. A fast analysis method for non-invasive imaging of blood flow in individual cerebral arteries using vessel-encoded arterial spin labelling angiography. *Medical image analysis* 2012;16:831-839

180. Lu H, Clingman C, Golay X, et al. Determining the longitudinal relaxation time (T1) of blood at 3.0 Tesla. *Magn Reson Med* 2004;52:679-682

181. Marchal G, Benali K, Iglesias S, et al. Voxel-based mapping of irreversible ischaemic damage with PET in acute stroke. *Brain* 1999;123:2387-2400

182. Albers GW, Thijs VN, Wechsler L, et al. Magnetic resonance imaging profiles predict clinical response to early reperfusion: the diffusion and perfusion imaging evaluation for understanding stroke evolution (DEFUSE) study. *Ann Neurol* 2006;60:508-517

183. Frackowiak RS, Lenzi GL, Jones T, et al. Quantitative measurement of regional cerebral blood flow and oxygen metabolism in man using 15O and positron emission tomography: theory, procedure, and normal values. *J Comput Assist Tomogr* 1980;4:727-736

184. Law I, Iida H, Holm S, et al. Quantitation of regional cerebral blood flow corrected for partial volume effect using O-15 water and PET: II. Normal values and gray matter blood flow response to visual activation. *J Cereb Blood Flow Metab* 2000;20:1252-1263

185. Leenders KL, Perani D, Lammertsma AA, et al. Cerebral blood flow, blood volume and oxygen utilization. Normal values and effect of age. *Brain* 1990;113 (Pt 1):27-47

186. Pantano P, Baron JC, Lebrun-Grandie P, et al. Regional cerebral blood flow and oxygen consumption in human aging. *Stroke* 1984;15:635-641

187. Ingvar DH, Cronqvist S, Ekberg R, et al. Normal values of regional cerebral blood flow in man, including flow and weight estimates of gray and white matter. A preliminary summary. *Acta neurologica Scandinavica Supplementum* 1965;14:72-78

188. Hoedt-Rasmussen K, Sveinsdottir E, Lassen NA. Regional cerebral blood flow in man determined by intra-arterial injection of radioactive inert gas. *Circ Res* 1966;18:237-247

189. Henry ME, Kaufman MJ, Lange N, et al. Test-retest reliability of DSC MRI CBV mapping in healthy volunteers. *Neuroreport* 2001;12:1567-1569

190. Gevers S, van Osch MJ, Bokkers RP, et al. Intra- and multicenter reproducibility of pulsed, continuous and pseudo-continuous arterial spin labeling methods for measuring cerebral perfusion. *J Cereb Blood Flow Metab* 2011;31:1706-1715

191. Qureshi AI. Acute hypertensive response in patients with stroke: pathophysiology and management. *Circulation* 2008;118:176-187

192. Kidwell CS, Saver JL, Mattiello J, et al. Diffusion-perfusion MRI characterization of post-recanalization hyperperfusion in humans. *Neurology* 2001;57:2015-2021

193. Markus R, Reutens DC, Kazui S, et al. Hypoxic tissue in ischaemic stroke: persistence and clinical consequences of spontaneous survival. *Brain* 2004;127:1427-1436

194. Darby DG, Barber PA, Gerraty RP, et al. Pathophysiological topography of acute ischemia by combined diffusion-weighted and perfusion MRI. *Stroke* 1999;30:2043-2052

195. Schabitz WR, Laage R, Vogt G, et al. AXIS: a trial of intravenous granulocyte colony-stimulating factor in acute ischemic stroke. *Stroke* 2010;41:2545-2551

196. Bi M, Ma Q, Zhang S, et al. Local mild hypothermia with thrombolysis for acute ischemic stroke within a 6-h window. *Clin Neurol Neurosur* 2011;113:768-773

197. Hacke W, Furlan AJ, Al-Rawi Y, et al. Intravenous desmoteplase in patients with acute ischaemic stroke selected by MRI perfusion-diffusion weighted imaging or perfusion CT (DIAS-2): a prospective, randomised, double-blind, placebo-controlled study. *Lancet Neurol* 2009;8:141-150

198. Fiehler J, von Bezold M, Kucinski T, et al. Cerebral blood flow predicts lesion growth in acute stroke patients. *Stroke* 2002;33:2421-2425

199. Kirino T. Delayed neuronal death in the gerbil hippocampus following ischemia. *Brain Res* 1982;239:57-69

200. Gidday JM. Cerebral preconditioning and ischaemic tolerance. *Nature reviews Neuroscience* 2006;7:437-448

201. Papadakis M, Hadley G, Xilouri M, et al. Tsc1 (hamartin) confers neuroprotection against ischemia by inducing autophagy. *Nat Med* 2013;19:351-357

202. Traylor M, Farrall M, Holliday EG, et al. Genetic risk factors for ischaemic stroke and its subtypes (the METASTROKE collaboration): a meta-analysis of genome-wide association studies. *Lancet Neurol* 2012;11:951-962

203. Huang S, Zhou S, Zhang Y, et al. Association of the Genetic Polymorphisms in Pre-MicroRNAs with Risk of Ischemic Stroke in a Chinese Population. *PLoS One* 2015;10:e0117007

204. Garcia-Bonilla L, Benakis C, Moore J, et al. Immune mechanisms in cerebral ischemic tolerance. *Frontiers in neuroscience* 2014;8:44

205. Nael K, Meshksar A, Liebeskind DS, et al. Periprocedural arterial spin labeling and dynamic susceptibility contrast perfusion in detection of cerebral blood flow in patients with acute ischemic syndrome. *Stroke* 2013;44:664-670

206. Kidwell CS. MRI biomarkers in acute ischemic stroke: a conceptual framework and historical analysis. *Stroke* 2013;44:570-578

207. Zhou J, van Zijl PC. Defining an Acidosis-Based Ischemic Penumbra from pH-Weighted MRI. *Transl Stroke Res* 2011;3:76-83

208. Nakada T, Houkin K, Hida K, et al. Rebound alkalosis and persistent lactate: multinuclear (1H, 13C, 31P) NMR spectroscopic studies in rats. *Magn Reson Med*: Wiley Subscription Services, Inc., A Wiley Company; 1991:9-14

209. Tomlinson FH, Anderson RE, Meyer FB. Acidic foci within the ischemic penumbra of the New Zealand white rabbit. *Stroke* 1993;24:2030-2039; discussion 2040

210. Jokivarsi KT, Grohn HI, Grohn OH, et al. Proton transfer ratio, lactate, and intracellular pH in acute cerebral ischemia. *Magn Reson Med* 2007;57:647-653

211. Naritomi H, Sasaki M, Kanashiro M, et al. Flow thresholds for cerebral energy disturbance and Na+ pump failure as studied by in vivo 31P and 23Na nuclear magnetic resonance spectroscopy. *J Cereb Blood Flow Metab* 1988;8:16-23

212. Roos A. Intracellular pH and buffering power of rat brain. *American Journal of Physiology--Legacy Content*; 1971

213. Kraig RP, Petito CK. Interrelation of Proton and Volume Regulation in Astrocytes. In: Ginsberg MD, Dietrich WD, eds. *Cerebrovascular Diseases: Sixteenth Research Conference*. Princeton: Raven Press, New York; 1989:239-246

214. Alberti KG, Nattrass M. Lactic acidosis. *Lancet* 1977;2:25-29

215. Crockard HA, Gadian DG, Frackowiak RS, et al. Acute cerebral ischaemia: concurrent changes in cerebral blood flow, energy metabolites, pH, and lactate measured with hydrogen clearance and 31P and 1H nuclear magnetic resonance spectroscopy. II. Changes during ischaemia. *J Cereb Blood Flow Metab* 1987;7:394-402

216. McVicar N, Li AX, Goncalves DF, et al. Quantitative tissue pH measurement during cerebral ischemia using amine and amide concentration-independent detection (AACID) with MRI. *J Cereb Blood Flow Metab* 2014;34:690-698

217. Nedergaard M, Kraig RP, Tanabe J, et al. Dynamics of interstitial and intracellular pH in evolving brain infarct. *Am J Physiol* 1991;260:R581-588

218. Allen KL, Busza AL, Proctor E, et al. Controllable graded cerebral ischaemia in the gerbil: studies of cerebral blood flow and energy metabolism by hydrogen clearance and 31P NMR spectroscopy. *NMR Biomed* 1993;6:181-186

219. Mabe H, Blomqvist P, Siesjo BK. Intracellular pH in the brain following transient ischemia. *J Cereb Blood Flow Metab* 1983;3:109-114

220. Cho SH, Kim DG, Kim DS, et al. Motor outcome according to the integrity of the corticospinal tract determined by diffusion tensor tractography in the early stage of corona radiata infarct. *Neurosci Lett* 2007;426:123-127

221. Sun PZ, Cheung JS, Wang E, et al. Association between pH-weighted endogenous amide proton chemical exchange saturation transfer MRI and tissue lactic acidosis during acute ischemic stroke. *J Cereb Blood Flow Metab* 2011;31:1743-1750

222. Sun PZ, Zhou J, Sun W, et al. Detection of the ischemic penumbra using pH-weighted MRI. *J Cereb Blood Flow Metab* 2007;27:1129-1136

223. Chopp M, Chen H, Vande Linde AM, et al. Time course of postischemic intracellular alkalosis reflects the duration of ischemia. *J Cereb Blood Flow Metab* 1990;10:860-865

224. Chopp M, Vande Linde AM, Chen H, et al. Chronic cerebral intracellular alkalosis following forebrain ischemic insult in rats. *Stroke* 1990;21:463-466

225. Yoshida S, Busto R, Martinez E, et al. Regional brain energy metabolism after complete versus incomplete ischemia in the rat in the absence of severe lactic acidosis. *J Cereb Blood Flow Metab* 1985;5:490-501

226. Nedergaard M, Goldman SA, Desai S, et al. Acid-induced death in neurons and glia. *J Neurosci* 1991;11:2489-2497

227. Kraig RP, Chesler M. Astrocytic acidosis in hyperglycemic and complete ischemia. *J Cereb Blood Flow Metab* 1990;10:104-114

228. Kraig RP, Petito CK, Plum F, et al. Hydrogen ions kill brain at concentrations reached in ischemia. *J Cereb Blood Flow Metab* 1987;7:379-386

229. Goldman SA, Pulsinelli WA, Clarke WY, et al. The effects of extracellular acidosis on neurons and glia in vitro. *J Cereb Blood Flow Metab* 1989;9:471-477

230. Kraig RP, Wagner RJ. Acid-induced changes of brain protein buffering. *Brain Res* 1987;410:390-394

231. Gao J, Duan B, Wang DG, et al. Coupling between NMDA receptor and acid-sensing ion channel contributes to ischemic neuronal death. *Neuron* 2005;48:635-646

232. Chu XP, Grasing KA, Wang JQ. Acid-sensing ion channels contribute to neurotoxicity. *Transl Stroke Res* 2014;5:69-78

233. O'Bryant Z, Vann KT, Xiong ZG. Translational strategies for neuroprotection in ischemic stroke--focusing on acid-sensing ion channel 1a. *Transl Stroke Res* 2014;5:59-68

234. Zeng WZ, Liu DS, Duan B, et al. Molecular mechanism of constitutive endocytosis of Acid-sensing ion channel 1a and its protective function in acidosis-induced neuronal death. *J Neurosci* 2013;33:7066-7078

235. Pignataro G, Simon RP, Xiong ZG. Prolonged activation of ASIC1a and the time window for neuroprotection in cerebral ischaemia. *Brain* 2007;130:151-158

236. Chesler M, Kraig RP. Intracellular pH of astrocytes increases rapidly with cortical stimulation. *Am J Physiol* 1987;253:R666-670

237. Chesler M, Kraig RP. Intracellular pH transients of mammalian astrocytes. *J Neurosci* 1989;9:2011-2019

238. Zollner JP, Hattingen E, Singer OC, et al. Changes of pH and Energy State in Subacute Human Ischemia Assessed by Multinuclear Magnetic Resonance Spectroscopy. *Stroke* 2015;46:441-446

239. Tietze A, Blicher J, Mikkelsen IK, et al. Assessment of ischemic penumbra in patients with hyperacute stroke using amide proton transfer (APT) chemical exchange saturation transfer (CEST) MRI. *NMR in biomedicine* 2014;27:163-174

240. Tee YK, Khrapitchev AA, Sibson NR, et al. Optimal sampling schedule for chemical exchange saturation transfer. *Magn Reson Med* 2013;70:1251-1262

241. Harston GW, Tee YK, Blockley N, et al. Identifying the ischaemic penumbra using pH-weighted magnetic resonance imaging. *Brain* 2015;138:36-42

242. Sun PZ, Benner T, Copen WA, et al. Early Experience of Translating pH-Weighted MRI to Image Human Subjects at 3 Tesla. *Stroke* 2010;41:S147-S151

243. Zhao X, Wen Z, Huang F, et al. Saturation power dependence of amide proton transfer image contrasts in human brain tumors and strokes at 3 T. *Magn Reson Med* 2011;66:1033-1041

244. Andrews RJ. Transhemispheric diaschisis. A review and comment. *Stroke* 1991;22:943-949

245. Feeney DM, Baron JC. Diaschisis. *Stroke* 1986;17:817-830

246. Wise R, Gibbs J, Frackowiak R, et al. No evidence for transhemispheric diaschisis after human cerebral infarction. *Stroke* 1986;17:853-861

247. Back T, Hoehn M, Mies G, et al. Penumbral tissue alkalosis in focal cerebral ischemia: Relationship to energy metabolism, blood flow, and steady potential. *Ann Neurol* 2000;47:485-492

248. Maclaren J, Herbst M, Speck O, et al. Prospective motion correction in brain imaging: a review. *Magn Reson Med* 2013;69:621-636

249. van Zijl PC, Zhou J, Mori N, et al. Mechanism of magnetization transfer during on-resonance water saturation. A new approach to detect mobile proteins, peptides, and lipids. *Magn Reson Med* 2003;49:440-449